Universidade de Aveiro
2012

Departamento de Engenharia Mecânica

Sylvio Michael Olim de Freitas

Nanofluids for heat exchanger improvement: a numerical approach

Universidade de Aveiro

2012

Departamento de Engenharia Mecânica

Sylvio Michael Olim de Freitas

Nanofluids for heat exchanger improvement: a numerical approach

Dissertação apresentada à Universidade de Aveiro para cumprimento dos requisitos necessários à obtenção do grau de Mestre em Engenharia Mecânica, realizada sob a orientação científica da Doutora Mónica Sandra Abrantes de Oliveira Correia, Professora Auxiliar do Departamento de Engenharia Mecânica da Universidade de Aveiro.

Dedico este trabalho aos meus pais

o júri

presidente	Prof. Doutor Nelson Amadeu Dias Martins Professor Auxiliar do Departamento de Engenharia Mecânica da Universidade de Aveiro
arguente	Doutor Jorge Humberto de Melo Rosa Amorim Estagiário de Pós-doutoramento do Departamento de Ambiente e Ordenamento da Universidade de Aveiro
orientadora	Prof. Doutora Mónica Sandra Abrantes de Oliveira Professora Auxiliar do Departamento de Engenharia Mecânica da Universidade de Aveiro

agradecimentos

Ao findar uma longa e enriquecedora fase da minha vida, constato que não há espaço adequado para agradecer às tantas pessoas que me motivaram e ajudaram no meu percurso.

O meu profundo apreço é endereçado à Doutora Mónica Sandra Abrantes de Oliveira Correia, professora e orientadora, por proporcionar-me esta e outras oportunidades cativantes e enriquecedoras neste trajecto académico. Sua calma, capacidade de motivação e nível de conhecimento não aparentam ter limites.

Um agradecimento especial ao (iminente) Doutor Hugo Miguel Filipe Calisto, pela orientação relativa ao desenvolvimento do modelo numérico e estimada ajuda na adequação ao *software* utilizado. Por meio da referida iminência, não pôde desempenhar oficialmente o cargo, mas foi um óptimo co-orientador.

Quero agradecer e manifestar meu afecto aos meus queridos pais pelo apoio incondicional, sem eles nada disto teria sido possível, minha mãe pelo seu carinho infinito e meu pai pela sua dedicação sistemática. Obrigado por sempre acreditarem nas minhas capacidades.

Um profundo agradecimento à Sara (*my one and only*), pela ajuda, a entrega, a compreensão e o carinho; bem como à sua maravilhosa família pela simpatia sem paralelo.

Aos meus amigos, em particular ao Carlos, e restantes bons colegas, deixo meu agradecimento.

Por fim, mas não menos importante, deixo um agradecimento a todos os autores das (imensas) publicações que servem de base para o Capítulo 2 da presente tese. Foi gratificante constatar que, mesmo espalhados pelo mundo, trabalham com o objectivo comum de compreender os nanofluidos e acelerar sua aplicação industrial, assim tornando o planeta um pouco mais verde para as gerações que se seguem. Suas peças contribuíram significativamente para meu conhecimento de nanofluidos, o que poderá, no futuro, vir a ser útil.

palavras-chave Nanotubo de carbono, nanofluido, convecção, convecção forçada, permutador de calor, modelação numérica, mecanismos de transferência de calor

resumo No panorama industrial, as últimas décadas ficaram marcadas pelo aparecimento do conceito de sustentabilidade, consequência da crescente escassez de recursos e o desaparecimento de ecossistemas. Os resultados da poluição excessiva têm sido notórios, como o buraco do ozono ou a intensificação de fenómenos meteorológicos adversos comprovam. Cientes da aproximação a um ponto de irreversibilidade, governos e indústrias perseguem o objectivo comum de proteger o ambiente e racionalizar consumos energéticos, com vista a garantir a sobrevivência das gerações futuras. Permutadores de calor desempenham um papel fundamental no aquecimento, arrefecimento e recuperação energética, tendo também sido alvo da implementação de medidas que promovem o aumento da sua eficiência com vista a contribuir para a sustentabilidade dos sistemas térmicos nos quais operam. A principal limitação dos actuais permutadores é o baixo desempenho calorífico dos fluidos operantes tipicamente empregues, como óleo, glicóis ou água. De forma a preencher esta lacuna, surgiram recentemente os nanofluidos, suspensões de nanopartículas, possuidores de melhores propriedades de transferência de calor, em fluidos comuns. Estes revelam aumentos substanciais no desempenho, permitindo antever um aumento da eficiência dos dispositivos quando aplicado. De momento, o desconhecimento dos parâmetros mais influentes para a transferência anómala de calor, está a restringir a sua aplicabilidade industrial. Para o estudo da transferência de calor, por convecção, de um nanofluido, composto por água destilada e nanotubos de carbono, um modelo numérico é proposto e validado com base em dados experimentais. As propriedades mais relevantes dos fluidos em estudos desta natureza, o coeficiente de convecção e o número de Nusselt, são obtidos através da análise ao escoamento no interior de um tubo aquecido (aço inox). Os dados obtidos para o nanofluido são posteriormente comparados aos valores correspondentes para a água destilada e às correlações teóricas comuns. Propõe-se, adicionalmente, o estudo e debate do contributo de alguns dos mecanismos comuns à transferência de calor, por intermédio de testes paramétricos individuais.

keywords Carbon nanotube, nanofluid, convective heat transfer, forced convection, heat exchanger, numerical modelling, heat transfer mechanisms

abstract

In the industrial panorama, the last decades have been marked by the advent of the concept of sustainability, consequence of growing resource scarcity and ecosystem destruction. Excessive pollution has led to notorious concerns, such as ozone layer depletion or severe climatic events. In order to guarantee the safety of future generations, governments and industries share the common goal of environment preservation and rational energy expenditure, before a point of no return is reached. Heat exchangers perform an important role in heating, cooling and heat recovery, having also been subjected to the implementation of measures that promote efficiency in order to ultimately contribute to the sustainability of the systems in which they operate. The main limitation of current exchangers is the poor heat transfer behaviour of common operating fluids, such as oil, glycols or water. In order to fulfil the requirement of improved fluid heat transfer, the recent advent of nanofluids, high heat transfer nanoparticle suspensions in base fluids, has taken place. These have displayed substantial heat transfer performances, allowing to foresee increases in device efficiency once applied. At present the mechanisms, responsible for the anomalous enhancements, remain unknown, thus restricting industrial applicability. For the convective heat transfer study of a nanofluid, with carbon nanotubes suspended in deionized water, a numerical model is proposed and validated based on experimental data. The relevant fluid properties used for such investigations, the heat transfer coefficient and the Nusselt number, are obtained for fluid flow through a heated tube (stainless steel). The acquired results for the nanofluid are then compared to the matching data for deionized water and to common theoretical correlations. Additionally, a study and debate concerning the contribution of typical heat transfer mechanisms, evaluated individually under parametric testing, is proposed.

Contents

List of Figures

List of Tables

List of Symbols

A	Heat Transfer Area
A_{ext}	Outer Tube Surface Area
bf	Base Fluid
$CCVD$	Catalytic Chemical Vapour Deposition
CFD	Computational Fluid Dynamics
CHE	Compact Heat Exchanger
c_P	Specific Heat Capacity
CNT	Carbon Nanotube
D	Test Tube Inner Diameter
DIW	Deionized Water
$DWCNT$	Double-walled Carbon Nanotube
EG	Ethylene Glycol
exp	Experimental
h	Convective Heat Transfer Coefficient
k	Thermal Conductivity
k_f	Thermal Conductivity of Base Fluid
k_{eff}	Effective Thermal Conductivity
k_P	Thermal Conductivity of Solid Particle
L	Test Tube Length
M	Molar Mass
$\dot{m}$	Mass Flow Rate
$MWCNT$	Multi-walled Carbon Nanotube
n	Particle Shape Factor
nf	Nanofluid
np	Nanoparticle
Nu	Nusselt Number
num	Numerical
Pe	Peclet Number
PHE	Plate Heat Exchanger
Pr	Prandtl Number
Q_{in}	Power Transfer to the Fluid
Q''_{in}	Heat Flux to the Fluid
q	Power
q''	Surface Heat Flux
q_{cw}''	Constant Wall Heat Flux
Re	Reynolds Number
$SWCNT$	Single-walled Carbon Nanotube
$\bar{T}_f$	Axial Mean Fluid Temperature
$T_{f,in}$	Fluid Temperature at Inlet
$T_{f,out}$	Fluid Temperature at Outlet
T_{out}	Fluid Temperature at Outlet

T_s	Tube Surface Temperature
$T_{w,\,out}$	Tube Temperature at Outlet
THW	Transient Hot-wire
U	Overall Heat Transfer Coefficient
u	Fluid Velocity
u_{in}	Fluid Velocity at Inlet
x	Axial Position
ϕ	Volume Fraction
3ω	3-omega
ρ	Density
μ	Dynamic Viscosity

Chapter Guide

Chapter 1 – Introduction

The motivation for nanofluids and its connection to the main objectives for the current thesis are outlined. Brief concepts and basic definitions are also discussed.

Chapter 2 – Literature Review

An investigation into the notion of sustainable development and its role in energy management is conducted. Additionally, a comprehensive study of current heat exchanging technology and typical operating fluids is proposed. Once an adequate understanding is established, one can proceed to comprehend nanofluids and the important role they can play in improving heat exchanger performance for sustainable development. This chapter posteriorly served as foundation for the chapter of a book regarding carbon nanotube science.

Chapter 3 – Experimental Model

Dedicated to the presentation of the experimental setup employed by Silva (2010), which is the foundation for numerical model development. Both the setup and the experimental procedure are concisely explained, as well as other relevant factors.

Chapter 4 – Numerical Model

The parameters associated to the numerical model development are presented and thoroughly discussed. Once accomplished, the model undertakes a validation procedure based on the experimental data described in the previous chapter.

Chapter 5 – Heat Transfer Mechanism Analysis

Some possible heat transfer enhancement mechanisms of the nanofluid are submitted to parametric testing in an attempt to gain some insight into the contribution of each. The obtained data is compared to theoretical correlations and discussed, if such assumptions are conclusive.

Chapter 6 – Conclusions

Reserved for a critical debate of the current study, which includes an assessment of the used software and a discussion on the suitability of nanofluid employment based on the obtained results. Finally, a few thoughts on possible model developments, with a view to improve result accuracy, are discussed.

Chapter 1

Introduction

1.1. Nanofluid Motivation

Ever since the World Commission on Environment and Development (WCED) addressed the issue, in June 1987, sustainable development has gained global awareness, leading governments and businesses in most industrialized countries to commit to reorienting policies in order to avoid the deterioration of natural resources and human environment. According to the WCED the aim of sustainable development is to meet present needs without compromising the future generations in meeting their own needs, essentially maintaining economic and social growth without depleting the world's natural resource supply and preserving its ecosystems. With the purpose of achieving this, today's engineers and scientists are challenged to develop innovative products and services that minimize the use of resources whilst preventing the generation of pollution throughout their life cycles.

For thermal systems, a major topic of sustainable development is rational energy management. As a result of industrial development and population increase the global energy demand continues to rise, despite limited resources, which has led to soaring prices and, consequently, contributed to the current global economic crisis. The undergoing reform in the energy sector is deemed critical for the future of sustainable development and measures, such as environmental protection policies or higher levels of regulation, are in place. Improved energy technologies and cleaner energy usage have become top priorities, the main focus being on the maximization of overall system efficiency. Over the last decades steps have been taken in reviewing and improving the existing technologies as well as developing new ones, for instance renewable energies or improved means of energy transport. Despite this, energy-related greenhouse gas emissions still account for around 70% of total emissions, including methane and carbon dioxide, mainly produced by fossil fuel combustion (Bazmi et al. 2011). New challenges in thermal system design are also thriving, sharing the common aim of gaining heat transfer intensification at reduced energy loss.

In a wide variety of industries heat exchangers play a significant part in energy conservation, conversion and recovery, as well as in system implementation for new technologies. Besides construction simplicity and high efficiencies, that minimize production and operating costs, they also allow process integration, enabling exchanges between processes, thus reducing energy requirements. Additionally, they provide a significant contribution in environmental protection, performing key roles in waste heat recovery and in pollution prevention/control systems, such as systems that decrease air pollutant emissions or pollutants in wastewater discharges.

Over the years, improvements in material science have allowed for progressive component downscaling in most industries. Heat exchanger design has evolved in the same manner, with the development of increased transfer surface devices with reduced hydraulic diameters, leading to higher system efficiencies when compared to older designs. Despite these successful improvements, recent demands call for smaller size technologies and higher thermal load interactions. The advent of micro-scale system components, allied to the growing concerns in sustainable development, has pushed toward the requirement for augmented heat transfer performances at reduced material and operating expenses. In order to achieve increased heat

dissipation, one can apply either of two methods: passive and active techniques. More widely used, active techniques bear the inconvenience of requiring external energy sources, adding higher controllability and significant heat transfer intensification, as efficient heat pumps prove, leading to faster heat transfer processes. Passive techniques, such as fluid property modification or heat exchanging surface geometry enhancement, have more potential from a sustainable development point of view.

At present, the main limitation of passive technique employment is the low heat exchange performance of typical heat transfer fluids, the thermal conductivity of water being the highest, at roughly 0.6 W/m K, supporting this notion. On the other end of the scale, many common metals or metal oxides have thermal conductivities that are several orders higher. Therefore it is coherent to assume that the addition of solid particles to a base liquid could increase its overall thermal conductivity. This has been known ever since Maxwell first presented the idea of suspending metallic particles in order to improve the heat transfer of fluids, in the latter 19^{th} century. Since then, numerous theoretical and experimental studies found that suspended mili- and micrometre sized particles tend to agglomerate and settle down rapidly, which leads to channel clogging, rendering them unfeasible for use in micro-channel flows. The high relative mass of the particles was also noted to promote channel corrosion quite easily. It wasn't until the advent of nanotechnology that the opportunity to produce particles at a nano-scale presented itself.

As recently as 1995, Choi proposed the term nanofluid to designate the colloidal suspension of nano-sized particles, in which one critical dimension is lower than 100 nm, in a base fluid. According to Choi nanofluids constitute a new type of functional composite material, developed with the distinctive purpose of enhancing the thermal performance of heat transfer fluids, whilst offering a stable quasi-single phase arrangement. Presently, the most common nanoparticles used for nanofluids have spherical or tubular geometries, carbon nanotube (CNT) nanofluids exhibiting significantly higher heat transfer enhancements than spherical nanofluids, which indicate that these will promote top efficiencies when used in heat exchanging devices.

1.2. Nanofluid Heat Transfer

Increases in heat transfer using nanofluids have indeed been found experimentally, however the formulation of the mechanisms responsible for these increases is far from consensual. Thorough experimentation with a vast variety of nanofluids has determined that the enhancement of thermal conductivity is influenced by a variety of parameters, paving the way for the development of several mathematical models. Despite this, the degree of dependence on each parameter in the observed enhancements remains unknown.

In order to apply nanofluids in heat exchanging systems, a full knowledge of their convective heat transfer behaviour is required. However, experimental studies in this area are still scarce, far rarer is the available literature involving numerical models. Most of the studies employ nanofluids in heated tubes, acting as heat exchangers between heating devices and fluids, with the Nusselt number (Nu) typically characterizing their convective heat transfer capabilities, the majority demonstrating a superior heat transfer performance of nanofluids when compared to their base fluids alone. Still, consensual results are yet to be established, the same going for possible heat transfer parameters responsible for such enhancements. At present, the lack of experimental and numerical investigations into convective heat transfer is a significant factor that is limiting application in industrial systems.

1.3. Challenges for the Present Thesis

Despite the extensive research on nanofluids, a precise description of the experimentally displayed anomalous heat transfer enhancements is still a paramount limitation. The uncertainties surrounding the influence of several factors to the observed uncharacteristic heat transfer enhancements remain a source of speculation amongst the scientific community. Additionally, most existing studies are focused on nanofluid thermal conductivity, rather than the convective heat transfer performance. In order to gain an adequate understanding of such fluid behaviours, Silva (2010) developed a specialized facility for CNT nanofluid research at the University of Aveiro's Department of Mechanical Engineering. Here, preparation of a CNT/water nanofluid was carried out, followed by experimental measurements of the fluid thermal conductivity, viscosity and convective heat transfer. The resulting data was consequently employed to calculate the convective heat transfer coefficient (h) and the Nusselt number (Nu), which displayed significant enhancements over the corresponding values of the base fluid alone.

With the purpose of achieving a better understanding of the witnessed heat transfer behaviours, the current thesis proposes a numerical approach to the forced convective heat transfer setup of the experimental study of flow in a heated circular tube. Essentially, this involves system modelling using Computational Fluid Dynamics (CFD) software, which is followed by model validation using the experimental data observed by Silva (2010). The obtained numerical results can then be analysed and compared to the matching experimental data, allowing conclusions regarding possible heat transfer enhancements using nanofluids, as well as the legitimacy of the experimental setup. Yet, the main advantage of a successful numerical model will be the possibility of examining the individual contributions of select properties to the viewed global heat transfer enhancements.

Nanofluid science is still at a premature stage of development, so obviously there is still no dedicated simulation software or CFD software upgrade exclusively dedicated to nanofluids. Therefore, the proposed numerical model can bear the inconvenience of existing uncontrollable factors that may interfere with obtained results. Due to this, the modelling process is expected to be a complex one and the validity of the results, at times, questionable. Hence, a critical stance must be permanently preserved, quite especially when evaluating the roles played by the available parameters in the increased heat transfer capabilities displayed by the nanofluids.

In order to correctly establish a numerical approach for nanofluid employment in heat exchangers, a comprehensive understanding of heat exchanger technology, common operating fluid properties and performed nanofluid studies is fundamental. This is proposed with Chapter 2, an exhaustive, but required, critical literature review that also presents the concepts of sustainability and nanofluid science, along with associated investigations. After an adequate understanding is accomplished, Chapter 3 covers the essential topics regarding the experimental setup, performed by Silva (2010), which serves as foundation for the numerical model, presented in Chapter 4. In this chapter, special attention is paid to the modelling process that involves mesh features and boundary condition definitions. Once the numerical model is deemed test-worthy validation can be undertaken, taking in account the obtained experimental data. Consequent comparisons between experimental, theoretical and numerical results are then established, after which conclusions regarding model rationality can be made. To gain some insight into the influence of a few mechanisms to the improved performance, results yielded through parametric property

testing are described in Chapter 5. Finally, conclusions regarding the performed study, as well as future model developments are reserved for Chapter 6.

Chapter 2

Literature Review

2.1. Sustainable Development

In order to fully understand the role that nanofluids can perform in reducing energy dependence, an understanding of sustainable development, as well as energy usage and its impact on the environment, bears relevance. A brief, historic review of the concepts of sustainability and sustainable development is proposed, followed by a diminutive investigation into the connection between energy management and its consequences to ecosystems. Here it is also important to comprehend the changes that can be generally applied and the main guidelines behind environmental policy moulding.

2.1.1. Definitions

The abundant resources available in the early stages of industrialization imposed a development approach based on the concept that most resources would be unlimited. Over a century has passed and, presently, risk of resource depletion is globally perceived. Ever since the United Nations Plenary Meeting at its General Assembly in 1987, where the Brundtland Commission on behalf of the World Commission on Environment and Development (WCED) addressed the issue, sustainability has become an international effort, governments and businesses in most industrialized countries have become committed to avoid the deterioration of natural resources and human environment. The basic concept of sustainability is to meet the present needs without conceding the capability of future generations in meeting their own needs, i.e., without depleting the world's natural resources. In order to achieve this, the Brundtland Commission proposed several strategic requirements: stimulating growth, improving growth quality, meeting essential human necessities, maintaining a supportable level of population, preserving resource base, reorienting technologies and merging environment and economics in decision making (WCED, 1987).

Based on this concept, the European Commission later defined sustainable development, affiliating sustainability with environmental matters (EC, 1992). Sustainable development is considered the most important reference for environmental policy, having significant effects on policy modelling. Multiple directives aim to reduce the environmental impact of human activity, with growing focus on the role of science in assisting the sensible management of the environment for the survival and the future development of mankind (Afgan et al., 1998; Zaccai, 2012).

2.1.2. Energy and Environment

It is well-known that energy management plays an important role in sustainable development. Energy resources are needed for collective development, but natural resource scarcity and economic growth act in opposition to each other (Afgan et al., 1998). Over the last decades, population growth and technological progress have directed the increase of energetic requirements, also bearing the consequence of increased environmental problems which threaten the future of manhood. Industry's high dependence on burning fossil fuels is regarded the main culprit of climate change and, quite expectedly, industrialized countries are primary contributors toward global emissions (Omer, 2007).

There is robust scientific evidence that the average temperature of the planet's surface is rising, a consequence of the increasing concentrations of greenhouse gases (especially CO_2) in the atmosphere. These proceed to trap heat radiated from the planet's surface, thus increasing the Earth's surface temperature (Dincer, 1997). A predicted global temperature increase, of between 1.5 and 4.5°C, can lead to catastrophic environmental impacts, such as severe weather events, sea level rise, floods or droughts (Omer, 2007).

Since the signing of the Kyoto Protocol in 1997, policies with a view to reducing emissions and gaining awareness to fossil fuel dependence have emerged and are in place. The common aim of such policies is to encourage and promote measures capable of enhancing long term sustainability through technological improvement, decreased energy consumption and cleaner energy source usage (renewable energies), thus decreasing the influence of the bond shared by productivity and resource depletion. Energy usage can be reduced by minimizing demand, employing rational management or recovering heat (Omer, 2007). Although pollutant reductions have been observed in some regions, complemented by an increase in green products available in markets, these remain inadequate improvements as far as major ecological impacts are concerned, particularly in climate change and biodiversity loss (Zaccai, 2012).

2.2. Heat Exchangers

The present topic aims to describe heat exchangers and respective applications. Nowadays, heat exchangers exist in a wide variety of industries, sizes and functions, which translates to several different classifications. In order to gain an extensive scope of the most common device types used, an approach to the main classification systems is proposed. Once a necessary understanding is obtained, measures that allow heat transfer enhancement, fundamental in a sustainable development point of view, can then be reviewed and comprehended.

2.2.1. Heat Exchanger Applications

A heat exchanger is a device used to transfer thermal energy between two or more fluids, between a solid surface and a fluid, or between solid particulates and a fluid. To achieve heat transfer, the exchanging fluids are required to be at different temperatures and in thermal contact (Shah and Sekulic, 2003). Heat exchangers can be employed in any system requiring the transfer of thermal energy from one location to another, fundamental in system or substance temperature control.

Common applications include heating, or cooling, of fluid streams and evaporation, or condensation, of single- or multicomponent streams. Such applications are required in a wide variety of industries and industrial processes, such as HVAC systems, power production, sanitation, waste management, chemical processing or refrigeration.

2.2.2. Heat Exchanger Types

Due to such a vast applicability, a wide array of heat exchanger types can be employed, leading to many different classifications. Categories used in such groupings include transfer processes, flow configurations, surface compactness or construction arrangements.

2.2.2.1. Transfer Process

When classified according to the transfer process involved, as in Figure 1, heat exchangers can be direct-contact or indirect-contact types. The most common type employed is the indirect-contact heat exchanger.

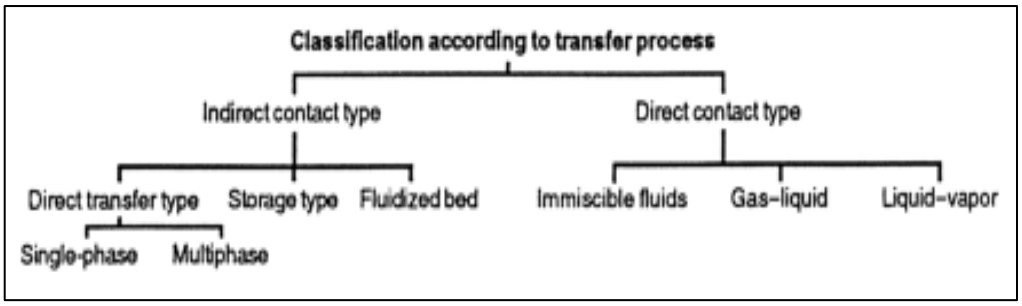

Figure 1 – Classification of heat exchangers, according to heat transfer process (Shah and Sekulic, 2003)

In direct-contact exchangers, heat transfer between fluids occurs through direct interaction, ideally without mixing or leakage. The fluids come into direct contact, exchange heat and are then separated. Advantages of these include a low cost and a lack of fouling (absence of transfer surface), the major drawback being the fact that applications are limited to situations in which direct contact of fluid streams is viable. They are particularly useful in applications involving mass transfer in addition to heat transfer, obtained through fluid phase-change; heat transfer involving only sensible heat is rare for this type of exchanger. Due to the increased enthalpy, latent heat transfer is responsible for the greater portion of energy transferred in this process. Immiscible fluids and phase-changing exchangers constitute sub-categories of the direct-contact type. (Shah and Sekulic, 2003)

As for the indirect-contact configuration, the fluid streams remain separate while the heat transfers through an impermeable surface via conduction. As can be observed in Fig. 1, these can be further categorized into direct-transfer, storage or fluidized-bed types. In a perspective of nanofluid employment, only direct-transfer exchangers shall be considered. In these, heat transfer between flowing streams, in separate passages, occurs continuously and the process can occur in single- or multi-phase flows. (Shah and Sekulic, 2003)

2.2.2.3. Surface Compactness

An exchanger's surface compactness is dependent on its surface area density, the ratio of its transfer surface area to its volume. A compact heat exchanger (CHE) is characterized by its large area density, greater than 700 m^2/m^3, for gas-to-fluid exchangers, just above 300 m^2/m^3 for liquid or phase-change exchangers. Additionally, a gas-to-fluid CHE has a maximum hydraulic diameter of 6 mm, when operating in a gas stream. The term micro heat exchanger is applied if the surface area density is at least 15000 m^2/m^3 or in cases in which the hydraulic diameter ranges from 1 µm to 100 µm. (Reay, 2002; Shah and Sekulic, 2003)

Compared to its conventional counterparts, the CHE presents reduced volume and weight, as well as a simplified design process. Performance-wise, crucial advantages are the increased operating efficiency and lower fluid inventory, essential in cost-cutting and long-term sustainability. The main purpose for CHE employment is to gain a specified performance within low mass and volume constraints. Due to these features, the CHE has become increasingly important in many

industrial processes, not only with its contribution to increased energy efficiency but also in more demanding applications, with complex requirements, such as compact reactors based on printed circuit heat exchangers. (Reay, 2002; Shah and Sekulic, 2003; Li et al., 2011)

2.2.2.4. Construction Features

Perhaps the most frequently used classification system for heat exchangers, construction types can be organized in four major groups, as described in Figure 2: tubular, plate, extended surface and regenerative. Other types, such as scraped surface exchangers or tank heaters are available, but these are specialized for more unique purposes, therefore will not be taken into consideration. (Shah and Sekulic, 2003)

Tubular exchangers are built of circular (typically), elliptical, rectangular or twisted tubes, which allow significant design flexibility. Geometries can be easily varied by modifying tube diameters, lengths or arrangements. This type of exchanger is predominantly used in liquid-to-liquid and liquid-to-phase-change heat transfer applications, being designed for high pressure differences between fluids or relatively to the surrounding environment. These can be further classified into shell-and-tube, double-pipe and spiral tube exchangers. (Shah and Sekulic, 2003)

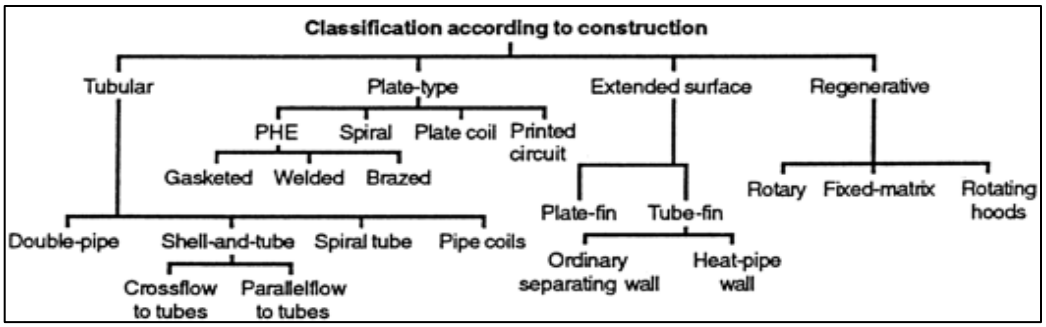

Figure 2 - Classification of heat exchangers, according to construction features (Shah and Sekulic, 2003)

The shell-and-tube configuration is basically a circuit of tubes tidily mounted in a cylindrical shell, with which the tube axis is parallel. One fluid flows inside the tube while the other flows across (cross-flow) or along (parallel-flow) the tube. Perhaps the simplest heat exchanger, the double-pipe configuration typically consists of two concentric pipes, with the inner pipe smooth or finned. Fluids flow, separately, inside the inner pipe and in the passage between pipes. Double-pipe exchangers are commonly used in small-capacity applications and are advantageous in flow distribution and disassembly for maintenance. Spiral-tubes are basically spiral coils fitted in a shell, with the purpose of gaining extended transfer surfaces. (Shah and Sekulic, 2003)

In the plate-type configuration, exchangers are constructed of packed thin plates, either smooth or corrugated (Shah and Sekulic, 2003). As can be partially attained by the observation of plate-type CHE attributes in Table 1, these are normally unable to accommodate high temperatures or pressures, rendering them most suitable for low temperature and pressure difference heat transfer applications (Reay, 2002). Depending on required parameters, such as leak tightness, plate type exchangers can be classified as plate heat exchangers (PHE), spiral, lamella, plate coil or printed circuit exchangers (Shah and Sekulic, 2003).

Within the PHE category, exchangers can be gasketed (plate-and-frame), welded (partially or totally), or brazed, the most common being the gasketed PHE. Main advantages of PHE are

compactness, size and pass arrangement flexibilities, installation simplicity and heat recovery capability (Sunden et al., 2005).

In the gasketed PHE, plates are holed for the passage of fluids, each containing a flanking gasket which seals the channels formed upon compression of the frame, when assembled. The fluids flow in alternate channels, promoting heat transfer between adjacent channels. Augmented heat transfer can be obtained through the employment of corrugated plates, as these increase the transfer area and stimulate turbulence within the channels. The accommodation of gaskets originates the restriction of a set fluid compatibility, prohibiting the application of corrosive fluids. Welded PHE overcome the confinements, limited operation pressures and temperatures and noncorrosive fluid requirements, of the gasketed counterparts but also complicate disassembly and decrease design flexibility. Due to welding cost contention, the plate size is typically larger than the gasketed PHE. These can be further categorized into platular-plate, Bavex-plate or Packinox-plate exchangers, also designated stacked PHE. Brazed-plate exchangers are compact PHE for high temperature and pressure duties, comprising of stacked plates confined to two termination plates, all brazed. (Pinto and Gut, 2004; Shah and Sekulic, 2003)

The spiral-plate exchanger essentially consists of two material strips, provided with welded studs for plate spacing, wrapped helically around a mandrel to form dual spiral channels in which the fluids flow in a long single passage. Due to this passage, these exchangers are more useful for viscous fluids and slurries than other exchanger types, in which such fluids normally contribute to fouling. If fouling does occur, localized fluid velocity in the channel increases, thus decreasing the fouling rate. Disadvantages of this configuration are the typical low operating pressures, limited size and the difficulty in conducting maintenance operations. (Shah and Sekulic, 2003)

In printed-circuit heat exchangers, plates are grooved using the same techniques as those employed in printed circuit board manufacturing. Stacks of chemically carved plates are bonded to create an exchanger block in which different fluid streams follow different groove patterns. For large heat transfer duties, several blocks can be welded together, guaranteeing design flexibility. Other advantages of this exchanger type are its high efficiencies and surface area densities, as can be observed in Table 1. (Shah and Sekulic, 2003)

Basic components of plate coil exchangers are called panel-coils and these are made to fit, in shape and size, the desired system in which heat transfer is to take place. They function as heat sinks or heat sources, when subjected to cooling requirements or heating requirements, respectively. Allied to the wide variety of shapes and sizes, the main advantage of the plate coil type is the relatively low cost. (Shah and Sekulic, 2003)

Extended surface heat exchangers serve the purpose of increasing the heat transfer area and the exchanger compactness, typically achieved through the addition of fins. These exist in a variety of geometries, the most common being plate-fin and tube-fin exchangers. The plate-fin type consists of corrugated fins, which form individual flow passages, sandwiched between parallel plates, which separate the fluid streams. Tube-fin exchangers can be separating wall (conventional) or heat-pipe wall (specialized) types. In the first type, conductive heat transfer occurs through a tube wall. The heat-pipe type differs in wall structure, in this instance built of closed tubes. Regenerators are storage-type heat exchangers, improving efficiency by returning energy to the system. (DOE, 1992; Shah and Sekulic, 2003)

2.2.3. Heat Transfer Enhancement

As mentioned earlier, heat transfer between fluids is one of the most required processes in engineering. The simultaneous effect of regulations concerning increased energy efficiency and lower environmental impact continues to effect heat exchanger technology (Meyer and Liebenberg, 2007). Therefore, as far as sustainable development is concerned, it is rational to contemplate measures of heat transfer enhancement, especially those employable at minimal exergetic cost and harm to the environment. Increases in heat transfer present a difficult challenge for engineers and demand for higher operational capacities is continuous (Paul et al., 2010). Industrial systems are increasingly pushing toward micro- and nano-scale equipment, such as micro-electromechanical (MEM) devices, leading to a greater demand for compactness and flexibility in heat exchanger design (Ohadi and Buckley, 2001). In addition, many applications now require higher peak operating temperatures, to minimize both fossil fuel consumption and greenhouse gas emissions, originating high temperature heat exchangers with temperatures in excess of 650 °C (Aquaro and Pieve, 2007; Ohadi and Buckley, 2001). Therefore, the main objectives in heat exchanger design have become size reduction, capacity upgrades on available heat exchangers and pumping power reduction (Liebenberg et al., 2002).

Increasing heat exchanger performance translates essentially to increasing the device's overall heat transfer coefficient (U), thermodynamically related to the heat transfer surface area (A), the heat transfer duty (q) and the temperature difference between hot and cold fluids (Incropera and DeWitt, 2001; Lunsford, 2006). This coefficient can also be determined as function of exchanger transport properties, depending on convective heat transfer (h) and thermal conductivity (k) coefficients, as well as fouling considerations (Lunsford, 2006).

In order to achieve desired heat transfer augmentation, various techniques can be used. These are separated in two major groups: active and passive enhancement methods. Active techniques require external activation or power supply, whereas passive techniques neglect such needs (Meyer and Liebenberg, 2007). It is also possible to combine both active and passive techniques on heat exchangers, in what is designated as compound enhancement, but involves complex design and has limited applicability (Dewan et al., 2004).

2.2.3.1. Active Techniques

Due to the necessity of external energy sources, active techniques are only used if passive techniques are subject to constraints in obtaining the desired enhancement for a given heat transfer system. Major disadvantages are the greater fixed cost, as well as noise, safety and reliability concerns (Webb, 1994). Another important obstacle is the higher energy consumption required, contradicting some of the premises of sustainable development (Meyer and Liebenberg, 2007). The most common active techniques are: fluid and surface vibration, mechanical aids, electrostatic fields, gas injection/vapour suction or jet impingement.

In order to increase thermal transfer quantities, mechanical assistance produces fluid stir or surface rotation via mechanical means, such as surface scrapers or rotating heat exchanger ducts (Bergles, 1983). Low or high frequency surface vibration can be employed in obtaining single-phase heat transfer enhancement and can be produced by devices like piezoelectric transducers (Heffington, 2001). Fluid vibration is more practical than the surface counterpart. Presenting a wider range of frequencies, about 1 Hz to ultrasound, this technique is mostly applied to single-phase fluids, but has been known to damage heat transfer devices and tubes (Cheng et al., 2009).

Strong electrostatic fields, produced by direct or alternating current, cause bulk mixing of dielectric fluids between a charged and a receiving electrode, in the vicinity of the heat transfer surface, thus increasing heat transfer. For two-phase heat transfer augmentation, as well as for single-phase requirements, electrohydrodynamics (EHD) is beneficial (Laohalertdecha et al., 2007). Injection or suction techniques essentially consist of gas injection, with the purpose of enlarging single-phase flows for heat transfer enhancement, and vapour removal, from single-phase fluids, respectively (Meyer and Liebenberg, 2007). Finally, jet impingement involves liquid spraying on the hot surface, spreading a thin film that is then evaporated (Xia, 2002). Spray cooling uses less fluid, while covering a larger area than the imposed liquid jet, this for the same expelling orifice size (Pavlova et al., 2008).

2.2.3.2. Passive Techniques

The majority of viable enhancement techniques are passive, the decisive factors being the non-requirement of external power input and the additional power needed to enhance the heat transfer being extracted from the available system power, ultimately leading to pressure drop (Dewan et al., 2004). The most conventional method of increasing heat transfer is to increase the transfer area, either increasing the exchanger size or increasing its compactness (Eastman, 2005). Techniques to achieve this goal include extended surfaces, inserts, coiled or twisted tubes and surface treatments (Lunsford, 2006).

Perhaps the oldest technique in heat transfer enhancement, finning consists of inserting fins in the vicinity of the desired heat transfer location within the exchanger. This is usually desirable for fluids with low convective heat transfer coefficients, where fins increase its value with added turbulence and also increase the heat transfer surface, contributing to an increase in thermal conductivity (Lunsford, 2006). Fin designs are evaluated by fin efficiency, which consequently lead to an optimized fin height and area. Wen and Ho (2009), conducting a comparative experimental study into fin geometry influence on heat transfer enhancement, found that a compounded type fin had a superior convective heat transfer coefficient, but higher pressure drop, than both plate fins and corrugated fins. Corrugated and fluted fin types have been found to be the most adequate for turbulent single-phase flow, due to a reasonable pressure drop increment (Pethkool et al., 2011). It has also been found that modulated surfaces significantly increase friction losses, thus augmenting exchanger heat transfer capabilities (Pantzali et al., 2009a).

For enhancement in situations with strict size constraints, a frequent technique is the use of inserts (inserts, turbulators or static mixers) in the flow channel, promoting turbulent heat transfer enhancement close to the transfer surface, thus reducing the thermal boundary layer thickness (Lunsford, 2006). Baffles can be employed in directing fluid flow efficiently through heat exchangers but have been associated to leakage and inefficient area filling (Van Der Ploeg and Masters, 1997). Twisted or coiled tubes and tapes include geometrical arrangements for forced flow and turbulence creation, thus increasing convective heat transfer coefficients (Lunsford, 2006).

Surface treatment techniques include coating, roughening or tension application (Sachdeva, 2010). Surface coating consists of droplet or wetted film deposition on the heat transfer surface through condensation, which increases the heat transfer coefficient of exchangers (Sachdeva, 2010). Roughened surfaces are obtained by machining, surface restructuring or adjacent roughness surface placing in the vicinity of the primary heat transfer surface (Sachdeva, 2010). Kandlikar et al. (2001) found that channel roughness increased transferred heat quantities, in tubes, as a function of decreasing tube diameter.

Another common enhancement technique is vortex generation, geometrical protuberances that produce high friction vortices to enhance convective heat transfer (Aris et al., 2011). The respective coefficient is increased via boundary layer development and flow destabilization intensification that result from the vortex formation (Fiebig, 1998). Vortex types can be classified in two categories: longitudinal, generating vortices with parallel axis relatively to the fluid flow, and transverse, vortices with transverse axis to the flow (Fiebig, 1998). The longitudinal vortices, longer lasting, are found to be more suitable for cases in which pressure drop is of upmost importance (Sachdeva, 2010).

2.3. Heat Transfer Fluids

The main limitation of the heat transfer enhancement technique's effectiveness is the poor thermal performance of the employed fluids, obstructing increases in performance and compactness of heat exchangers (Trisakri and Wongwises, 2007). In what regards heat transfer performance, the fundamental thermo-physical properties of fluids are convective heat transfer, thermal conductivity, viscosity, and specific heat capacity at constant pressure (Incropera and DeWitt, 2001).

2.3.1. Conventional Fluids

Of the conventional heat transfer fluids used in cooling processes, water is the most common, having a higher thermal performance than glycols or engine oil and being low-priced. When freeze conditions or the need to increase the fluid boiling point exist, the addition of ethylene or propylene glycol is frequent, providing freeze and burst protection. Both glycols have inferior thermal transfer properties than water and superior densities, resulting in higher flow-rates or heat transfer surface areas, leading to increased pressure drop, energetic requirements and equipment decay (Kurt and Kayfeci, 2009). Another disadvantage of glycol employment is the corrosion due to acid production when in contact with air, but can be minimized through the addition of corrosion inhibitors. Of the two, ethylene glycol has a better heat transfer performance but propylene glycol has lower toxicity, important for non-toxic heat transfer applications. Engine oils can accumulate various functions specific to individual parts of engines, including heat dissipation, friction reduction, detergency and area sealing (Abou-Ziyan, 2004). Oils also have inferior thermal transfer properties than water, being most suitable for heat transfer duties in which the fluid has increased boiling point requirements. The success rate of engine oils depends on the complex additives that are blended into these, being categorized as chemically active, with the capacity of interaction with metals at low oxidation and degradation costs, and chemically inert, which improve physical properties and effective performance (Abou-Ziyan, 2004; Korcek et al., 2001).

2.3.2. Thermophysical Properties

The most relevant thermophysical properties of conventional fluids, with a view to application in heat transfer, can be compared from the observation of the following tables (Table 1, 2 and 3).

Table 1 - Thermophysical Properties of Water (Engineering Toolbox)

Property	Units	Value
Thermal Conductivity @ 300 K	$W/m\,K$	0.613
Dynamic Viscosity @ 303 K	$N\,s/m^2$	$0.798\,x\,10^{-3}$
Kinematic Viscosity @ 303 K	m^2/s	$0.801\,x\,10^{-6}$
Density @ 303 K	Kg/m^3	995.7
Specific Heat Capacity @ 303 K	$KJ/Kg\,K$	4.179

Table 2 - Thermophysical Properties of Glycols (Engineering Toolbox)

Property	Units	Ethylene Glycol	Propylene Glycol
Thermal Conductivity @ 300 K	$W/m\,K$	0.258	0.147
Dynamic Viscosity @ 300 K	$N\,s/m^2$	$4.8\,x\,10^{-3}$	$0.798\,x\,10^{-3}$
Kinematic Viscosity @ 294 K	m^2/s	$17.8\,x\,10^{-6}$	$52\,x\,10^{-6}$
Density @ 298 K	Kg/m^3	1096.78	965.27
Specific Heat Capacity @ 295 K	$KJ/Kg\,K$	2.36	2.5

Table 3 - Thermophysical Properties of Engine Oil (Engineering Toolbox)

Property	Units	Value
Thermal Conductivity @ 300 K	$W/m\,K$	0.145
Dynamic Viscosity @ 293 K	$N\,s/m^2$	$319\,x\,10^{-3}$
Density @ 295 K	Kg/m^3	1114.62
Specific Heat Capacity @ 295 K	$KJ/Kg\,K$	2.3927

2.4. Nanofluids

For heat transfer enhancement, the alternative to the conventional approach of increasing device size or altering component geometry is improving fluid performance. As was observed in the preceding tables, conventional fluids have poor thermal properties that constitute a paramount limitation in heat transfer enhancement. Following a general trend for system miniaturization with improved heat transfer requirements, experimental studies into the addition of particles, with higher thermal performance, to these fluids have taken place. This has led to the development of nanofluids, nano-sized solid particles suspended in conventional fluids (base fluids) with the purpose of increasing heat transfer performance.

2.4.1. Incentive for Nanofluids

It is well known that solid materials tend to have much higher thermal conductivities than fluids, as can be observed in Table 4. With this in mind, it is rational to assume that the thermal conductivity of fluids can be achieved by solid addition. However, it has been found that solid

particles, of micrometric and millimetric magnitudes, added to fluids provoke an insignificant increase to the combined thermal conductivity (Choi, 1998). Other issues related to the large particles are sedimentation, severe clogging problems, kinetic energy increases in interactions with surfaces, pipeline erosion and high viscosity with consequent pressure drop increase (Choi, 1998; Eastman, 2005). Due to these limitations, heat transfer fluid enhancement via solid particle addition could not fully develop. However, modern material processing technologies provided the possibility of nano-scaled material production, which has originated the emergence of nanofluids, at a time in which heat transfer requirements are summiting. Due to the smaller size, nanoparticles exhibit higher mobility and less particle interaction, allowing for improved stability and heat transfer. Such factors are significant in reducing pumping power, fluid inventory and eliminating clogging issues, thus increasing global interest in nanofluid research.

Table 4 - Thermal Conductivities of Solid Materials (Han, 2008)

Material	**Thermal Conductivity** [W/m K]
Diamond	2300
Carbon Nanotubes	2000
Silver	429
Copper	401
Aluminium	237
Silicon	148
Silicon Carbide (SiC)	120
Alumina (Al_2O_3)	40

2.4.2. A Brief History of Nanofluids

Experimental investigation in fluid thermal conductivity enhancement dates back to as early as 1873, when James Maxwell theoretically proposed the integration of metallic particles to achieve increased thermal conductivities of fluids, benefiting from the superior heat transfer performances of metals (Choi, 1998). In subsequent studies, experimental investigation was conducted using metallic particles of micrometre and millimetre magnitudes to create the colloidal suspensions or slurries. However, the particles were too large and led to a variety of problems, such as particle agglomeration, sedimentation, large pressure drop and pipeline erosion with troublesome consequences like channel clogging and surface abrasion (Han, 2008). From a chemical point of view, it was found that these fluids had poor molecular composition, lacking re-dissolving capabilities and irreproducible catalytic activities, leading to untrustworthy results (Botha 2007). During the following decades, restraints in downscaling methods and auxiliary technologies undermined the preparation and testing of smaller magnitude particles, preventing further experimental investigation.

With the advent of nanotechnology, production of atomic scale materials became possible, the first being roughly spherical, and progress in heat transfer testing of colloidal suspensions was achieved. In 1993, Masuda et al. published an article investigating the thermal conductivity and viscosity of suspensions of Al_2O_3, SiO_2 and TiO_2 in water. In the same year, Grimm dispersed aluminium particles measuring 80 nm to 1 µm, with loadings ranging from 0.5 to 10 vol. %, claiming

a 100 % increase in thermal conductivity before the problematic rapid settling of the particles. The coining of the term nanofluid is attributed to S.U.S. Choi and J.A. Eastman following work at Argonne National Laboratory, having made nanofluids with oxide nanoparticles and carbon nanotubes (Choi, 1998; Williams, 2006).

2.4.3. Nanofluid Tailoring

As previously referred, nanofluid preparation is a complex process due to a number of factors with a high degree of difficulty in maintaining under control. Masuda et al. (1993) found that particle instabilities resulted in agglomerations, while Grim (1993) had to conduct experiments in an accelerated fashion due to imminent particle settling. Nowadays, nanofluid development is based on two methods: the one-step method and the two-step method, the latter being the method employed in earlier investigations. The most important elements when considering a mass production approach are the nanoparticle materials and the host liquids. It is vital that nanoparticles have high dispersability and stability in base fluids, as well as chemical compatibility with the host fluid. In most experiments documented in literature, nanoparticles made of oxide ceramics (such as Al_2O_3 and CuO), nitride ceramics (AlN and SiN), carbide ceramics (SiC and TiC), metals (Cu, Ag, Fe and Au), semiconductors (TiO_2 and SiC), carbon nanotubes (CNT) and composites were applied. The most common base fluids are water, oil and ethylene glycol. (Botha 2007; Choi 1998; Keblinski et al. 2005; Mohammed et al. 2010)

2.4.3.1. Nanoparticle Preparation

A nanoparticle is a quasi-zero dimensioned object in which all characteristic linear dimensions are of the nano-size order of magnitude (Gubin et al. 2005). Much progress has been made in the mass-production of nano-phase powders, with average particle sizes having already breached the 10 nm mark, i.e., single figures (Choi 1998). The production of nanoscale materials can be attained via several means, including fluidic-structured assembly (particle confinement), rigid template synthesis, liquid-phase and gas-phase processing. Each of these methods follows one of three key processing approaches: preparation from macroscopic materials by dispersion; chemical synthesis with change in substance composition and growth up to the nano-size stage or transformations of nanoparticles with composition change. (Gubin et al. 2005)

Essential features in nanoparticle production are particle shapes, sizes and magnetic properties. Preparations of nanoparticles in the gas or solid phase using high-energy treatment of the material are denominated physical methods; while solution syntheses at moderate temperatures are known as chemical methods (Gubin et al., 2005). Physical methods include condensation procedures, involving vaporisation or evaporation of source materials with posterior condensation into particles, or nano-dispersion of compact materials (Choi 1998; Gubin et al., 2005). Chemical methods, such as compound thermolysis, compound dispersion, compound reduction, reverse micelle synthesis, chemical vapour deposition, micro-emulsions, thermal spraying or synthesis at phase-change interfaces, are more widely used (Gubin et al., 2005; Yu et al., 2008; Wen and Ho, 2009). The high energy consumption and expensive equipment costs of the physical methods render them less attractive in a perspective of cost contention.

CNTs are tubular carbon-based allotropes, obtained from graphitic carbon, that can be categorized as single-wall carbon nanotubes (SWCNTs), structured with a single graphene cylinder, and double- (DWCNTs) or multi-walled carbon nanotubes (MWCNTs), consisting of two or several nested cylinders, respectively (Botha, 2007; Keidar and Waas, 2004; Popov, 2004). These

can be catalytically produced by decomposition of carbon containing compounds (precursors), such as C_2H_2, CH_4, C_2H_4 or C_2H_6, over metal particles (catalysts), with growth occurring at the base or the tip of the tube, in a needle-like structure (José-Yacamán et al., 1993). The process is often designated as catalytic chemical vapour deposition (CCVD), in which tube length depends on the chemical reaction time; while tube diameter is influenced by the diameter of the particle from which growth occurs (José-Yacamán et al., 1993). CNTs manufactured by CCVD typically exhibit high thicknesses, often consisting of large particle aggregates (Esumi et al., 1996). Other CNT production techniques have been extensively researched; including arc-discharge, laser ablation, pyrolysis and enhanced plasma vapour deposition (Antisari et al., 2003; Cho et al., 2002; Duncan et al., 2007; Esumi et al., 1996; Hernadi et al., 1996; Hilding et al., 2003; José-Yacamán et al., 1993; Keidar and Waas, 2004; Kingston et al., 2004; Merchan-Merchan et al., 2010; Nasiri et al., 2011; Popov, 2004; Schnitzler and Zarbin, 2008; Tsitzios et al., 2006). The arc-discharge technique comprises the vaporization of one of two carbon rods, anode and cathode placed end-to-end, with an electric current passing through the pair and consuming the anode, the resulting soot containing the nanotubes (Duncan et al., 2007). Due to high temperature processing, the technique produces highly graphitized tubes in smaller quantities than chemical techniques, rendering the process an expensive one, but useful in producing small diameter MWCNTs (Duncan et al., 2007; Esumi et al., 1996). Arc discharge and laser ablation are the most common techniques used in SWCNT synthesis (Shi et al., 2000).

2.4.3.2. Nanofluid Tailoring: Two-Step Method

Basically, the first step of the process relates to the nanoparticle powder production, the second to the dispersion in the base fluid. This method is advantageous for mass production considerations, benefiting from the high production quantity of the inert gas condensation technique (Romano et al., 1997). In addition, nanoparticles are produced under clean conditions, minimizing surface coatings and contaminants (Lee et al., 1999). An important handicap of this production method is the cluster-forming during the second step, acting to prevent the adequate nanoparticle dispersion within the base fluids (Yu et al., 2008). It is also believed that this method is only suitable for nanofluids containing oxide nanoparticles in deionized water (DIW), not the case of nanofluids containing heavier metallic nanoparticles (Eastman et al., 2001).

As for the process of obtaining the nanofluid, the first step involves nanoparticle preparation by chemical reaction, vapour condensation, organic decomposition or mechanical actuation (Agostiano et al., 2000; Guo et al., 2000; Jiang et al., 1999; Talapin et al., 2002; Wegner et al., 2002). Inert gas condensation (IGC) is a common technique, able to produce a wide variety of nano-powders, having already been commercialized (Eastman, 2005). The fact that these can be obtained commercially in large quantities offers an economic advantage over other methods (Botha, 2007). As previously mentioned, the major drawbacks of the two-step method occur during the second step, i.e., when the produced nanoparticles from the first step are dispersed in the base fluids assisted by mechanical agitation (stirring) or ultrasound (Hwang et al., 2008). The main problem is the poor resulting dispersion, with high instability, which can lead to the agglomeration of the nanoparticles (Eastman, 2005). In order to minimize the effects of poor dispersion, steric barriers (surfactants) are typically employed (Gubin et al., 2005). Once absorbed on the surfaces of the nanoparticles, surfactant molecules create a barrier for agglomeration prevention and particle solubility, thus guaranteeing long term stability (Han, 2008).

CNT based nanofluids are typically tailored via the two-step method, the first step involving the assembly of carbon atoms obtained by graphite sublimation or by the decomposition of

precursor molecules (Antisari et al., 2003). This step of the process is fundamental, as the CNT property dependence on the tube structure demonstrates (Edgar and Spencer, 2006; Xie and Chen, 2009). Nasiri et al. (2011) compared the thermal conductivity behaviour of different CNT nanofluids prepared using different techniques, concluding that the nanotube processing technique is clearly influential in nanofluid performances. Physical and chemical entanglement of the tubes also constitutes a major problem for the first step, if not properly dealt with both types can interfere with particle stability and heat transfer capabilities (Hilding et al., 2003; Lamas et al., 2012). Greatly entangled materials are difficult to disperse in liquids, resulting in aggregation and poor mechanical and transport properties (Hilding et al., 2003). Size control and impurities are also typical and problematic occurrences, impurities require removal before the second step of the process, i.e., suspension of the CNTs in the base fluid, can be conducted (Hilding et al., 2003). The powdered nanotubes are then suspended in the base fluid, with or without surfactant (Popov, 2004).

2.4.3.3. Nanofluid Tailoring: One-Step Method

In this method nanoparticle production and dispersion in the base fluid occurs in a single step. Being a more recent method than the two-step counterpart, there a fewer one-step techniques, the most common being direct evaporation (a modified IGC technique), chemical vapour condensation and chemical precipitation (Choi and Eastman 2001; Eastman et al., 2005).

Comparatively to the two-step IGC technique, nanofluids obtained by direct evaporation present less agglomeration issues, result of the solidification, from gas-phase, inside the base fluid (Eastman, 2005; Eastman et al., 2001). Amongst the technique limitations, the most significant is the small sample size, which limits the process mass production for commercialization (Eastman, 2005; Yu et al., 2008). Another limitation is the low vapour pressure restriction to liquids, which can vaporize at low to moderate temperatures (Eastman, 2005). Particle size control is also an issue when employing this technique (Eastman, 2005; Eastman et al., 2001).

Size control need not be a problem as it is possible with the chemical vapour condensation technique. Nanoparticle powder is directly deposited into the base fluids, which results in higher clustering than direct evaporation. Chemical synthesis techniques, such as precipitation, can produce small, mono-disperse nanoparticles with reduced agglomeration. However, the effect of surface molecules on the nanofluid thermal properties remains unknown, few studies have employed nanofluids obtained using such techniques. CNTs have also been obtained via one-step techniques, such as carbon plasma discharge directly in water. (Eastman, 2005; Hsin et al., 2001)

2.4.3.4. Modes of Particle Stabilization

Particle agglomeration can be prevented by balancing attractive forces between the nanoparticles within the fluid, obtainable through the employment of two common mechanisms: electrostatic (also known as mechanical or physical) stabilization or steric (chemical) stabilization (Botha, 2007; Nasiri et al., 2011). Mechanic stabilization generally includes ultrasonication, i.e., different pressure wave generation which provokes cavitation and consequent particle deagglomeration. It consists of the placement of an electric charge on particle surfaces with the purpose of guaranteeing kinetic stability. The absorption of ions to the electrophilic metal surface during the process creates an electrical multi-layer, resulting in repulsive electric forces between nano-clusters (Juillerat et al., 2005; Warad et al., 2005). Electrostatic stabilization is pH sensitive and of limited use, steric stabilization being most frequently applied (Botha, 2007). This chemical methodology consists of bulky material, such as polymer or surfactant, layer addition to the particles, which provides a steric barrier enabling cluster prevention (Aiken III and Finke, 1999;

Egorova and Revina, 2002; Rensmo et al., 2002). An alternative mechanism of stabilization, involving the addition of charged nanoparticles to microspheres, has recently been reported. The stabilization is obtained through the addition of small charged nanoparticle concentrations which repel Van der Waals attraction forces (Karanikas and Louis, 2004).

CNT nanofluids have been found to have greater instability than spherical particle nanofluids, a consequence of the tendency to assemble into bundles or ropes which results from the stronger Van der Waal attractive forces between carbon surfaces, intensified by the higher nanotube specific areas (Nasiri et al., 2011; Vaisman et al., 2006). Nanotube morphology and attractive forces between tubes are highly influential in successful dispersions (Hilding et al., 2003). CNTs are usually suspended with the assistance of steric stabilization, be it via surfactant employment or by functionalization techniques, which generally involves nanotube treatment with acids at high temperatures (Keblinski et al., 2005; Nasiri et al., 2011). Functionalization also aids in effectively preventing nanotube aggregation (Sahoo et al., 2010). As with the spherical nanoparticles, electrostatic (or physical) stabilization is typically avoided, as it has also been found to cause destruction to CNTs (Lamas et al., 2012). According to Hilding et al. (2003) the most important challenges in CNT nanofluid production are the chemical and morphological purification of the nanotubes, the uniform and reproducible dispersion and the orientation of the nanotubes in liquid and melt phases. The use of the mentioned surfactants is advantageous in interface absorption and accumulation in supra-molecular structures, thus aiding a uniform dispersion (Vaisman et al., 2006). Nasiri et al. (2011) experimentally concluded that functionalized suspensions present better stability, dispersion and thermal conductivity than suspensions obtained through ultrasonication, translating a smaller tendency for agglomeration and precipitation. The same authors also found that the thermal conductivity of all suspensions decrease with time, the reduction rate varying with the preparation method. However, an experimental study using plasma coating on MWCNT nanoparticles to improve stability was successfully conducted by Kim et al. (2010). A desired nanotube orientation can be obtained through shear flows, elongational flows or by electric and magnetic field application (Hilding et al., 2003).

2.4.4. Conductive Heat Transfer

Being below the critical length scale, the physical properties of nanoparticles differ from conventional bulk solids, serving as motivation for a large number of studies on nanofluid behaviour. Most of these studies echo higher heat transfer performances than that of the base fluids alone, though some contradictory results have been reported (Khanafer and Vafai, 2011). Experiments have shown that the thermal conductivity (k) of nanofluids depends on a large number of parameters, but an accurate, consensual prediction of its variation with these parameters is yet to be established (Paul et al., 2010).

2.4.4.1. Experimental Investigation

2.4.4.1.1. Measurement Methods

Measurement of k for liquids can be a difficult task, this due to the necessity of establishing a steady one-dimensional temperature field. The measurements should be taken in a reduced timeframe, so that convection currents cannot develop, while liquid heating should take place from above to facilitate heat conduction in a layer wise manner. The most common measurement methods are the transient hot-wire method (THW), cylindrical cell method, temperature oscillation

method and 3-omega method (3ω). Figure 3 classifies these techniques according to the liquid flow state. (Cahill, 1990; Eastman, 2005; Kurt and Kayfeci, 2009; Paul et al., 2010; Peña et al., 2008; Yoo et al., 2007)

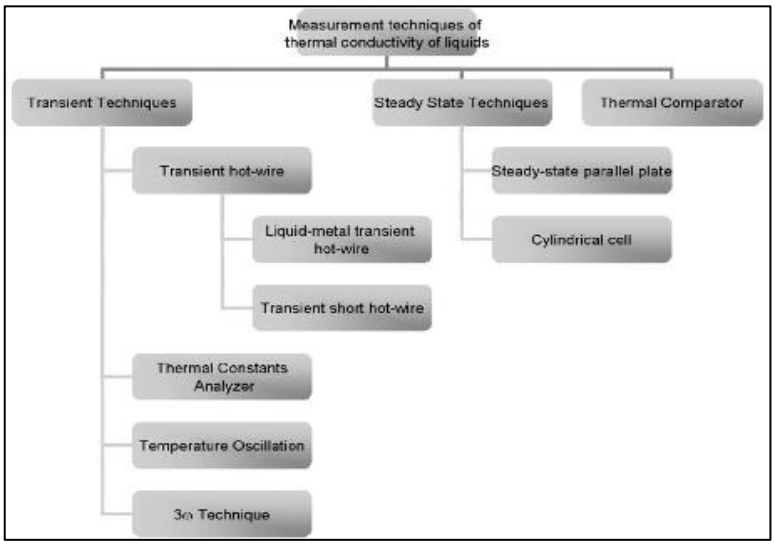

Figure 3- Nanofluid thermal conductivity measurement techniques (Paul et al., 2010)

The THW technique is the most exploited method, consisting of the measurement of temperature and time response of a platinum wire, acting as a probe, subjected to an abrupt electrical pulse (Paul et al., 2010; Peña et al., 2008). The wire, heated resistively, usually employing a Wheatstone bridge resistor setup, is suspended in the nanofluid with the purpose of increasing its temperature (Eastman, 2005; Paul et al., 2010). The temperature increase of the fluid, measured by the wire, depends on its k, which is calculated from the temperature-time profile of the wire (Eastman, 2005; Hong et al., 2006; Murshed et al., 2005; Peña et al., 2008; Zhang et al., 2007). This method has several advantages, the most significant being the capacity to eliminate experimental errors associated to natural convection, as well as the relatively accelerated measurement process (Paul et al., 2010). The main drawback is the need for a chemical wire coating for measurements in electrically conducting fluids (Eastman et al., 2005; Peña et al., 2008).

Another popular technique is 3ω, also a transient state technique that is similar to the THW technique, using a radial heat flow from an element serving as both nanofluid heater and thermometer (Oh et al., 2008; Paul et al., 2010). This technique uses temperature oscillation rather than time dependent response, in which a sinusoidal current at frequency ω passes through a metal wire and generates a heat wave at frequency 2ω, deduced by a voltage component at 3ω (Paul et al., 2010). The thermal conductivity of the fluid is then determined by the slope of the 2ω wire temperature rise (Ding et al., 2007).

Of the steady state techniques, perhaps the most common is the cylindrical cell, in which the space between two concentric cylinders is filled with the nanofluid and acted upon by an electrical heater. k is then obtained via Fourier's equation after temperature measurement using thermocouples. (Paul et al., 2010)

In recent years, non-invasive optical measurement techniques, such as optical beam deflection, forced Rayleigh scattering, hotwire-laser beam displacement or thermal lensing, have been proposed with a view to improve accuracy and reproducibility, as well as decreasing measurement times (Ali et al., 2010; Putnam et al., 2006; Rusconi et al., 2006; Schmidt et al.,

2008; Venerus et al., 2006). Due to the fact that the aforementioned invasive measurement techniques promote an unavoidable interference, these techniques are expected to produce more accurate results because detectors and heaters are separate (Kleinstreuer and Feng, 2011; Rusconi et al., 2006). Reduced measurement times are also important, longer times allow for the effect of natural convection, which contributes to over-predictions of the measured thermal conductivity (Hosseini et al., 2011; Kleinstreuer and Feng, 2011).

2.4.4.1.2. Experimental Studies

Over the last decade, a large number of experimental studies investigating the effective thermal conductivity (k_{eff}) of nanofluids have been conducted. Most have shown increases in thermal conductivity of nanofluids, even at diminutive particle volume fractions, when compared to base fluids, in most cases exceeding the predictions of theoretical models developed for suspensions of larger particles. The studies have also revealed that k depends on several parameters and that these dependencies cannot be discarded when investigating heat transfer mechanisms of nanofluids (Ding et al., 2007; Murshed et al., 2008; Wen and Ho, 2009; Xie et al., 2011).

2.4.4.1.2.1. Spherical Particle Nanofluids

Due to being inexpensive, alumina (Al_2O_3) and copper oxide (CuO) nanoparticles have been targeted for most experimental studies. Eastman et al. (1997) measured the thermal conductivity of Al_2O_3, CuO and Cu nanoparticles suspended in water and HE-200 oil. A 60 % increase in k of the CuO/water nanofluid was obtained, comparatively to that of the water alone, this for a 5 % volume fraction of nanoparticles. It was also concluded that Cu nanoparticles obtained via a one-step method resulted in larger improvements than that of CuO nanoparticles produced with a two-step method, as can be observed in Table 5. Later, Lee et al. (1999) conducted a similar experiment using different combinations of nanofluid, based on Al_2O_3 and CuO nanoparticles dispersed in water and ethylene glycol base fluids, having obtained a 20 % enhancement in k for the CuO/EG nanofluid at 4 vol. %. The results revealed that k of nanofluids were dependent on the conductivities of the nanoparticles and the base fluids. Other experiments using nanofluids with Al_2O_3 and CuO nanoparticles led to similar results (Eastman et al., 2001; Lee et al., 2008; Li and Peterson, 2006; Liu et al., 2006; Murshed et al., 2006; Oh et al., 2008; Wang et al., 1999; Xie et al., 2002; Xuan and Li, 1999). Gowda et al. (2010) reported that higher acidities improve dispersion capabilities and that the viscosity of base fluids reduces Brownian velocity of nanoparticles, thus minimizing sedimentation, both contributing to improved k. Williams (2006) found that k of Al_2O_3-water nanofluids increased with particle loading in a linear fashion up until the 4 vol. % mark, manifesting a decrease in dependence for higher loadings. A summary of these and other experimental studies is established with Table 5.

Table 5 – Summary of Experimental Studies of k in Spherical Particle Nanofluids

Authors (Year)	Measurement Technique	Nanoparticle Material	Base Fluid	Enhancement in k (Vol. Fraction)
Eastman et al. (1997)	THW	Al_2O_3	Water	29% (5 $vol.\%$)
		CuO	Water	60% (5 $vol.\%$
		Cu	Oil	44% (0.05 $vol.\%$)
Lee et al. (1999)	THW	Al_2O_3	EG	18% (5 $vol.\%$)
		CuO	EG	22% (4 $vol.\%$)
Wang et al. (1999)	Steady state	Al_2O_3	Water	12% (3 $vol.\%$)
		Al_2O_3	EG	26% (5 $vol.\%$)
Xuan and Li (1999)	THW	Cu	Water	54% (5 $vol.\%$)
Eastman et al. (2001)	THW	Cu	EG	40% (0.3 $vol.\%$)
		CuO	EG	22% (4 $vol.\%$)
Xie et al. (2002)	THW	Al_2O_3	EG	30% (5 $vol.\%$)
Hong et al. (2005)	THW	Fe	EG	11.5% (0.55 $vol.\%$)
Li and Peterson (2006)	Steady state	CuO	Water	52% (6 $vol.\%$)
		Al_2O_3	Water	30% (10 $vol.\%$)
Murshed et al. (2006)	THW	Al_2O_3	Water	24 % (5 $vol.\%$)
Liu et al. (2006)	THW	CuO	EG	23% (5 $vol.\%$)
Lee et al. (2008)	THW	Al_2O_3	Water	1.44% (0.3 $vol.\%$)
Oh et al. (2008)	*3ω*	Al_2O_3	DIW	20% (4 $vol.\%$)

4.4.1.2.2. CNT Nanofluids

Measurements of k in CNTs have also been reported, the first conducted by Choi et al. (2001). The main difference was the larger increase of k for all tested nanoparticles, as high as 300 % for 3 vol. % in epoxy, revealing a non-linearity with nanotube loadings (Choi et al., 2001; Choi et al., 2003). The authors speculated on the possibility that CNT bundling could be highly influential for thermal transport properties. Wen and Ding (2004) demonstrated that k_{eff} of CNT-water nanofluids increased with increasing temperatures. Kim et al. (2010) reported a 25 % enhancement using plasma nano-coated (≈ 2 nm thickness) MWCNT at 0.01 vol. %. Pantzali et al. (2008) found that CNT concentration and stabilizing surfactant volume affects k in MWCNT nanofluids. Nasiri et al. (2011) conducted a thorough investigation into enhancements in k of various types of CNT nanofluids tailored using three different dispersion methods: functionalization, probe ultrasonication and bath ultrasonication. The comparison of observed results demonstrated the dependence of k on the tailoring process employed, with the functionalized CNT nanofluids exhibiting the highest enhancement. Additionally, the authors found that k of all samples decreased with time. As with the case of spherical particle nanofluids, a summary of experimental studies for CNT nanofluids is available in Table 6.

Essentially, experimental investigation has shown that nanofluids have enhanced k, which may depend on volume fractions, particle materials, particle sizes, particle shapes, base fluid

properties, temperature, fluid flow and acidity. The degree of influence of these on k remains unknown. Unexpected discrepancies in experimental data have also been reported, Ju et al. (2008) demonstrated that the THW measurement method returned erroneous results when performed immediately after sonication, employed for improved dispersion.

Table 6 - Summary of Experimental Studies of k *in CNT Nanofluids*

Authors (Year)	Measurement Technique	Nanoparticle Material	Base Fluid	Enhancement in k (Particle Fraction)
Choi et al. (2001)	THW	MWCNT	Oil	160% $(1\ vol.\%)$
Choi et al. (2003)	THW	SWCNT	Epoxy	300% $(3\ vol.\%)$
Xie et al. (2003)	THW	MWCNT	Water	6% $(1\ vol.\%)$
Wen and Ding (2004)	THW	CNT	Water	23.7% $(0.8\ vol.\%, 293K)$ 31% $(0.8\ vol.\%, 315K)$
Liu et al. (2005)	THW	MWCNT	EG	12.4% $(1\ vol.\%)$
Hong et al. (2007)	Thermal Constants Analysis	CNT + Fe_2O_3	Water	50% $(0.03\ wt.\%)$
Pantzali et al. (2008)	THW	MWCNT	Water	20% $(1vol.\%, 300K)$
Jiang et al. (2009)	Transient Plane Source	CNT	R113	$104\ \%$ $(1\ vol.\%)$
Kim et al. (2010)	THW	Plasma ct. MWCNT	Water	25% $(0.01\ vol.\%)$
Nasiri et al. (2011)	THW	SWCNT DWCNT MWCNT	Water	Highest for SWCNT

2.4.4.2. Theoretical Studies

At present there are no globally precise analytic formulas able to predict k of nanofluids, most resulting in inferior values when compared to experimental results (Trisaksri et al., 2007; Xue and Xu, 2005).

2.4.4.2.1. Classic Models

Earlier theoretical models are derived from the Maxwell model (1881), a semi-empiric correlation used to describe the effective thermal conductivity (k_{eff}) of larger scale spherical solid suspensions in liquids, with emphasis on k of the solid particles (k_P) and base liquids (k_f) used, as well as the volume fraction (ϕ) of solid particles (Han, 2008; Mujumdar and Wang, 2008; Trisakri and Wongwises, 2007). However, despite working best for low concentrations of solid particles, the Maxwell model was rapidly found to under-predict k_{eff} of smaller nano-scaled suspensions, also failing for non-spherical particle suspensions (Mujumdar and Wang, 2008; Trisakri and Wongwises, 2007).

$$k_{eff} = \frac{k_P + 2k_b + 2(k_P - k_b)\phi}{k_P + 2k_b - (k_P - k_b)\phi} k_b \quad \text{(Eq. 1)}$$

In 1935, Bruggeman proposed a similar model that didn't present the low volume fraction constraint of its predecessor, satisfactorily agreeing with early experimental data (Choi, 1998; Mujumdar and Wang, 2008).

Later, the Hamilton and Crosser model (1962) introduced an empirical particle shape factor (n), dependent on sphericity, to account for its effect, obtaining the same result as the Maxwell model when particles are spherical (Mujumdar and Wang, 2008; Trisakri and Wongwises, 2007).

$$k_{eff} = \frac{k_P + (n-1)k_b - (n-1)(k_P - k_b)\phi}{k_P + (n-1)k_b - (k_P - k_b)\phi} k_b \quad \text{(Eq. 2)}$$

The aforementioned, commonly classified as classic, models were conceptualized for larger order particle diameters than those of nanoparticles and assumed diffusive heat transport in both solid and liquid, making for questionable accuracy. In addition, these do not take into account several possible k enhancement mechanisms, such as particle Brownian motion, liquid layering at the liquid-particle interface, the nature of heat transport of the nanoparticles and the effects of particle clustering (Keblinski et al., 2002). Such considerations were subsequently employed in several theoretical models, exclusively formulated for nanofluids.

2.4.4.2.2. Spherical Particle Nanofluids

2.4.4.2.2.1. Liquid Layer (Nano-layer) Based Models

When in proximity to solid surfaces, liquid molecules tend to layer structurally, creating intermediate (solid-liquid) state layers, referred to by some authors as solid-like nano-layers, which act as a thermal bridge between solid nanoparticle and base liquid, thus elevating layer conductivity (Trisakri and Wongwises, 2007). In solid-solid interfaces, the interface resistance, or Kapitza resistance, is a barrier to heat transfer, thus reducing the overall k_{eff}. In contrast, the contact resistance in solid-liquid interfaces of particle suspensions in liquid is far less influential, about two orders of magnitude lower, leading authors to expect the aforementioned enhancements of k (Huxtable et al., 2003; Yu and Choi, 2003).

Taking this theory into account, Yu and Choi (2003) proposed a modified Maxwell model with a modified particle thermal conductivity (k_{Pe}), assuming a shell type nano-layer, in which the k of the nano-layer to the particle conductivity ratio (γ) and nano-layer thickness to nanoparticle thickness ratio (β) are introduced. The predictions for k were found to be more in agreement for spherical nanoparticles with diameters inferior to 10 nm (Khanafer and Vafai, 2011; Trisakri and Wongwises, 2007; Yu and Choi, 2003).

$$\gamma = \frac{k_{layer}}{k_P};\ \beta = \frac{e_{layer}}{e_P};\ k_{Pe} = \frac{[2(1-\gamma) + (1+\beta)^3(1+2\gamma)\gamma]}{-(1-\gamma) + (1+\beta)^3(1+2\gamma)} k_P;$$

$$k_{eff} = \frac{k_{Pe} + 2k_b + 2(k_{Pe} - k_b)(1-\beta)^3\phi}{k_{Pe} + 2k_b - (k_{Pe} - k_b)(1-\beta)^3\phi} k_b \quad \text{(Eq. 3)}$$

A year later, the same authors projected a modified Hamilton and Crosser model to also include the effect of the nano-layer (Mujumdar and Wang, 2008). Xue (2003) developed a model based on the effects of the nano-layer and also on the average polarization theory, later revealed

inaccurate due to incorrect values of parameters such as the depolarization factor (Kim et al., 2004).

Xie et al. (2005) also studied the nano-layer effect on k, based on Fourier's heat conduction law, using a similar nano-layer behavioural approach to that of Yu and Choi (2003), the main difference residing in the assumption that k of the nano-layer varied linearly in the radial direction, rather than being constant. In their model, k_{eff} depends on the nano-layer thickness, nanoparticle size, volume fraction and k of fluid, nanoparticle and nano-layer. It was found that obtained theoretical results were in agreement with only some of the experimental data, leading the authors to conclude that nano-layer formation is not the only mechanism responsible for the enhanced k observed (Xie et al., 2005).

The model developed by Xue and Xu (2005) assumed a specific k for the liquid layer, defining a "complex particle" conductivity as the combined k of nanoparticle and nano-layer. k_{eff} of the nanofluid was then determined via the application of Bruggeman's effective media theory (1935). The model was found to be in good agreement with experimental data of CuO nanofluids (Lee et al., 1999).

Leong et al. (2006) proposed a static nano-layer based model for spherical particles, which takes volume fraction, particle size, k of the layers and layer thickness into account. When compared to experimental data, the model produces the most precise results for CuO nanofluids (Leong et al., 2006). In 2009, Sitprasert et al. (2009) created a modified version of the Leong et al. model (2006) taking the effect of the temperature on k and thickness of the nano-layer into account. The authors concluded that the model was accurate in predicting changes in k of nanofluids due to changes in volume fraction and temperature for different nanoparticle sizes.

2.4.4.2.2.2. Brownian Motion Based Models

Brownian motion consists of particle movement through liquid, allowing collisions which enable direct heat transfer between particles in contact with each other (Botha, 2007; Keblinski et al., 2002; Mujumdar and Wang, 2008; Murshed and Castro, 2011). Due to particle tininess, Brownian motion has been considered as a possible mechanism for the anomalous k of nanofluids (Evans et al., 2006; Keblinski et al., 2002). Some authors argued that Brownian particles generate long velocity fields in the surrounding fluids which, in large volumes of fluid, can transport substantial amounts of heat (Jang and Choi, 2004; Prasher et al., 2005). However, most authors have found that the Brownian motion effect on heat transfer enhancement is minimal. Botha (2007) proposed that the movement of nanoparticles due to Brownian motion is too slow to transport significant heat quantities. Evans et al. (2006) conducted a kinetic theory analysis, supported by molecular dynamics simulations of heat flow, demonstrating that hydrodynamic effects associated with Brownian motion have a minor effect on k of nanofluids.

Based on the Maxwell model, Xuan et al. (2003) proposed a theoretical model centred on the theory of Brownian motion and the diffusive aggregation, which also accounts for particle size, concentration and temperature effects on k_{eff}. They found that the effect of particle aggregation and nanofluid temperature were the essential factors behind enhancements of k.

The following year, Jang and Choi (2004) modelled k considering four modes of energy transport: heat conduction in the base fluid, heat conduction of the nanoparticles, collisions between nanoparticles due to Brownian motion and micro-convection caused by the random motion of nanoparticles. They concluded that the collisions between nanoparticles were found to be

negligible when compared to the alternative modes of energy transport, altering the initial model equation to only include the three remaining modes.

Koo and Kleinstreuer (2004) proposed that k of nanofluids is composed of the effects of two parts: static k (using the Maxwell model) and dynamic (associated to Brownian motion) k. They created a parameter, β, to account for interactions between nanoparticles and the fluid molecules around them, as well as a parameter, f, to increase the temperature dependency of the model, rendering the model a highly complex one.

Similarly, Xu et al. (2006) modelled k to be the sum of the contributions of the static and dynamic conductivities. In this case, the static term is obtained using the Hamilton and Crosser model, whereas the dynamic term considered the flow over the nanoparticles and the fractal distribution of the nanoparticle sizes. Due to the fact that the effect of Brownian motion decreases with higher particle sizes, the global enhancement in k predicted by the model was found to decrease with the increase in particle size.

Chon et al. (2005) projected an empirical correlation for k of Al_2O_3 based nanofluids as a function of particle size and temperature. When compared to experimental results they found that k increases with increasing temperatures and decreasing particle sizes. They concluded that both the Reynolds number and Brownian motion were responsible for anomalous enhancements in k, the temperature increasing Brownian velocity of the nanoparticles.

2.4.4.2.2.3. Clustering Based Models

When suspended in base fluids, nanoparticles tend to form clusters that can result in speedy heat transport along extended distances, which can significantly enhance k of nanofluids (Evans et al., 2008; Hong et al., 2006; Wang et al., 2003; Xuan et al., 2003). Kwak and Kim (2005) established that enhancements in k occur with viscosity increases for low nanoparticle volume fractions, indicating the effect of aggregation. Hong et al. (2006) confirmed this effect by scattering Fe nanoparticles and observing a consequent cluster formation, leading to significant k increases. To further emphasize the effect of clustering, Venerus et al. (2006) and Putnam et al. (2006) failed to find any unexpected heat transfer improvements for well dispersed, non-aggregated nanofluids, indicating that clustering could play an important role in the anomalous performances of other studies. Evans et al. (2008) used the homogenization theory, validated using a Monte Carlo simulation, to demonstrate that an increase in cluster size is accompanied by an increase in k_{eff}. However, they also found that by increasing particle volume fractions, the resulting clusters revealed smaller gains in k. The aforementioned Xuan et al. (2003) theoretical model, associating Brownian motion and particle aggregation, led the authors to conclude that larger clusters decelerate nanoparticle movement thus decreasing the enhancement of k.

Feng et al. (2007) proposed a model based on nanoparticle clustering and nano-layer formation, being a function of the nanoparticle volume fraction and size, nano-layer thickness and k of both particle and base fluid. They found that the enhancement of k depended on the nanoparticle size, enhancements increasing with particle size decrease due to the shorter distances between particles.

Chen et al. (2009) incorporated the effect of clustering to the Hamilton and Crosser model, obtaining a model dependent on the cluster radius. They experimentally measured the viscosity of both spherical and tubular TiO_2 nanoparticles in water and in ethylene glycol, having found that the

experimental data for conductivity augmentation was in good agreement with their theoretical model.

2.4.4.2.3. Tubular Particle Nanofluids

When considering the influence of particle geometry in k enhancement predictions, non-spherical particles require alternative formulations to the previously mentioned models. Otherwise, expected model precision losses and result discrepancies will occur. Typically, tubular particles are treated as cylinders. As early as 1962 this necessary distinction was incorporated in the Hamilton and Crosser model, where the empirical shape factor (n) assumes different values for spherical (n=3) and cylindrical (n=6) particles (Narvaez et al. 2010). As a result of their experimental study, which culminated in the aforementioned theoretical model based on cluster formation, Chen et al. (2009) also employed different shape factor values for spherical (n=3) and cylindrical (n=5) nanoparticles. In the case of the cylindrical particles (nanotubes), k along transverse and longitudinal directions was applied to account for nanotube diameter and length conductivity distributions.

2.4.4.2.3.1. The Percolation Effect

In comparison to metallic spherical nanoparticles, CNTs exhibit higher aspect ratios, reason for which percolation, due to aggregation, occurs far more frequently. The percolation theory predicts the existence of a critical particle concentration threshold, characterized by the formation of a continuous solid path, formed by highly conducting nanotubes coming into contact with each other, thus assisting the increase in k of several orders of magnitude (Lamas et al., 2012b; Martin et al., 2004; Sahoo et al., 2010). Patel et al. (2008) consider heat percolation as one of the main culprits for the higher k exhibited by CNTs.

Xie and Chen (2009), producing CNT nanofluids via ball milling, found that longer milling times lead to higher aggregation levels, which promote percolation, having concluded that the positive influence of aggregation surpasses the negative effect of aspect ratio deterioration that results from excessive milling. The percolation threshold of CNTs depends on nanotube dispersion, alignment, aspect ratio and surface modifications (Sahoo et al., 2010).

Munson-McGee (1991) found that a reduction of the threshold can be obtained with an increase in aspect ratio, demonstrating that the critical volume of cylindrical particles can vary from less than 1% to just over 20%, whereas Biercuk et al. (2002) indicated that the threshold for SWCNTs is approximately equal to the inverse of the aspect ratio, which was roughly 1000 in value, and that the percolation network formation occurs at inferior loadings, even for randomly oriented nanotubes.

Martin et al. (2004) established that the threshold for MWCNTs could be controlled by diffusion during particle dispersion. The same authors also consider that reported inconsistencies between experimental observation and the statistical percolation theory are owed to the lack of considerations with regard to inter-particle interactions, neglecting the effects of Van der Waals forces and Coulomb interactions due to static particle charging, and kinetic effects, such as particle Brownian motion. They also predicted that aging high aspect ratio nanotube dispersions would lead to lowered percolation thresholds.

Lamas et al. (2012b), backed by theoretical studies of Biercuk et al. (2002) and Nan et al. (2003), indicate discontinuities in k, attributed to Kapitza resistances, credited to play a significant

role in defining the percolation threshold. These interfacial thermal resistances were recognized to depend on the bonding strength between CNTs and the surrounding medium, as well as low functionalization levels (Shenogin et al., 2004; Xue et al., 2003). The dependence of the Kapitza resistance on the strength of liquid-solid interactions was found to exhibit two distinct regimes: an exponential dependence for weak bonding and a power law dependence for strong bonding, in which thermal resistance is inversely proportional to the solid-liquid connection strength (Xue et al., 2003). Shenogin et al. (2004) found that the functionalization of SWCNTs leads to significant decreases of the referred thermal resistances, but they also witnessed drops in k with increases in functionalized atom fractions. They used the effective medium theory to predict that this dependence could be eliminated for highly functionalized CNTs.

2.4.4.2.3.2. Theoretical Models for CNT Nanofluids

The previously mentioned Hamilton and Crosser model (1962) was the first to enable the prediction of k_{eff} of non-spherical particles. However, this classic model was formulated for larger sized particles than the nano-sized ones employed in nanofluids, as revealed in 2.4.4.2.1., being found to under-predict $k_{eff}$of CNT nanofluids. Nan et al. (2003) presented a simple formula based on Maxwell's effective medium model, accounting for high particle aspect ratios and volume fractions. However, the model was later found to over-predict k, this due to the authors having neglected the influence of the interfacial thermal resistances (Lamas et al., 2012b).

These conclusions led the authors to propose a modified model the following year, formulated to include, to some extent, the interface thermal resistance effect on k (Nan et al., 2004). According to this revised model, k_{eff} is a function of the volume fraction and β coefficients along the transverse direction (β_X) and the longitudinal direction (β_Z). These coefficients depend on k in each direction (k_{11}^c and k_{33}^c), in turn influenced by the particle thermal conductivity (k_P), nanotube diameter (d) and length (L), as well as the radius in which Kapitza resistance is influential (a_k). The Kapitza radius is a function of interface thermal resistance (R_k) and (k_b). The model was found to lack precision for increasing volume fractions and also doesn't account for percolation effects, CNTs assumed to be isolated from each other (Xue, 2006a).

$$k_{eff} = \frac{3 + \phi(\beta_X + \beta_Z)}{3 - \phi(\beta_X)} k_b \quad \text{(Eq. 4)}$$

$$\beta_X = \frac{2(k_{11}^c - k_b)}{k_{11}^c + k_b};\ \beta_Z = \frac{k_{33}^c}{k_b} - 1$$

$$k_{11}^c = \frac{k_p}{1 + \frac{2a_k}{d}\frac{k_p}{k_b}};\ k_{33}^c = \frac{k_p}{1 + \frac{2a_k}{L}\frac{k_p}{k_b}};\ a_k = R_k k_b = 8 \times 10^{-8} \frac{m^2 K}{W} x\ k_b$$

Xue (2006a) proposed a theoretical model which incorporates interfacial thermal resistances using an average polarization theory, as well as simultaneously considering the effects of nanotube dimensions and concentrations. The deduced expression leads the author to state that increases in k can be obtained via an increase in nanotube length, regardless of the corresponding diameter, which indicates that thermal variations along the transversal direction can be neglected.

$$9(1-\phi)\frac{k_{eff} - k_b}{2k_{eff} + k_m} + \phi\left[\frac{k_{eff} - k_{33}^c}{k_{eff} + 0.14\,{}^{d}/_{L}\left(k_{33}^c - k_{eff}\right)} + 4\frac{k_{eff} - k_{11}^c}{2k_{eff} + {}^{1}/_{2}\left(k_{11}^c - k_{eff}\right)}\right] = 0 \quad \text{(Eq. 5)}$$

The same author also proposed a Maxwell-based model to account for the effect of the nanotube orientation distribution, founded on the discontinuity theory of dispersions in a continuous phase (Xue, 2006b). Once again, the effect of percolation was overlooked and the model only predicts increases in k_{eff} for increases in particle volume fraction (Lamas et al., 2012b).

$$k_{eff} = \frac{1 - \phi + 2\phi \frac{k_p}{k_p - k_b} ln \frac{k_p + k_b}{2k_b}}{1 - \phi + 2\phi \frac{k_b}{k_p - k_b} ln \frac{k_p + k_b}{2k_b}} k_b \quad \text{(Eq. 6)}$$

Sastry et al. (2008) presented a model based on percolation and the contact resistance in the consequent thermal resistance network. A dimensionless parameter was introduced to represent the effect of percolation, it being a function of conductance between CNTs (G), CNT length (L_i) and particle volume fraction. According to their model, k_{eff} depends on the number of parallel CNT chains (M), the number of connected segments (N) over a distance (X), CNT diameter (d) and the heat transfer area (A).

$$M = \frac{4\phi X^3}{\pi d^2 L N};\ k_{eff} = \frac{X}{A}\left(\sum_{i=1}^{N} \frac{1}{\frac{k_b A}{dx_i} + \frac{M}{\frac{L_i}{\pi k_p d^2} + \frac{2}{G d^2}}} \right)^{-1} \quad \text{(Eq. 7)}$$

Based on the Sastry et al. (2008) model, Koo et al. (2008) proposed a revised model which takes the non-linear k enhancement with particle concentration increases into account using the excluded volume concept, where the excluded volume is the volume surrounding an object in which the centre of an identical object should be missing in order to avoid object inter-penetration. According to their model, the role of percolation is represented not only by the dimensionless parameter, but also by the number of contacts per cylinder (N_c) of randomly oriented cylinders, quantified by the product of the excluded volume and the CNT volume fraction, as follows:

$$N_c = \frac{\pi}{2} L^2 d \frac{\phi}{\pi/4\, d^2 L} = 2\phi \left(\frac{L}{d}\right) \quad \text{(Eq. 8)}$$

Patel et al. (2008) derived a model for CNT nanofluids based on a spherical particle model of k previously proposed by Hemanth et al. (2004), announcing a reasonable enhancement trend prediction for both oil and water based CNT nanofluids. Additionally, two paths for heat flow are assumed: one through the base liquid and another through the CNTs; both considered to be acting in parallel to each other. According to the model, k_{eff} is a function of the base liquid molecular size (r_b), the average CNT diameter (d) and ϕ of CNTs.

$$k_{eff} = \left(1 + \frac{k_p\, \phi\, r_b}{k_b [1 - \phi] d}\right) k_b \quad \text{(Eq. 9)}$$

With a view to predict the effects of anisotropy, aspect ratio, non-straightness, CNT volume fraction and interfacial thermal resistance on k_{eff}, Deng et al. (2007) and Deng and Zheng (2009) proposed several analytical formulas. The most significant of these models takes into account a non-straightness of CNTs (η), a high thermal anisotropy of CNTs ($k_{11}^c / k_{33}^c \ll 1$), a random CNT orientation and a tube-end thermal resistance. The model also assumes the formation of CNT thermal cables, while the role played by the aspect ratio (p) is reflected by parameter H, as follows.

$$k_{eff} = 1 + \frac{\eta\phi/_3}{\frac{k_b}{\eta/_{k_{33}^c/(1+2R_k k_{33}^c/L)}} + H(\eta p)} k_b \quad \text{(Eq. 10)}$$

$$H = \frac{1}{p^2-1}\left[\frac{p}{\sqrt{p^2-1}} ln\left(p + \sqrt{p^2-1}\right) - 1\right]$$

2.4.5. Convective Heat Transfer

In order to employ nanofluids in concrete applications, a full understanding of their convective heat transfer features is essential. When compared to the reported studies of k, convective heat transfer research is scarce, little attention having been given to determining the convective heat transfer characteristics of nanofluids (Murshed et al., 2008; Pfautsch, 2008). However, in recent years this mode of heat exchange has gained more awareness, result of a necessary comprehension for practical application. Convective heat transfer can be divided into two categories: forced convection, with induced fluid flow through confined regions, and natural convection, with fluid motion due to buoyancy (Ding et al., 2007).

2.4.5.1. Forced Convection

Of the limited available literature, most studies are focused on the forced convective heat transfer of nanofluids in circular tubes. The convective heat transfer coefficient (h) depends on k, specific heat capacity (c_P), viscosity (μ), flow rate and density of fluids (Eastman, 2005). The fluid flow mode is of upmost importance, studies being conducted for both laminar and turbulent flows. Most of the reported investigations characterize the heat transfer with emphasis on h and the Nusselt number (Nu), which depends on the Reynolds number (Re) and the Prandtl number (Pr). These parameters are dependent of the nanofluid thermal transport properties, most significantly μ and k, which are a function of the temperature. Due to this, most experimental procedures involve the measurement of the fluid temperature in different regions along the tube. In experimental procedures, laminar flow convective heat transfer studies are frequently validated using the theoretical predictions of Shah, whereas turbulent flows are typically validated by the Gnielinski or the Dittus-Boelter equations, all characterized by Nu (He et al., 2007).

- Shah equation for laminar flows (D, tube diameter and x, axial position along tube axis):

$$Nu = \begin{cases} 1.953\left(RePr\,{}^{D}/_{x}\right)^{1/3}, & \left(RePr\,{}^{D}/_{x}\right) \geq 33.3 \\ 4.364 + 0.0722RePr\,{}^{D}/_{x}, & \left(RePr\,{}^{D}/_{x}\right) < 33.3 \end{cases} \quad \text{(Eq. 12)}$$

- Gnielinski equation for turbulent flows (f, friction factor $f \approx 0.078Re^{-1/4}$) :

$$Nu = \frac{f/2\,(Re - 10^3)Pr}{1 + 12.7(f/2)^{1/2}\left(Pr^{2/3} - 1\right)} \quad \text{(Eq. 13)}$$

- Dittus-Boelter equation for turbulent flows:

$$Nu = 0.023Re^{0.8}Pr^{0.4} \quad \text{(Eq. 14)}$$

2.4.5.1.1. Experimental Studies

2.4.5.1.1.1. Spherical Particle Nanofluids

2.4.5.1.1.1.1. Laminar Flow

Wen and Ding (2004a) evaluated the convective heat transfer performance of Al_2O_3/Deionized water nanofluids in a copper tube. The witnessed enhancement was most significant in the tube entrance region and increased with increasing particle volume fractions, Nu and Re. They also found that the increase in h surpassed that of k, especially at the tube entrance. This was attributed to a decrease in the thermal boundary layer thickness at the tube entrance, the authors speculating whether particle migration, Brownian motion or viscosity gradients were the mechanisms behind this. Table 7 presents a summary of all the reported heat transfer studies under laminar flow.

Heris et al. (2006 and 2007) examined h of Al_2O_3/water nanofluids (and CuO/water nanofluids, 2006) in a steel tube with an imposed constant wall temperature boundary condition, obtained via steam application through an outer tube. For several nanoparticle volume fractions, the experimental enhancements of h were related to the Peclet number (Pe), influenced by rates of advection and diffusion. The results were found to improve with increasing volume fractions and increasing Pe. In their earlier experiment, they found that the enhancement peaked at an optimum particle loading, posteriorly decreasing with increasing volume fractions. The same authors would later conduct similar experiments exclusively for Cu/water nanofluids (2009).

Li and Xuan (2002) and He et al. (2007) conducted thorough investigations into convective heat transfer and pressure drop of Cu/water and TiO_2/water nanofluids, respectively. As with previous experiments, the heat transfer was evaluated for nanofluid flows through a horizontal brass tube (Li and Xuan, 2002) and a vertical copper pipe (He et al., 2007). Li and Xuan (2002) indicated the significant influence of the nanoparticle volume fraction on h and the pressure drop. He et al. (2007) also concluded that thermal transport was found to increase with particle concentration, but also linearly increase with Re, whereas pressure drop was reported to be very close to that of the base liquid alone.

Hwang et al. (2009) investigated the performance of Al_2O_3 and water based nanofluids under a fully developed laminar flow in a steel tube. The heat transfer was found to be almost constant, indicating that nanofluids behave like single-phase fluids under fully developed laminar flow. h increased with volume fraction, registering a superior enhancement to that of k_{eff} at maximum loading, leading the authors to conclude that k plays a minor role in dynamic heat transfer.

With a view to demonstrate that nanofluids can be treated as homogeneous mixtures, Rea et al. (2009) studied the convective heat transfer and pressure loss of Al_2O_3 and ZrO_2 based nanofluids across a steel tube. The heat transfer enhancement for Al_2O_3 was significantly higher than that of ZrO_2 and the pressure loss increased with higher particle loadings. With Nu being evaluated by the Shah equation, the best heat dissipation performances were observed in the tube entrance region, i.e., the laminar development region.

In the same year, Anoop et al. (2009) analysed the effect of nanoparticle size on h of Al_2O_3/water nanofluids in a copper tube, comparing the performances of two distinct average sized nanoparticles: 45 nm and 150 nm. The smaller particle size exhibited the better performance,

indicating that nanoparticle size decrease will enhance h in a developing laminar flow. In both circumstances, the increase in h expressively surpassed the measured k. Chandrasekar et al. (2010) experimentally investigated the effect of employing wire coil inserts to Al_2O_3/water nanofluid flow in a copper tube. The initial enhancement of Nu, due to the nanofluid alone, was boosted by the addition of two wire coils to the heat transfer test system (12.24 % vs. 21.53 %).

Table 7 - Summary of Experimental Studies of Forced Convective Heat Transfer, under Laminar Flow, of Spherical Particle Nanofluids

Author (Year)	Nanofluid	Volume Fraction	Tube Dimensions	Heat Transfer Enhancement
Li and Xuan (2002)	Cu/Water	$0.3 - 2$ %	$L = 0.8\ m$ $d = 10\ mm$	60% for h at 2 $vol.$%
Wen and Ding (2004a)	Al_2O_3/Water	$0.6 - 1.6$ %	$L = 0.97\ m$ $d = 4.5\ mm$	47% for h at 1.6 $vol.$% and $Re = 1600$; 41% at $Re = 1050$
Heris et al. (2006)	Al_2O_3/Water CuO/Water	$0.2 - 3$ %	$L = 1\ m$ $d = 6\ mm$	29% for h at 2.5 $vol.$% and $Pe = 5000$ (Al_2O_3)
Heris et al. (2007)	Al_2O_3/Water	$0.2 - 2.5$ %	$L = 1\ m$ $d = 6\ mm$	40% for h at 2.5 $vol.$% and $Pe = 6000$
He et al. (2007)	TiO_2/Water	$0.2 - 1.1$ %	$L = 1.83\ m$ $d = 6.3\ mm$	12% for h at 1.1 $vol.$% and $Re = 1500$
Chun et al. (2008)	Al_2O_3/Oil	$0.2 - 0.5$ %	$L = 5\ m$ $d = 6.35\ mm$	13% for h at 0.5 $vol.$% and $Re \approx 400$
Hwang et al. (2009)	Al_2O_3/Water	0.01 – 0.3 %	$L = 2.5\ m$ $d = 1.8\ mm$	8% for h; 1.44 % for k; 0.3 $vol.$% at $Re \approx 735$
Kolade et al. (2009)	Al_2O_3/Water Al_2O_3/Oil	2 %	$L = 1.8\ m$ $d = 5\ mm$	Maximum: 6% for k at $Re = 1200$ (Al_2O_3/Water)
Rea et al. (2009)	Al_2O_3/Water ZrO_2/Water	$0.6 - 6$ % $0.3 - 1.3$ %	$L = 1.01\ m$ $d = 4.5\ mm$	27% for h at 6 $vol.$% and $Re = 1600$ (Al_2O_3)
Anoop et al. (2009)	Al_2O_3/Water	$0.1 - 1$ %	$L = 1.2\ m$ $d = 4.75\ mm$	25% for h at 1 $vol.$% and $Re = 1550$
Heris et al. (2009)	Cu/Water	$0.2 - 2.5$ %	$L = 1\ m$ $d = 6\ mm$	45% for h at 2 $vol.$% and $Pe = 6700$
Chandrasekar et al. (2010)	Al_2O_3/Water	0.1 %	$L = 0.8\ m$ $d = 4.85\ mm$	21.53% for Nu at $Re = 2275$, with inserts

2.4.5.1.1.1.2. Turbulent Flow

Pak and Cho (1998) evaluated the heat transfer performance of Al_2O_3 and TiO_2 particle nanofluids, at Re varying from 10^4 to 10^5, in a steel tube for which a constant wall heat flux boundary condition was considered. The enhancement of h increased with increasing particle volume fractions, as displayed in Table 8. He et al. (2007) conducted an experimental study to determine the enhancement of h for TiO_2 nanofluids for laminar and turbulent flows. For turbulent flow regimes the enhancement of h was greater, particle volume fraction being more influential than for laminar flows. On the downside, the pressure drop was higher and began displaying exponential increases for high Re.

A different approach was taken by Nguyen et al. (2007), using a heated aluminium block to simulate an operating CPU microprocessor. Particle size, loading and Re were found to be influential. The enhancement was found to grow with the level of turbulence in the fluid flow. Fotukian and Esfahany (2010) evaluated the heat transfer of low concentration Al_2O_3/water nanofluids in a copper tube. Unexpectedly, they found that the enhancement decreased with increasing Re, contradicting theoretical predictions. The pressure drop increased with nanoparticle loadings, but varied inconsistently with Re. Hojjat et al. (2011) studied three different nanofluids, all using an aqueous solution of carboxymethyl cellulose (CMC) for base fluid. For all the tested nanofluids, h and Nu increased significantly with an increase of Pe.

Table 8 - Summary of Experimental Studies of Forced Convective Heat Transfer, under Turbulent Flow, of Spherical Particle Nanofluids

Author (Year)	Nanofluid	Volume Fraction	Tube Dimensions	Heat Transfer Enhancement
Pak and Cho (1998)	Al_2O_3/Water TiO_2/Water	$1 - 10\ \%$	$L = 0.48\ m$ $d = 10.7\ mm$	75% for h at $2.4\ vol.\%$; 75% at $1.34\ vol.\%$ (Al_2O_3)
Li and Ding (2002)	Cu/Water	$0.3 - 2\ \%$	$L = 0.8\ m$ $d = 10\ mm$	60% for h at $2\ vol.\%$
Williams (2006)	Al_2O_3/Water ZrO_2/Water	$0.9 - 3.6\ \%$ $0.2 - 0.9\ \%$	$L = 3\ m$ $d = 12.7\ mm$	Max. Nu enhancement at $3.6\ vol.\%$ (Al_2O_3)
He et al. (2007)	TiO_2/Water	$0.2 - 1.1\ \%$	$L = 1.83\ m$ $d = 6.3\ mm$	40% for h at $1.1\ vol.\%$ and $Re = 5900$
Nguyen et al. (2007)	Al_2O_3/Water	$1 - 6.8\ \%$	Heated block: $60\ x\ 60\ x\ 75\ mm$	40% for h at $6.8\ vol.\%$ and $Re = 7000$
Kulkami et al. (2008)	SiO_2/Water + EG	$2 - 10\ \%$	$L = 1\ m$ $d = 3.14\ mm$	16% for h at $10\ vol.\%$ and $Re = 10000$
Yu et al. (2009)	SiC/Water	$3.7\ \%$	$L = 0.58\ m$ $d = 2.27\ mm$	60% for h at $Re = 6000$
Fotukian and Esfahany (2009)	Al_2O_3/Water	$0.03 - 0.13\ \%$	$d = 6.3\ mm$	48% for h at $0.054\ vol.\%$ and $Re = 9950$
Sundar and Sharma (2010)	Al_2O_3/Water	$0.02 - 0.5\ \%$	$L = 1.5\ m$ $d = 4.5\ mm$	80.19% for h at $0.5\ vol.\%$ and $Re = 22000$ (inserts)
Hojjat et al. (2011)	CuO/CMC	$0.1 - 1.5\ \%$	$L = 2.11\ m$ $d = 10\ mm$	71% for h at $0.5\ vol.\%$

2.4.5.1.1.2. Tubular Particle Nanofluids

2.4.5.1.1.2.1. Laminar Flow

Ding et al. (2006) studied the heat transport properties of MWCNT/water nanofluids along a uniformly heated copper tube. The experimental data demonstrated good agreement with the Shah equation for laminar flows under the constant heat flux boundary condition. As with the spherical studies, h was found to increase significantly with nanotube concentration and Re. It was also found to be minimally affected by the fluid acidity. The highest values of h were witnessed in the tube entrance region, leading the authors to indicate the creation of multiple artificial entrances along tubes, to maximize the heat transfer via boundary layer degradation, for future studies.

Amrollahi et al. (2010) conducted a similar experiment for both laminar and turbulent flows, using functionalized MWCNT nanofluids. Their experiment resulted in less significant enhancements of h when compared to the previous study.

Garg et al. (2009) prepared an experimental study to evaluate the influence of the ultrasonication times, during MWCNT/water nanofluid preparation, on the heat transfer performance. To that effect, four distinct samples, with ultrasonication times ranging from 20 to 80 minutes, were prepared. h was analysed along a copper tube, under a constant heat flux condition, with Re varying between 600 and 1200. As with previous studies, h was highest in the entry region but its maximum enhancement was found to occur in the developed boundary layer region. The increase of Re resulted in a decrease of the h. The authors found that the optimum ultrasonication time was 40 minutes, above which the tube breakage rate increased.

Silva (2010) and Abreu et al. (2012) conducted similar experiments to evaluate the convective heat transfer of low particle concentration MWCNT/water nanofluids along a stainless steel tube, under the constant wall heat flux boundary condition. In both investigations the enhancement of h was greatly superior to that observed for k, reported to be maximum in the tube entry region. Table 9 offers a summary of the mentioned experimental studies.

Table 9 - Summary of Experimental Studies of Forced Convective Heat Transfer, under Laminar Flow, of Tubular Particle Nanofluids

Author (Year)	Nanofluid	Nanotube Loading	Tube Dimensions	Heat Transfer Enhancement
Ding et al. (2006)	MWCNT/Water	$0.1 - 0.5\ wt.\%$	$L = 0.97\ m$ $d = 4.5\ mm$	375% for h at $0.5\ wt.\%$ and $Re = 800$
Garg et al. (2009)	MWCNT/Water	$0.25\ wt.\%$	$L = 0.914\ m$ $d = 1.55\ mm$	32% for h at $Re = 600$; 29% at $Re = 900$
Kolade et al. (2009)	MWCNT/Water	$0.2\ vol.\%$	$L = 1.8\ m$ $d = 5\ mm$	10% for k at $Re = 1200$
Amrollahi et al. (2010)	MWCNT/Water	$0.1 - 0.25\ wt.\%$	$L = 1\ m$ $d = 11.4\ mm$	12% for h at $0.12\ wt.\%$ and 40% at $0.25\ wt.\%$
Silva (2010)	MWCNT/Water	$0.25\ vol.\%$	$L = 1.2\ m$ $d = 6\ mm$	105% for h at $Re = 2060$
Abreu et al. (2012)	MWCNT/Water	$0.25 - 0.5\ vol.\%$	$L = 1.2\ m$ $d = 6\ mm$	94% for h at $0.5\ vol.\%$ and $Re = 2061$

2.4.5.1.1.2.2. Turbulent Flow

Despite extensive research, limited experimental investigations of tubular particle nanofluids were found; these are summarized in Table 10. Amrohalli et al. (2010) evaluated the heat transfer enhancement of functionalized MWCNT/water nanofluids for both laminar and turbulent flow modes. h in turbulent flows displayed a greater increase than the values obtained for laminar flows and the enhancement decreased with increasing temperatures. It was also found to become constant with increasing Re in the tube entry region.

Liu and Liao (2010) studied the heat transfer behaviour of CNT dispersions in an aqueous solution of cetyltrimethyl ammonium chloride (CTAC), purposely used to reduce drag. The heat

transfer enhancement was found to be greater with higher temperatures, even when the drag reduction is insignificant, and higher particle loadings. The dependence of h on the Re was noticed to be minimal.

Table 10 - Summary of Experimental Studies of Forced Convective Heat Transfer, under Turbulent Flow, of Tubular Particle Nanofluids

Author (Year)	Nanofluid	Nanotube Loading	Tube Dimensions	Heat Transfer Enhancement
Amrollahi et al. (2010)	MWCNT/Water	$0.1 - 0.25\ wt.\%$	$L = 1\ m$ $d = 11.4\ mm$	25% for h at $0.12\ wt.\%$ and $Re = 4778$
Liu and Liao (2009)	CNT/CTAC	$0.5 - 4\ wt.\%$	$L = 1.08\ m$ $d = 25.6\ mm$	70% for h at $2\ wt.\%$ and 40% at $4\ wt.\%$; $Re = 45000$

2.4.5.1.1.3. Studies Using Alternative Heat Exchanger Types

Most experimental studies reported in the available literature investigate the convective heat transfer along a singular tube. However, some authors have presented research studies involving alternative, more complex types of heat exchangers for nanofluid employment. Due to the experimental singularity of most of these studies, a lack of certainty of the obtained data is a concern; more research is required before these results can be properly compared and scrutinized.

Mapa and Mazhar (2005) studied the laminar flow heat transfer of a CuO/water nanofluid in a mini shell and tube heat exchanger, consisting of two flow loops across 37 tubes, each with a heat transfer area of 0.05 m^2. At very low particle concentrations the heat flow rate increased, compared to that of water alone, with the mass flow rate, the increase stabilizing once an optimum flow rate was achieved. The authors also found that higher particle concentrations lead to heat transfer increases that also vary with varying flow rates.

Pantzali et al. (2009) experimentally and numerically investigated h of CuO/water nanofluids operating in a miniature PHE with a corrugated surface. For a nanoparticle concentration of 4 vol. %, the enhancement in h was just over 10 %. However, the friction losses resulting from modulated surface employment were found to be 2.5 times larger than that of a flat plate. In the same year, Pantzali et al. (2009a) studied the efficacy of CuO, Al_2O_3 and CNT particles suspended in water at 4 vol. % in a herring-bone type PHE, consisting of 16 corrugated steel plates. When operating with laminar flows, the authors concluded that the use of nanofluids can be beneficial, whereas for turbulent flow they concluded that the enhancement in h with nanofluids can only be achieved if the increase in k is accompanied by a marginal increase in nanofluid viscosity.

Mare et al. (2011) investigated the heat transfer performances of Al_2O_3/water and CNT/water nanofluids operating at low temperatures (T_{max}=10°C) in a 20-plate PHE. Both nanofluids were tested in laminar flows, Re ranging between 35 and 195. Despite the inferior particle loading (0.55 vol. %), the CNT nanofluid exhibited the highest enhancement of h, 50 % vs. 42 %, than that of the Al_2O_3 nanofluid (1 vol. %). In conclusion, the authors insisted that the influence of viscosity and pressure drop are important, needing to be taken into account before nanofluid application to these heat exchangers.

Pandey and Nema (2012) and Lotfi et al. (2012) conducted similar experiments for Al_2O_3/water nanofluids in a corrugated PHE and MWCNT/water nanofluids in a shell and tube heat exchanger, respectively. Experimenting with different particle volume fractions in counter-flow, Pandey and Nema (2012) found that, above the optimum particle loading of 2 vol. %, h decreased with increasing concentrations (up to 4 vol. %), indicating that the effect of the viscosity increase surpasses the effect of the enhancement of k. The maximum enhancement of h, 111.5%, was registered at 2 vol. % and Pe=5134. Lotfi et al. (2012) used two distinct heating powers, 280 and 630 W, noting a higher enhancement for the higher heating power.

Rafati et al. (2012) tested three different nanofluids (Al_2O_3, SiO_2 and TiO_2 dispersed in a mixture of water and EG) in the cooling of an operating Phenom II X4 965 quad-core computer processor. The largest processor temperature decrease, of 5.5°C, was obtained with the Al_2O_3 nanofluid at 1 vol. %.

2.4.5.1.2. Theoretical Studies

Despite a recent boom in interest, theoretic models of convective heat transfer remain scarce, most are derived from classical correlations, such as the aforementioned Shah or Dittus-Boelter equations for laminar and turbulent flow, respectively. This bears the consequence of only being valid for specific nanofluids over small parameter variations (Wang and Mujumdar, 2008).

Pak and Cho (1998), following their experimental study of the heat transfer performance of Al_2O_3/water and TiO_2/water nanofluids under turbulent flow conditions, proposed the following correlation, a modified version of the Dittus-Boelter equation.

$$Nu = 0.021 {Re_{nf}}^{0.8} {Pr_{nf}}^{0.5} \quad \text{(Eq. 15)}$$

Xuan and Roetzel (2000) derived correlations for h of nanofluids proposing two different approaches: the first treating nanofluids as single-phase fluids, the second assuming nanofluids as solid-liquid mixtures. The first method assumes that classical correlations for pure fluids can be applied to predicting h. The second approach continues to treat the nanofluid as a single-phase fluid but also takes into account the heat transfer enhancement due to the thermal dispersion that results from random particle motion. Both approaches indicated that the enhancement depends on increases of k and chaotic particle motion, which accelerates energy exchanges. For their second approach, k_{eff} of the nanofluid is given by the sum of the contributions of the single-phase thermal conductivity of the nanofluid (k_{nf}) and the thermal conductivity of the dispersion (k_d), as follows.

$$k_{eff} = k_{nf} + k_d;\ k_d = C(\rho c_P)_{nf} \mu_X \phi d_P r_0 \quad \text{(Eq. 16)}$$

Based on the thermal dispersion and their experimental results for Cu/water nanofluids, Li and Xuan (2002) proposed a model for predicting h of nanofluids inside circular tubes. In this proposed correlation, the thermal dispersion promoted by micro-convection and micro-diffusion is quantified by Pe. Based on their experimental data for both laminar and turbulent flows, the following correlations were proposed.

- Laminar flows: $Nu = 0.4328\left(1.0 + 110285\phi^{0.754} {Pe_d}^{0.218}\right) {Re_{nf}}^{0.333} {Pr_{nf}}^{0.4}$ (Eq. 17)
- Turbulent flows: $Nu = 0.0059\left(1.0 + 7.6286\phi^{0.6886} {Pe_d}^{0.01}\right) {Re_{nf}}^{0.9238} {Pr_{nf}}^{0.4}$ (Eq. 18)

Ding and Wen (2005) focused on particle migration derived from Brownian motion, as well as shear stress and viscosity gradients, indicating a non-uniform property distribution that causes

radial variations in thermophysical properties, most notably of temperature and flow velocity, thus being proposed as a possible enhancement mechanism in heat transfer of nanofluids.

A comprehensive study of different analytical approaches was conducted by Mansour et al. (2007), in which laminar and turbulent flows, for an Al_2O_3/water nanofluid, were considered and common correlations used for nanofluids were evaluated for fully developed streams in a tube subjected to a constant heat flux boundary condition. Their analysis was focused on the determination of the c_P, μ and k, followed by pressure drop and heat transfer correlation studies for singular tube conditions using distinct particle volume fractions. The most significant discrepancies were found for the laminar flow cases, some contradictory.

2.4.5.2. Natural Convection

The natural convection of nanofluids bares importance in the chemical and food industries, having been found to be influenced by liquid unstable density distributions, which result from temperature and particle distribution differences due to particle sedimentation (Kang et al., 2001; Okada and Suzuki, 1997).

Few experimental and analytical studies to ascertain the natural convective heat transfer behaviour of nanofluids have been performed. Kang et al. (2001) and Putra et al. (2003) conducted similar experiments using cylindrical and rectangular vessels, respectively; in which the nanofluid was heated from one side (or wall) and cooled from the other. Kang et al. (2001) found that the formation and deterioration of multiple layers around SiO_2 nanoparticles occurred, these influenced by the increase of the temperature gradient between opposite sides. Putra et al. (2003) found that the enhancement of k of CuO/water nanofluids was higher than that of Al_2O_3/water nanofluids, both displaying improved convection than that of common slurries but inferior to that of the base fluid. Additionally, both nanofluids' natural convective heat transfer properties were found to deteriorate with an increase in particle concentration and density, characterized by decreasing Nu.

Analytic studies conducted by Khanafer et al. (2003) and Kim et al. (2004) led the authors to conclude that natural convective heat transfer increased with the particle volume fraction (at any Grashof number), contradicting the experimental conclusions of Putra et al. (2003).

2.4.6. Numerical Studies

Of the two approaches identified by Xuan and Roetzel (2000), the simpler single-phase assumption for nanofluids has been found to be numerically more efficient, result of its reduced computational workloads (Wang and Mujumdar, 2008). The advantage of this approach resides in the assumption that the base fluid and the nanoparticles are in thermal equilibrium as well as equal velocities (Kalbasi and Saeedi, 2012).

Maiga et al. (2004) developed a numeric model to simulate the flow of Al_2O_3/water and Al_2O_3/EG nanofluids, under both laminar and turbulent flows, applying single-phase and constant wall heat flux conditions to a circular tube (L=1 m, d=10 mm). Flow symmetry was assumed and, for turbulent flow, the semi-empirical K-Ɛ model was used to describe the nanofluids. Results demonstrated a higher heat transfer enhancement of the EG based nanofluid, increasing with growing particle loads.

Applying the same theoretical considerations, Roy et al. (2004) numerically evaluated the thermal performance and wall shear stress of nanofluids in a radial cooling system, subjected to

laminar, uniform velocity flows. The obtained data indicates increases in h for growing particle volume fraction and Re. More recently, a similar numerical study was conducted by Kalbasi and Saeedi (2012) to assess the thermal performance of a CuO/water nanofluid in a tube.

Xuan et al. (2005) proposed a thermal Lattice Boltzmann model for flow and energy transport simulation of a Cu/water nanofluid. The distinguishing feature of this model is the hypothesis of particle location at a series of lattices, presenting a Boltzmann distribution within these. Another relevant feature is the temperature independence with regard to particle density distribution. The model predicted an enhancement of 27 % to the nanofluid Nu over that of water alone.

Following their previously cited experimental investigations with Al_2O_3/water nanofluids under laminar flow, Heris et al. (2007a) established a model which employed the thermal dispersion theoretical hypothesis, proposed by Xuan and Roetzel (2000). Simulations indicated that enhancements of h could be maximized through the simultaneous effect of volume fraction increase and nanoparticle size decrease.

Employing the two-phase approach, Behzadmehr et al. (2007) numerically investigated the turbulent flow of a nanofluid through a tube. The model takes into account both nanoparticle and base fluid molecule velocity gradients and uses a numerical solution to enable the application of the constant wall heat flux boundary condition. The authors performed a simulation using the experimental data gathered by Li and Xuan (2002), claiming good agreement for the Cu/water nanofluids, contrary to the single-phase assumption for the same experimental data.

Pfautsch (2008) conducted a numerical analysis of the thermal transfer behaviour of Al_2O_3/water and Al_2O_3/EG nanofluids in a flat PHE assuming fluid and nanoparticle continuity, as well as momentum conservation via the Navier-Stokes equation. Due to a high non-linearity of the governing equations, simulations were performed employing the finite difference method. Results demonstrated that h for laminar flow increases dramatically with particle size reduction and volume fraction increase. For well dispersed particles in water the maximum enhancement was predicted to be 130 %, whereas for EG the enhancement was significantly higher (275 %).

More recently, Mohammed et al. (2011) conceived a model of an aluminium square micro-channel heat exchanger (25 channels) with the intent to evaluate the thermal performance of four nanofluids (Al_2O_3, SiO_2, Ag and TiO_2) under laminar flow. They assumed single-phase fluids and steady-state flow, while simulations followed the finite volume methodology. Simulations proved the better performance of the Al_2O_3 nanofluid and the disadvantageous increase in pumping requirements with increasing Re.

Kalteh et al. (2011) proposed a two-phase model to study the behaviour of a Cu/water nanofluid in an isothermally heated parallel plate micro-channel. Once again, the governing mass, momentum and energy equations were solved via the finite volume method using a non-uniform mesh. Perhaps anticipating the more anomalous behaviour reported in experimental studies for singular tube exchangers, the mesh was most refined in the micro-channel entry region. Consequent simulations demonstrated independence between particle viscosity and Nu at Re=100. As with the Behzadmehr et al. (2007) model, a comparison with the homogeneous single-phase assumption indicated the higher precision of the two-phase approach.

A unique numerical study was established by Manca et al. (2011) in assessing the heat transfer enhancement resultant of an Al_2O_3/water nanofluid employed in confined slot jet

impingement on a heated wall. The single-phase approach was used and the impingement temperature was considered constant. Other relevant considerations included steady-state, turbulent and constant property flow conditions, as well as nanofluid incompressibility.

Heris et al. (2012) performed numerical simulations to evaluate the thermal behaviour of Al_2O_3, CuO and Cu nanoparticle suspensions in water under constant wall temperature boundary conditions when transiting through a square duct, which is less penalizing in pressure drop but limited in heat transfer when compared to the circular profiles. In an analogous approach to that taken by Kalteh et al. (2011), the model was composed of a non-uniform mesh, finer elements packed in the duct entrance region. Of the tested nanofluids, the Cu/water presented the best thermal characteristics, Al_2O_3 displaying the worst.

Chapter 3

Experimental Model

For the exclusive purpose of experimental studies in nanofluid behaviour, a single-station multi-measurement structure was proposed and constructed by Silva (2010) in response to the requirement of a nanofluid preparation and test facility. The structure is composed of three independent sections: one for different nanofluid preparation, under controlled atmospheric conditions for contaminant minimization; another for conductive heat transfer measurements, using the THW method; and a convective heat transfer test section.

3.1. Nanofluid Conception

Nanoparticle preparation followed a two-step method. MWCNTs, acquired from Cheap Tubes Inc. (Table 11), where they were obtained under a CCVD technique, were diluted in a surfactant composed of sulphuric and nitric acids, for improved homogeneity and functionalized group stimulation, thus employing the chemical treatment of nanotubes proposed by Esumi et al. (1996). The next step of the preparation consisted of particle dispersion in the base fluid (DIW), with the purpose of achieving a stable nanofluid with a nanoparticle concentration of 0.25 vol. %. Colloidal stability was attained after an hour long ultrasonication period, followed by a 24 hour period of inactivity to ensure the absence of sedimentation before application.

Table 11 – Relevant Properties of employed CNTs (Cheap Tubes Inc.)

Property	**Value**
Outer diameter	$50 - 80\ nm$
Inner diameter	$5 - 10\ nm$
Length	$10 - 20\ \mu m$
Purity	$> 95\%$
Specific surface area	$60\ m^2/g$
Electric conductivity	$> 100\ S/cm$
Ash	$> 1{,}5\ wt.\%$
Density	$\sim 2{,}1\ g/cm^3$

Preceding MWCNT dispersion in DIW, the result of the chemical treatment on the particle surfaces was assessed using scanning electron microscopy (SEM). This procedure allows the observation of nanoparticle morphology and also allows a continuous surveillance of the required nanoparticle deagglomeration. Following the preparation of the nanofluid, its colloidal stability was assessed using ultraviolet-visible spectrophotometry, resulting in observed absorption rate drops of 12 % and 18 % after 72 and 100 hour periods, respectively, thus rendering the nanofluid test-worthy.

3.2. Property Measurements

3.2.1. Thermal Conductivity

The thermal conductivity (k) of the base fluid and the tailored nanofluid were measured using the THW, as described in the literature review. The variation of k as a function of the operating fluid temperature was determined using a Decagon KD2 Pro Thermal Properties Analyser, acquired for the task. These variations were registered for temperatures ranging from 283.15 K to 333.15 K, segmented in 10 K intervals.

3.2.2. Dynamic Viscosity

Nanofluid viscosity (μ) was determined using an oscillation rheometer, typically employed to measure elastic properties of low viscosity fluids. Due to the increased number of required set parameters, rheology is a less effective technique than viscometry. Additionally, oscillatory torque and phase are influenced by the inertia triggered by the operating rheometer (Franck, 2003). For the determination of the nanofluid viscosity, the oscillatory shear velocities were varied from 0 to 600 s^{-1}, at a constant temperature.

3.2.3. Density and Specific Heat Capacity

Both properties were theoretically calculated using similar correlations, in which separate material properties are employed as a function of the respective volume fraction of each in the particle/fluid mixture.

$$\rho_{nf} = (\phi \times \rho)_{np} + (\phi \times \rho)_{bf} \quad \text{(Eq. 19)}$$

$$c_{P,nf} = (\phi \times c_P)_{np} + (\phi \times c_P)_{bf} \quad \text{(Eq. 20)}$$

3.2.4. Results

Table 12 summarizes the experimental results obtained for the discussed thermophysical parameters of each employed operating fluid, at 300 K.

Table 12 – Experimental Thermophysical Properties of Tested Fluids at 300 K (Silva 2010)

Property	Units	DIW	0.25 vol. % CNT/DIW nanofluid
Density ($\boldsymbol{\rho}$)	kg/m^3	997	1197
Specific heat capacity ($\boldsymbol{c_p}$)	$J/kg\ K$	4179	4384
Dynamic viscosity ($\boldsymbol{\mu}$)	$N\ s/m^2$	0.000855	0.00135
Thermal Conductivity ($\boldsymbol{k}$)	$W/m\ K$	0.605	0.626

3.3. Convective Heat Transfer Measurement

3.3.1. Setup and Procedure

The experimental circuit for the measurement of forced convective heat transfer is composed of a test area, a peristaltic pump, a tubular indirect contact heat exchanger, a fluid storage vessel and data acquiring equipment. The operating fluid is pumped out of the storage container and transported, through silicone tubes, to the test area. After flowing through the test tube, the fluid proceeds to the heat exchanger, where it is cooled by indirect heat interaction with Kyro 30 refrigerating fluid, before returning to the vessel, thus concluding a cycle. A visual representation of the process can be observed in Figure 4.

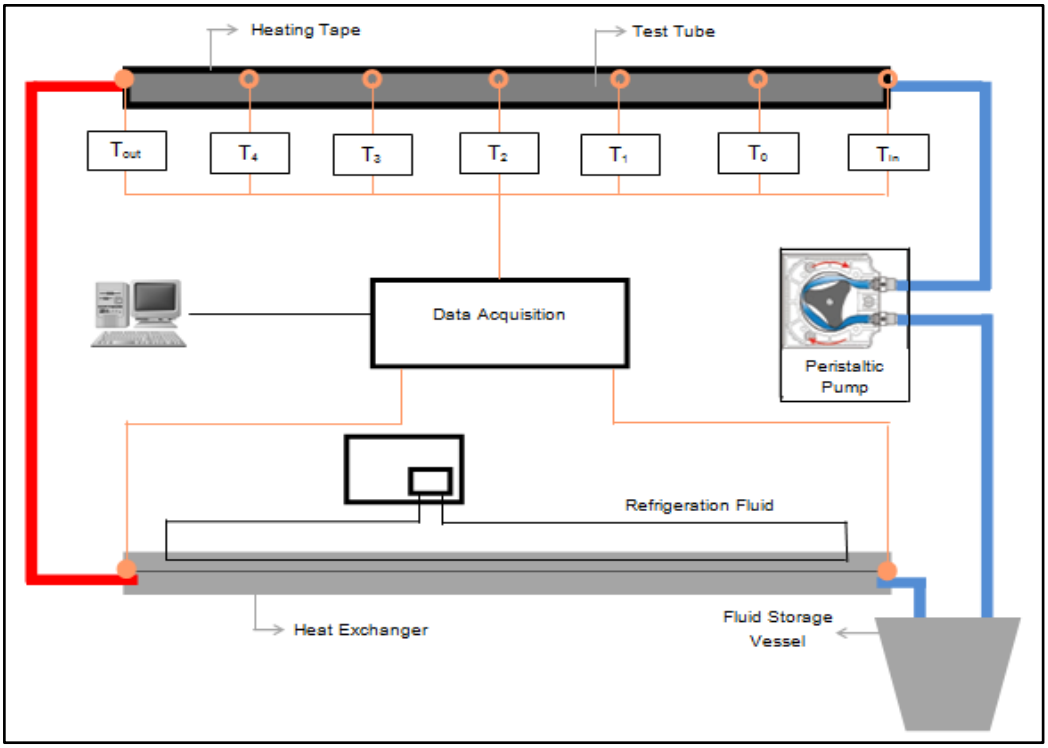

Figure 4 – Experimental circuit schematic for forced convective heat transfer studies (adapted from Silva, 2010).

The test section consists of a 1200 mm-long circular stainless steel (grade 316) tube, with interior and exterior diameters of 6 and 8 mm, respectively, operating as a heat exchanger between the tube inner surface and the operating fluid. The tube is heated using rubber heating tape, the power input controlled by a potentiometer. A constant wall heat flux, and consequent isothermal characteristics on the tube surface, is ensured by the minimization of heat losses, achieved by wrapping aluminium foil around the tube and posterior polyethylene foam coating for maximized thermal isolation.

This straightforward setup allows the temperature measurement of the operating fluid at the tube inlet and outlet, as well as the exterior tube surface temperature at intermediate positions along its longitudinal axis. To this purpose, seven k-type thermocouples, positioned on the mentioned positions, were used to obtain temperature measurements of rationally spaced locations, as described in Table 13. Both fluid temperature measurement thermocouples, at tube

inlet and outlet, were approximately positioned along the fluid flow axis (tube centre). In order to enable a fully developed fluid flow at the first measurement point, a 110 mm pre-segment is provided, calculated using the hydrodynamic entry length expressions for laminar and turbulent flows. Further setup information can be viewed in the thesis conducted by Silva (2010).

Table 13 – Thermocouple Positions along the Test Tube (Silva, 2010)

Measurement Point	Measurement Target	Axial Tube Position $[mm]$	x/D
T_{in}	Fluid	0	0
T_0	Tube Surface	210	33
T_1		420	70
T_2		610	102
T_3		810	135
T_4		1000	167
T_{out}	Fluid	1200	200

3.3.2. Setup Calibration

In order to validate the experimental results, multiple calibration procedures were employed. The setup was validated using the obtained experimental results for DIW, with its well established properties, then relating them to the corresponding theoretical results, calculated via mathematical formulation.

The adiabatic properties of the tube's thermal isolation were theoretically evaluated by the application of a thermal energy balance, using fluid temperature variation, between tube inlet and outlet, as governing property. This temperature variation was also experimentally monitored and the error between experimental and theoretical data quantified, at different flow conditions. At low Re (Re<1500) the results displayed higher discrepancies, leading the author to detect a problem associated to the peristaltic pump. This component manifested inaptness in maintaining continuous fluid flows, enabling flow oscillations that jeopardize a steady passage through the consecutive tube regions. Another pump limitation was its incapacity to sustain fully developed turbulent flows. This intrinsic difficulty ultimately limited experiments to laminar flows only, with Re ranging from 1236 to 2060.

Measurement repeatability was guaranteed following five distinct fluid passages, executed during five different days, through the tube using similar entry conditions for each. As for component calibration, the thermocouples were attuned using a fixed-point cell and appropriate data-acquiring software, the associated error found to be just below 2% or ±0.2 K.

3.3.2.1. Mathematical Formulation

The convective heat transfer performance of operating fluids is typically characterized by h, a property that cannot be directly measured. However, it can be indirectly obtained through the use of theoretical correlations of experimentally measurable properties, such as the temperature. For a uniaxial fluid flow through a tube, the experimental heat transfer coefficient (h_{exp}), at a given position in the uniaxial direction (x), was calculated as a function of the heat transfer rate, between

fluid and tube (q''), and the difference between axial mean fluid temperature ($\overline{T_f}$) and tube surface temperature (T_s) in each position (x), as follows in Equation 21.

$$h_{exp}(x) = \frac{q''}{T_s(x) - \overline{T_f}(x)} \quad \text{(Eq. 21)}$$

The heat transfer rate to the fluid is the quotient between the incoming power (q) and the heat transfer area between fluid and tube (A), this last term the inner tube surface area. The total heat transfer depends on fluid mass flow ($\dot{m}$) and specific heat capacity (c_P), as well as its temperature variation within the tube, experimentally quantified by the difference between tube inlet ($T_{f,in}$) and outlet ($T_{f,out}$) fluid temperatures. The heat transfer area depends on the tube inner diameter (D) and length (L), as described in Eq. 22.

$$q'' = \frac{q}{A} = \frac{\dot{m} \times c_P \times (T_{f,out} - T_{f,in})}{\pi \times D \times L} \quad \text{(Eq. 22)}$$

In order to establish a comparison between experimental and theoretical heat transfer properties at the intermediate points of the tube, the following theoretical formula for fluid mean temperature ($\overline{T_f}$) in any point along a uniaxial flow was employed (Eq. 23). The formula establishes a temperature dependence on the flow perimeter (P), as well as fluid mass flow ($\dot{m}$), specific heat capacity (c_P), heat transfer rate (q'') and uniaxial position (x).

$$\overline{T_f}(x) = \overline{T}_{f,in} + \frac{q'' \times P}{\dot{m} \times c_P} \times x \quad \text{(Eq. 23)}$$

To complete the experimental model validation, the experimental Nusselt number (Nu_{exp}), for any position along the tube axis, was obtained via Eq. 24, dependent on h_{exp}, D and fluid thermal conductivity (k_f).

$$Nu_{exp}(x) = \frac{h_{xp}(x) \times D}{k_f} \quad \text{(Eq. 24)}$$

As described in the literature review, experimental models for forced convective heat transfer studies are validated using the Shah equation (Eq. 12), for laminar flows, and the Gnielski or Dittus-Boelter equations (Eq. 13 and 14, respectively), for turbulent flows. All three formulas express a theoretical Nu, dependent on both Re and Pr, obtained through Eq. 25 and 26. Due to the aforementioned pump incapacity to supply turbulent flows, only the Shah equation was considered for experimental model validation.

$$Re = \frac{4 \times \dot{m}}{\pi \times \mu \times D} \quad \text{(Eq. 25)}$$

$$Pr = \frac{c_P \times \mu}{k} \quad \text{(Eq. 26)}$$

Chapter 4

Numerical Model

4.1. Initial Considerations

In order to develop the numerical model, using CFD simulation software, the experimental data obtained by Silva (2010), summarized in the previous chapter, was used. Consequently, a valid numerical model should yield similar heat transfer results to that of the experimental model, when tested under similar setup parameters. The main purpose of numerical model development is to allow a precise prediction of the forced convective heat transfer performance for the experimental nanofluid, particularly in the intermediate positions of the tube.

Experimentally, the fluid temperature at these positions ($\overline{T_f}$) was calculated via Eq. 23, from which the positional h_{exp} and, consequently, Nu_{exp} were determined. A successful numerical approach will allow a precise positional fluid temperature reading, thus increasing heat transfer result accuracy.

At the outset, a total of three numerical nanofluid models were to be developed using both the single-phase and the two-phase fluid approaches suggested by Xuan and Roetzel (2000), i.e., the nanofluid assumed a single-phase fluid and the nanofluid considered a solid-liquid dual-phase mixture. However, the two-phase approach involves a significant increase in required parameters, most of which lack any corresponding experimental data. In addition, there is no established nanoparticle behaviour model within the base fluid, so having to assume that nanoparticles behave in accordance to any given theoretical model implies a loss of accuracy. Therefore, to keep such uncontrollable parameters at a minimum, the single-phase approach was selected. This choice also allows for a certain degree of software independence, important for the present proposal where software adequacy to such small sized particles is unclear.

Unlike typical numerical approaches, that employ uniform domain meshes, the developed mesh for the current setup required particular refinement at the interface between the fluid surface and the inner tube surface where the highest temperature gradients are expected to occur. As with any numerical investigation, a mesh independence study was mandatory.

4.2. Model Development

The numerical model was established using Ansys® CFX 13 fluid flow analysis software, consisting of a CAD modelled test tube, presenting the same geometry as the one used for the experimental study. As with the experimental procedure, the tube functions as an indirect-contact tubular heat exchanger between heating tape and fluid.

4.2.1. Geometry and Mesh Generation

4.2.1.1. Geometry Setup

To facilitate domain definition, for subsequent manipulation, a three part CAD model was created: one, the fluid domain (L=1200 mm, D=6 mm), and the remaining two, symmetrical parts of the tube (designated tubes 1 and 2). A visualization of the assembly is available in Figure 5. The

two-part tube configuration also safeguards the necessity of a user-imposed symmetry boundary condition, reducing computational processing requirements in demanding cases. The tube inlet was positioned at the axis origin, while the uniaxial flow direction was elected to be the positive direction of the x axis.

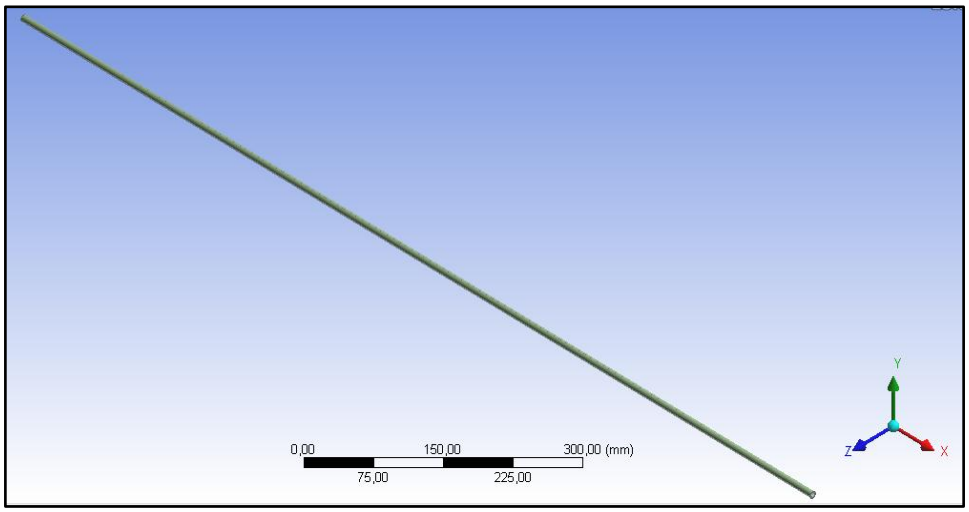

Figure 5 – Isometric view of the test tube geometry

4.2.1.2. Mesh Setup

Each of the domains employs a CFD simulation mesh method that uses tetrahedron type elements, these selected to be patch conforming, which enables 3D inflation at a desired boundary. Another feature of these meshes is the automatic smoothness and element growth control, promoting slick transitions and size variations, the latter manipulated by a specified growth factor. The alternative patch independent meshes, though better suited to boundary condition imposition, lack any type of local refinement capacity, rendering them less desirable to this setup.

4.2.1.2.1. Mesh Requirements

For controlled domain accuracy, the meshing process involves individual body and face element sizing manipulation. The separate-part element size management allows for local mesh refinements at particular regions of interest, particularly suitable for the current numerical approach. Additionally, the face element sizing process enhances the numerical simulation at the critical interface between the fluid surface and the inner tube surface. Naturally, smaller sized elements of the fluid domain at the material interface lead to the higher accuracy of the numerical model.

In addition to the smaller element size on the fluid domain surface, inflation layer meshing can be applied at the same boundary. This multilayer refinement further enhances the mesh at the fluid surface, thus increasing model accuracy in the complex near-wall region by using higher resolution elements where heat transfer from tube to fluid is expected to be at its highest, with large temperature gradients over small distances in perpendicular directions to that of the fluid flow. The total thickness control inflation option, where the number of layers, successive layer growth rate and maximum boundary thickness are set values, generates layers of equal heights.

4.2.1.2.2. Mesh Independence

The mesh quality is defined by its number of elements, each refinement offering higher quality and precision, but also increasing computational workloads. Mesh independence, i.e., the optimal point between mesh quality and pc workload, can be established when two successive refinements lead to equivalent results, the first of the two being the ideal mesh configuration.

In order to predict an adequate range of element sizes for value convergence testing, various theoretical formulas can be applied, but these become over-complex for separate part mesh assemblies, as well as local refinement procedures. Therefore, a coarse mesh was created and successive refinements developed, and simulated under the same input parameters for DIW, until a confident degree of independence was guaranteed. Due to the varying temperatures at both defined model domains, the fluid temperature at the outlet (T_{out}), in close proximity with the inner tube surface, and the tube outlet temperature ($T_{w,\,out}$) at 0.01 mm from the inner surface were the governing variables for the independence test. These measurement points were purposely selected to allow for a fully developed thermal interface between the developed fluid flow and the tube surface, as well as the outlet constituting a critical region. The element sizes of each of the three created meshes are described in Table 14 (organized from cruder to finer meshes).

Table 14 – Mesh Independence: Element Size Proposals

Model Domain	**Model Part**	**Mesh 1** $[mm]$	**Mesh 2** $[mm]$	**Mesh 3** $[mm]$
Fluid	Body	5	1	0.5
	Surface	0.05	0.01	0.005
Tube	Tube1	5	1	0.5
	Tube2	5	1	0.5
Number of Elements		1631982	2520747	4229153

Additionally, the applied inflation at the fluid domain surface also undertook successive refinements for each of the proposed meshes. Obviously, such a critical region demands minimal discretization errors. Therefore, the combined thickness of all layers was consecutively reduced to 0.15 mm and the number of layers successively increased to 12, as can be observed in Table 15.

Table 15 – Mesh Independence: Mesh Inflation Proposals

Parameter	**Mesh 1**	**Mesh 2**	**Mesh 3**
Number of Layers	8	10	12
Growth Rate	1.2	1.1	1
Maximum Thickness [mm]	1.5	0.15	0.1

The DIW simulation input parameters for independence testing, common to each of the tested meshes, as well as further mesh testing features, are presented in Appendix A.

The optimal mesh configuration was obtained between Mesh 2 and Mesh 3, when the difference between the consecutive mesh temperatures is negligible, recognizable tendencies in Figure 6. The temperature variations between these meshes are approximately 0.003 K, for the fluid temperature (T_{out}), and 0.001 K, for the tube temperature ($T_{w,\,out}$), hence mesh independence can be assumed.

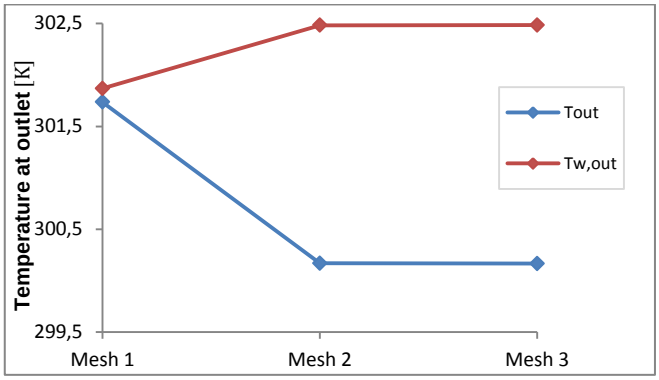

Figure 6 – Mesh independence: Temperatures at outlet for tested meshes

Due to the reduced computer workload without the loss of precision, Mesh 2 was elected to be employed for the present model, all residual targets reached before 80 iterations, as can be visualized in Appendix A. The following figures (Figure 7, 8 and 9) establish a visual representation of the generated part meshes.

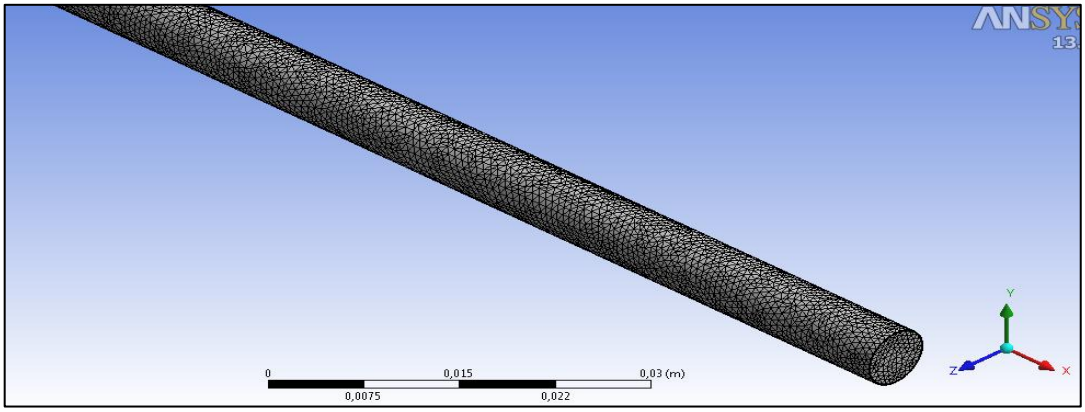

Figure 7 – Isometric view of the fluid domain mesh at the outlet region

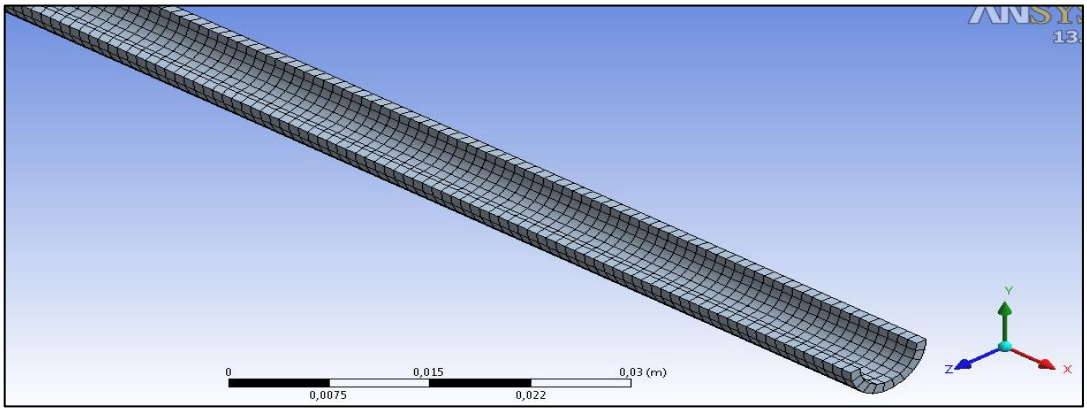

Figure 8 – Isometric view of the tube domain mesh in the outlet region

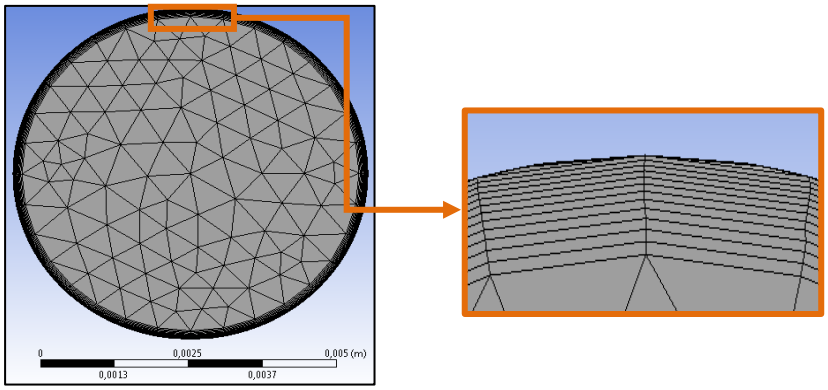

Figure 9 – View of the inflated boundary mesh layers at tube inlet

4.2.2. Material Definition

Each of the defined materials, including the single-phase CNT/DIW nanofluid, is established as a pure substance. During material definition, five fundamental input parameters were required to be specified, these summarized in Table 16. As can be observed, most of the fluid parameters are experimental results, an important advantage of the numerical approach using the single-phase nanofluid. The exception is the material molar mass; the pure substance molar masses correspond to the Periodic Table values, while the molar mass of the single-phase nanofluid results from Eq. 27, taking into account the volume fractions and pure substance masses of the dual-phase mixture:

$$M = (\phi \times M)_{np} + (\phi \times M)_{bf} \quad \text{(Eq. 27)}$$

The experimental tube domain material is stainless steel, grade 316 (UNS S31600 or EN1.4401), an austenitic steel with high corrosion resistance, but reduced k when compared to common steels (Atlas, 2011).

Table 16 – Material Input Parameters

Material	Input Parameter	Units	Value	Source
DIW	Molar mass (M)	g/mol	18.015	Periodic table
	Density (ρ)	kg/m^3	997	Table 12
	Heat capacity (c_P)	$J/kg\ K$	4179	
	Thermal conductivity (k)	$W/m\ K$	0.605	
	Dynamic viscosity (μ)	$N\ s/m^2$	0.000855	
CNT/DIW nanofluid	M	g/mol	17.999	Eq. 27
	ρ	kg/m^3	1197	Table 12
	c_P	$J/kg\ K$	4384	
	k	$W/m\ K$	0.626	
	μ	$N\ s/m^2$	0.00135	
Stainless Steel 316	M	$kg/kmol$	55.85	CFX library
	ρ	kg/m^3	8000	Atlas (2011)
	c_P	$J/kg\ K$	500	
	k	$W/m\ K$	16.3	

4.2.3. Boundary Conditions

In order to enable an adequate approximation to the fluid flow and heat transfer characteristics supplied by the remaining experimental apparatus, several assumptions were considered and a total of three boundary conditions were applied: one for the tube domain and two for the fluid domain. Additionally, a fluid-solid contact interface was used to account for the heat transfer between domains.

4.2.3.1. Model Assumptions

Before boundary conditions could be set, further suppositions regarding the system operating conditions were required to be made. Due to the fewer required specifications, all numerical simulations were conducted under a steady-state flow regime, assuming flow continuity. In comparison to a transient flow analysis, the disadvantage of an apparent precision loss is surpassed by the necessity to keep experimentally undetermined parameters at a minimum. In addition to the aforementioned single-phase fluid feature, the operating fluid was assumed incompressible. Additionally, all numerical simulations employed the K-Ɛ turbulence model.

The thermophysical properties of the stainless steel tube were assumed to be independent of the temperature. The same consideration was applied to the fluid properties, in this case less influential due to the expected temperature variations being confined to proximal values to that at which these were experimentally determined ($T = 300\ K$).

The heat supplied by the heating tape was considered to be evenly distributed along the tube surface. Additionally, heat interaction between the tape outer surface and the surrounding environment was neglected, the same with the tube's inlet and outlet faces, thus denoting a fully insulated setup.

4.2.3.2. Tube Domain

In the experimental study the tube was heated, at a quasi-constant heat rate, using heating tape. For the numerical model, the role performed by the heating tape is provided by a constant wall heat flux boundary condition, where the heat flux along the external tube surface is set to be the corresponding value experimentally used. As observed in the literature review, this is a compulsory boundary condition for numerical studies involving fluid flows within heated tubes, allowing the tube to act as a heat exchanger between the heating instrument and the operating fluid. With exception to the heat transfer surface between domains, the non-heated regions of tube, including the tube part junction surfaces and the inlet and outlet tube faces, were set to be adiabatic, thus guaranteeing an absence of unrealistic heat losses across these regions.

4.2.3.2. Fluid Domain

The two fluid boundary conditions are defined at the tube inlet and outlet. At the inlet, the domain flow direction (perpendicular to the boundary condition) and mass flow rate are specified. Additionally, the initial temperature and velocity (u), calculated using the following equation, of the entering fluid are set.

$$u = \frac{\dot{m}}{\rho \times A} \quad \text{(Eq. 28)}$$

In order for the model to account for local fluid recirculation, especially important for turbulent flows, a null relative pressure boundary condition is defined at the outlet.

4.2.3.3. Tube/Fluid Interface

The bulk of the heat quantity exchanged between both domains occurs at the interface between fluid wall and inner tube surface. In addition to the described refined mesh features, a domain interface with conservative contact heat flux was defined.

4.2.4. Temperature Prediction Situation

As described in the previous chapter, the experimental tube temperature measurements were obtained using thermocouples positioned on the outer tube surface at each point of the tube, specified in Table 13. The experimental tube surface temperatures were measured at the outer tube surface, while the fluid temperature measurements were taken at inlet and outlet, in the vicinity of the flow axis, whereas the intermediate position fluid temperatures were evaluated using Eq. 23. Numerically, the fluid temperatures can be directly obtained from the processed results. Therefore, numerical temperature predictions at two distinct domain positions are required:

- $T_f\ (x)$: The fluid temperature reading along the central axis of the fluid flow;
- $T_S\ (x)$: The tube external surface temperature measurement (4 mm from the fluid flow axis).

4.3. Model Validation

4.3.1. Proposed Simulations

The experimental results were validated via five independent experimental measurements for each Re, at each of the seven points of the test tube specified in Table 13. Re (Eq. 25) was controlled by fluid mass flow manipulation, this under peristaltic pumping power adjustment. For all the conducted experiments the heating power of the tape, wrapped around the tube and regulated by a potentiometer, was maintained at 108 W. (Silva, 2010)

For numerical model validation, the selected input values, for each Re, were the average of the five experimental temperature measurements of the fluid, at the inlet ($T_{f,in}$), as well as the respective fluid velocities (u_{in}). The constant wall heat flux value (q_{cw}''), performing the role of the heating tape, employed at the outer tube surface (A_{ext}), was calculated via the application of Eq. 22, i.e.:

$$q_{cw}'' = \frac{q}{A_{ext}} = \frac{q}{\pi \times D \times L} = \frac{108}{\pi \times 0.008 \times 1.2} = 3581.021\ W/m^2$$

Experimentally, heat transfer results were obtained for both DIW and the CNT/DIW nanofluid at three distinct Re. Therefore, the numerical model was validated by performing numerical simulations for each set of conditions, adding up to a total of six simulations. Table 17 designates each numerical simulation and displays its relevant input parameters.

Table 17 – Proposed Validation Simulations and Relevant Parameters

Simulation	Fluid	$\dot{m}$ $[Kg/s]$	μ $[N\,s/m^2]$	Re	$T_{f,in}$ $[K]$	u_{in} $[m/s]$
VAL1		0.004982		1236.51	296.85	0.1767
VAL2	DIW	0.006648	0.000855	1649.75	299.75	0.2358
VAL3		0.008304		2061.05	300.45	0.2947
VAL4		0.007860		1235.51	297.15	0.2322
VAL5	CNT/DIW	0.010494	0.001350	1649.55	297.25	0.3101
VAL6		0.013110		2060.33	297.05	0.3872

4.3.2. Validation Results

4.3.2.1. Temperature

Despite following a similar positional trend to that of the experimental measurements the numerical results display temperature under-prediction, for both fluid and tube domains. Possible mechanisms that may lead to these discrepancies will be discussed later. All involved temperatures, as well as temperature distribution representations, are tabled in Appendix B.

4.3.2.1.1. Tube Domain

The numerical surface temperatures positionally increase with the flow direction, demonstrating a general consistency with the experimental results. As with common heat exchangers, the effects of advection are highest in the fluid entry region, therefore the surface temperature would be expected to be at its lowest here. However, the numerical values exhibit a linear variation with the tube position, contrarily to the experimental temperatures, as can be observed in the Figure 10.

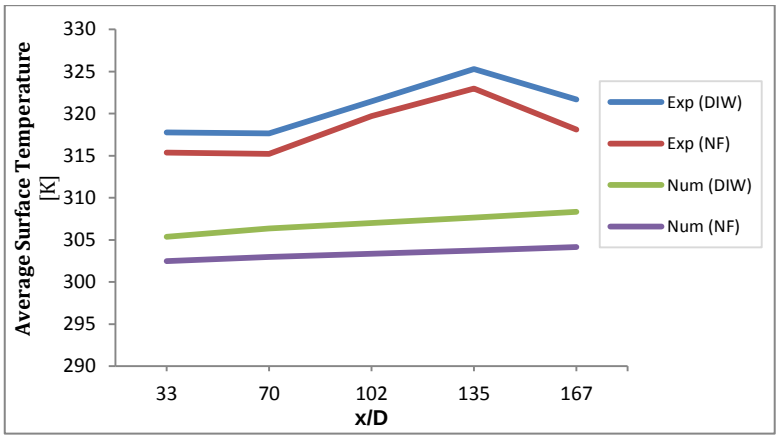

Figure 10 – Comparison of the experimental (Exp) and numerical (Num) average tube surface temperatures at each position.

Another immediate observation is the lower tube surface temperature when operating with the nanofluid, indicating a superior heat transfer performance over DIW alone. At first glance, this enhancement between fluids is superior for the numerical model; however the numerical data assumes the same initial tube temperature for all simulations, whereas for the experimental study this is not necessarily the case. The following figures (Fig. 11 and 12) compare the numerical tube surface temperature for both operating fluids, at the same Re. The apparent advantage of nanofluid employment is most visible from approximately x/D=33 onward (from left to right).

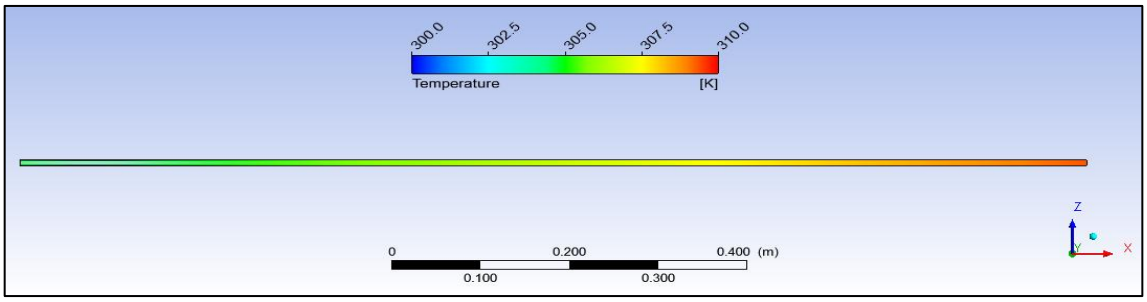

Figure 11 – Numerical tube surface temperatures for DIW at Re=1236.

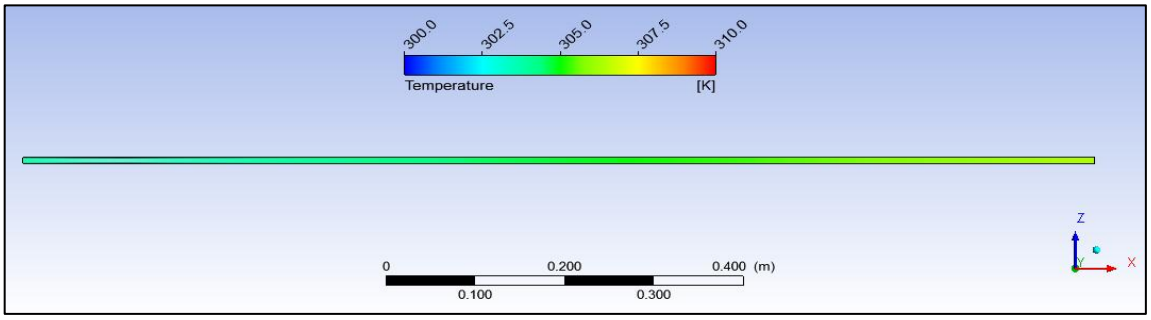

Figure 12 – Numerical tube surface temperatures for CNT/DIW nanofluid at Re=1236.

4.3.2.1.2. Fluid Domain

4.3.2.1.2.1. Intermediate Positions

As previously referred, the experimental setup only allowed for thermocouple placement at the inlet and outlet, the intermediate fluid temperatures being calculated theoretically using Eq. 23. When compared to the experimental data, the numerical results demonstrate a similar trend to that of the tube surface temperature variation with respective position. However, the experimental trend is more linear and discrepancies for the fluid domain are smaller, observable in Figure 13. Despite this, both sets of data exhibit higher average temperatures of DIW than the matching nanofluid temperatures.

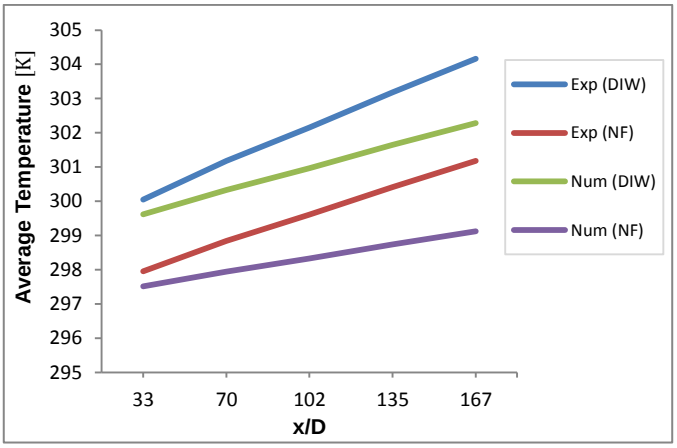

Figure 13 – Comparison of the experimental (Exp) and numerical (Num) average fluid temperatures at each position.

4.3.2.1.2.2. Outlet Temperatures

At the outlet, experimental and numerical temperatures generally display good agreement, result proximity increasing with increasing Re. As can be observed in the following table, the numerical data exhibits an under-predicting trend when matched to the experimental results.

Table 18 – Comparison of Experimental and Numerical Fluid Temperatures at Outlet

Simulation	Fluid	Re	T_{in} $[K]$	$T_{out,Exp}$ $[K]$	$T_{out,Num}$ $[K]$
VAL1		1236.51	296.85	308.15	301.90
VAL2	DIW	1649.75	299.75	303.65	303.52
VAL3		2061.05	300.45	302.65	303.46
VAL4		1235.51	297.15	305.65	300.20
VAL5	CNT/DIW	1649.55	297.25	300.55	299.53
VAL6		2060.33	297.05	299.85	298.87

Figure 14 enables the temperature distribution visualization of the nanofluid at the tube outlet. Despite the tiny gradients, one can observe that the maximum temperatures are quite expectedly reached at the tube/fluid interface, whereas the minimum fluid temperature is typically in the flow axis region (tube centre).

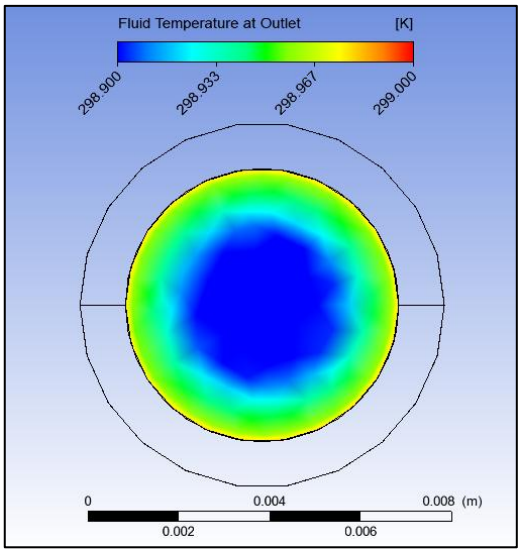

Figure 14 – Fluid temperature distribution at outlet for CNT/DIW nanofluid at Re=2060.

4.3.2.1.3. Temperature Divergence Mechanisms

Ideally, experimental and numerical results would be identical. However, the numerical model displays temperature under-predictions in both domains, most significantly in the tube domain. The primary culprit for the observed temperature discrepancies is the steady-state nature of the numerical analysis.

Experimentally, the fluid and the heating tape interact, via the tube, for different time intervals, ranging from 45 minutes to over 3 hours, with minute-to-minute temperature measurements that are consequently averaged. The prolonged time intervals involved enable vast quantities of heat to be transferred to fluid and tube domains, result of the continuous power supply of 108 W.

On the other hand, the numerical analysis is time independent, the power transferred to the tube is not accumulative. The defined heat flux (q_{cw}'') is transferred to the system in one drive, which accounts for the significant discrepancies reported for the tube surface temperatures. This notion is supported by the respective heat quantities entering the fluid, listed in Table 19. Obviously, a higher approximation between experimental and numerical data would be gained if the numerical model were to perform a transient analysis.

Other possible inconsistency mechanisms could derive from the experimental setup, such as local heat losses or irregular heat supplies at different tube locations. Also, there is no robust indication that the experimental setup is fully insulated. As for the experimental fluid temperatures, the two measurement thermocouples were roughly positioned near the flow axis, without any sort of visual aid. Naked-eye positioning for such a small diameter tube does have the potential to cause thermocouple misplacement or the non-alignment between inlet and outlet thermocouple measurement tips, leading to erroneous evaluations. Additionally, the intermediate fluid temperatures, calculated using Eq. 23, display over-prediction when compared to the numerical values taken along the flow axis. Again, this can be credited to the steady-state analysis returning decreased numerical heat fluxes entering the fluid without the extended timescale. However, from Eq. 23 one can also deduce that it lacks to account for heat transfer saturation, allowing the

average fluid temperature to increase infinitely for infinitely growing tube length, thus increasing the uncertainty associated to experimental h and Nu calculations.

Table 19 – Comparison of Experimental and Numerical Power and Heat Quantities Entering the Fluid

Simulation	Fluid	Re	$Q_{in,Exp}$ $[W]$	$Q''_{in,Exp}$ $[W/m^2]$	$Q_{in,Num}$ $[W]$	$Q''_{in,Num}$ $[W/m^2]$
VAL1	DIW	1236.51	244.151	10794.19	105.202	4651.102
VAL2		1649.75	104.995	4641.929	104.766	4631.806
VAL3		2061.05	95.133	4205.926	104.419	4616.495
VAL4	CNT/DIW	1235.51	290.839	12858.27	105.167	4649.519
VAL5		1649.55	152.734	6752.55	104.755	4631.323
VAL6		2060.33	165.150	7301.45	104.431	4616.987

4.3.2.2. Convective Heat Transfer Coefficient

Experimental and numerical coefficients were calculated via Eq. 21, the numerical results calculated using the fluid temperature readings from the flow axis, rather than the mean positional temperature ($\overline{T_f}$), calculated via Eq. 23, applied for experimental data treatment. Due to the total absence of heat losses, one would expect the numerical model to yield increased coefficients when compared to the experimental results. Additionally, typical heat exchanger behaviour predicts higher convective heat transfer in the fluid entry region, decreasing with trajectory length. Of the operating fluids, one can foresee coefficient enhancements of the nanofluid over DIW, as the experimental investigation, and most studies in the literature review, demonstrate. Another, practically, consensual conclusion from the literature review is the typical increase in heat transfer performance with increasing Re.

In general, the numerical model yields superior values of h to that of the matching experimental data. Due to the aforementioned full thermal insulation of the numerical setup, this was expected. However, both sets exhibit different coefficient variations at different tube positions. The numerical values are highest in the tube entry region and slightly decrease with tube length, except at x/D=135, where a slender increase in h is observed for both fluids, hardly visible in the following figure of average coefficients. Experimentally, the fluids display more abrupt variations, the highest coefficients viewed at x/D=70 and x/D=167, as is represented in Figure 15. This difference is most likely due to the steady-state flow defined for the numerical model.

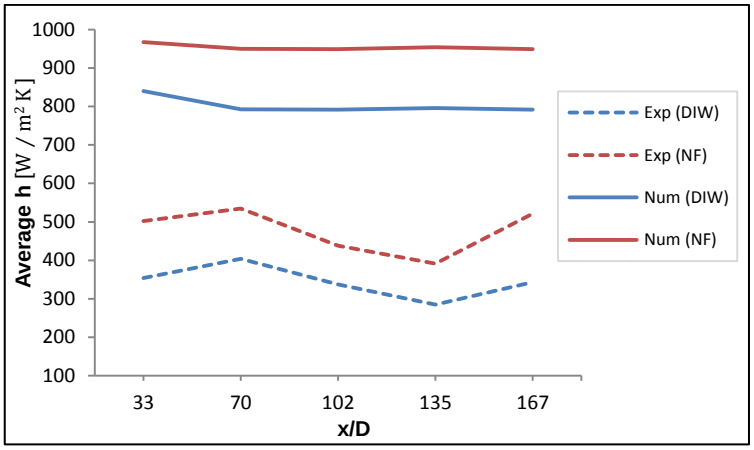

Figure 15 – Comparison of the experimental (Exp) and numerical (Num) average heat transfer coefficients at each position.

One of the main differences between the experimental and numerical results is the coefficient variation with varying Re, the models displaying opposite trends. The numerical model predicts increasing fluid heat transfer performances accompanying increasing Re, thus following the tendency reported in the majority of the experimental studies covered in Chapter 2, quite particularly the studies using MWCNT nanofluids conducted by Amrollahi et al. (2010) and Ding et al. (2006). This is also in agreement with the standard theoretical behaviour of common operating fluids circulating through heat exchangers.

On the other hand, the experimental results demonstrate a clear decrease in the heat transfer capabilities of both fluids with increasing Re, under mass flow rate increase, supporting the conclusion presented by Garg et al. (2009). A comparison between the data returned by each of the models is established in Figure 16. One may speculate over several mechanisms that contribute to this unexpected tendency, but there are two immediate candidates: the physical setup and the timescale setup.

The witnessed experimental decrease could be credited to an insufficient tube length, not enabling the fluid flow to fully develop before reaching the outlet. In such a case, the higher the mass flow rate the less thermodynamically developed the fluid flow, hence the decreasing heat transfer performances with increasing Re.

The observed tendency may also be caused by the varying experimental time intervals over long ranges. For shorter periods, one would expect an inferior global heat flux transmitted to the system which, as can be deduced from Eq. 21, will yield decreased coefficients. The experimental heat fluxes to the fluid, listed in Table 19, generally decrease with increasing mass flow rates. Lotfi et al. (2012) reached a similar conclusion after investigating nanofluid performance for different heating powers, finding that increased heating powers lead to improved fluid heat transfer performance.

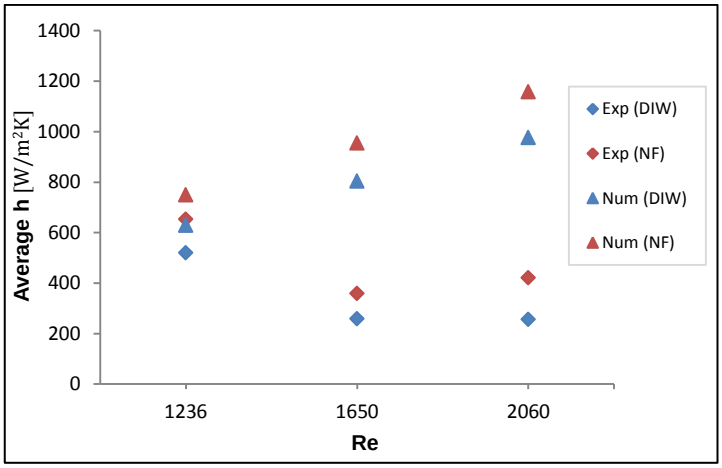

Figure 16 – Comparison of the experimental (Exp) and numerical (Num) average heat transfer coefficients as function of Re.

Perhaps the most significant of the observable trends in the previous figure is the superior heat transfer performance displayed by the nanofluid. This result is substantial, especially if one recalls the tiny nanoparticle concentration used, which bodes well for nanofluid applicability in the most demanding environments. The average enhancement of h of the nanofluid over DIW, as function of Re, is displayed Figure 17. Experimental and numerical data evolve in contradictory fashion, the numerical enhancement decreasing linearly at an extremely reduced rate. Despite the discrepancies, one can confidently conclude that nanofluid employment does indeed improve the overall efficiency of heat exchangers.

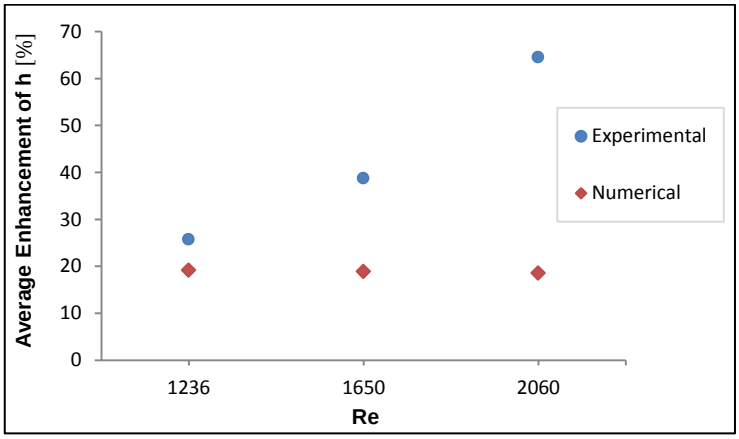

Figure 17 – Average heat transfer coefficient enhancements as function of Re.

In a positional analysis, similar trend divergences between experimental and numerical data can be observed in Figure 18. Numerically, the average enhancement is minimal in the tube entry region, varying subtly to its maximum at x/D=135. Again, this can be credited to the steady-state flow approach used for the numerical model. The variation of the experimental enhancements is more pronounced, result of the transient dynamical fluid behaviour, the maximum improvement being observed at x/D=167.

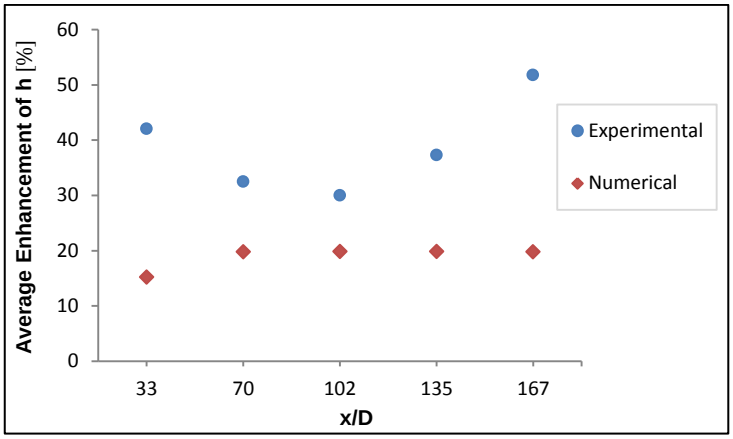

Figure 18 – Average heat transfer coefficient enhancements as function of position.

4.3.2.3. Nusselt Number

The Nusselt number is experimentally and numerically evaluated using Eq. 24. Due to the limitation of the peristaltic pump in guaranteeing turbulent flows, only laminar flows were tested during the validated experimental study, meaning that the inherent theoretical results for Nu originate from the formulation presented by Shah (Eq. 12). During the data processing, the experimental author mistakenly employed the conductivity of saturated water (k=0.613 W/m K) instead of the value of DIW, leading to slight under-predictions in Nu and Pr (Eq. 26) calculations. In the present study, corrections were made to Pr in order to calculate corrected theoretical results.

Essentially, Nu quantifies the contribution of advection over diffusion in the global fluid heat transfer. Heat transfer via advection is typically highest in the fluid entry region, where convection is at its maximum, effects of diffusion commonly most notorious in regions following full thermal boundary layer development. This tendency can be observed for the numerical and theoretical results displayed in Figure 19, as well as with most convective heat transfer investigations reported in the literature. As with the average values of h, the average experimental Nu unusually peaks at x/D=167, i.e., where the effect of an increased k, property of diffusive heat transfer, decreases Nu due to its maximized contribution. The lack of dynamic heat transfer, result of the imposed steady-state regime, is clear for the numerical data with its ever-present linearity. Despite exhibiting the most realistic of the trends, the Shah theoretical equation is found to generally over-predict the fluid heat transfer performances, perhaps due to having been formulated for larger diameter tubes, as proposed by Silva (2010).

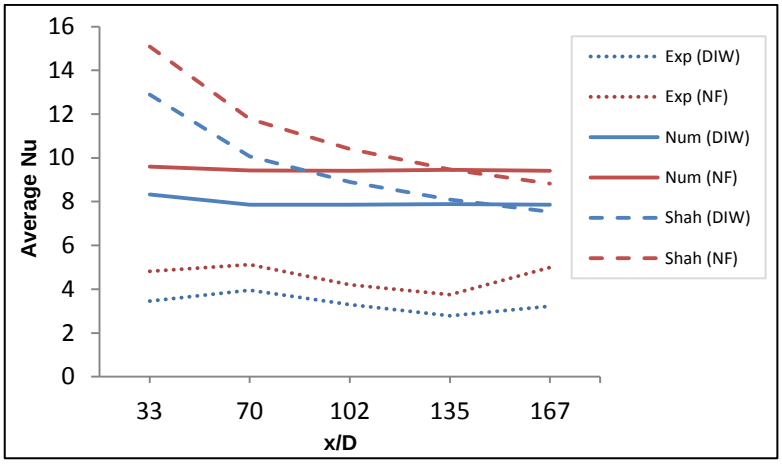

Figure 19 – Comparison of the experimental (Exp), theoretical (Shah) and numerical (Num) average Nusselt numbers as function of position.

As for the influence of Re, Nu follows a similar tendency to that of h, which implies divergent behaviours between models. While the experimental average Nu decreases with increasing Re, the numerical counterpart increases with the addition of turbulence to the flow. The tendency displayed by the numerical model is supported by the corresponding theoretical results, yielded by the Shah equation. This trend resemblance, also reported by Ding et al. (2006), can be observed in the Figure 20.

All models display improved heat transfer characteristics of the CNT/DIW nanofluid over that of the base fluid alone. The largest of these enhancements is the experimental value at Re=2060, which corresponds to an improvement of just over 60%. The numerical and theoretical enhancements exhibit an almost independence of Re, at least this can be affirmed for values ranging from 1236 to 2060. The numerical Nu enhancement demonstrates a slowly decreasing behaviour, whereas the enhancement of Nu using the Shah equation is almost constant at 16.9%.

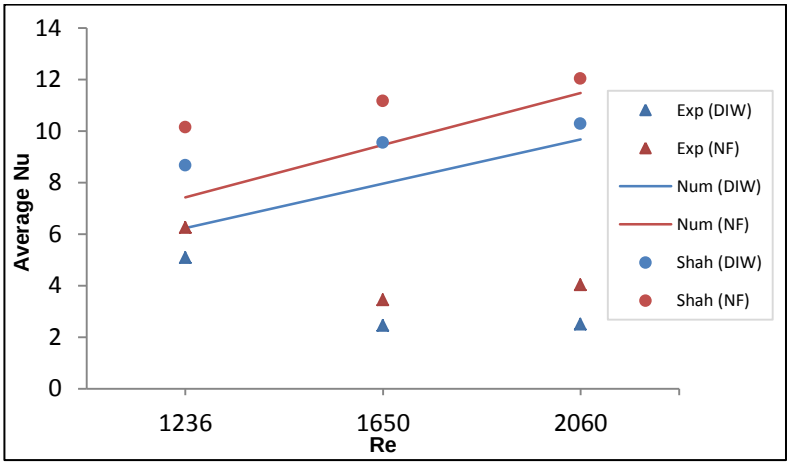

Figure 20 – Comparison of experimental (Exp), numerical (Num) and theoretical (Shah) average Nusselt numbers as function of Re.

Chapter 5

Heat Transfer Mechanism Analysis

5.1. Summary

Once an adequate validation is accomplished, the numerical model can be submitted to parametric testing with the intent of investigating the effect of possible mechanisms on the heat transfer enhancements of the CNT/DIW nanofluid over DIW. At this stage the disadvantage of employing the single-phase colloid approach for the nanofluid, proposed by Xuan and Roetzel (2000), becomes most confining. Evaluations of significant parameters associated to the nanotubes, which could be verified using a two-phase numerical model, cannot be performed. The investigation into the heat transfer contribution of particle properties such as aspect ratio, length or diameter could ultimately lead to a confident understanding of the roles played by Brownian motion or particle agglomeration in the witnessed heat transfer enhancements of nanofluids. However, there is still a lack of sufficient nanoparticle behavioural data to currently enable any accurate dual-phase predictions, as discussed previously. Nonetheless, the single-phase model still allows the parametric study of several of the possible enhancement mechanisms, debated in the literature review.

5.2. Fluid Parameters

5.2.1. Flow Rate

As covered in the literature review, it is well known that an increase in heat transfer performance can be achieved by turbulence induction in the operating fluid. A straightforward, but not necessarily the most efficient, manner of increasing Re is to intensify the fluid mass flow, quite especially for laminar flows. Typically, this leads to augmented fluid heat transfer capabilities, but does come at the cost of an increased necessary pumping power, which negatively contributes to energy rationalization. Obviously this form of turbulence generation should be avoided; however some heat transfer applications are far too demanding to allow for alternative, cost-friendly solutions. Therefore, nanofluid behaviour under turbulent flows merits an influence analysis.

In order to achieve a numerical estimate of the influence of the mass flow rate on the performance of the nanofluid, a total of eight simulations (FR1 to FR8) are proposed. To parametrically establish an estimate of the enhancement of the flow rate, a set of input parameters remain constant throughout the proposed studies. These, displayed in Table 20, originate from the closest approximation of the numerical model to the experimental heat transfer results, found to be at $Re \approx 1236$ (corresponding to VAL1 and VAL4 simulations from the previous chapter).

The purpose of the proposed simulations, listed in Table 21, is not only to assess the influence of turbulence to the heat transfer, but also to evaluate fluid behaviour at lower Re laminar flows than those already investigated. If the same nanofluid heat transfer enhancement levels witnessed at higher Re were to remain unchanged at $Re<1000$, this would deem nanofluid application beneficial in what concerns sustainability in heat transfer systems, the result of an efficient heat transfer with minimal energy requirements.

Table 20 – Fixed Parameters for Flow Rate Influence Simulations

Parameter	Units	Value
Dynamic viscosity (μ)	$\mathrm{N\,s/m^2}$	$0.000855\ (\mathrm{DIW});\ 0.00135\ (\mathrm{NF})$
Fluid inlet temperature ($\boldsymbol{T_{in}}$)	K	297
Specific heat capacity ($\boldsymbol{c_P}$)	$\mathrm{J/kg\,K}$	$4179\ (\mathrm{DIW});\ 4384\ (\mathrm{NF})$
Thermal conductivity ($\boldsymbol{k}$)	$\mathrm{W/m\,K}$	$0.605\ (\mathrm{DIW});\ 0.626\ (\mathrm{NF})$
Total heat flux ($\boldsymbol{q_{cw}''}$)	$\mathrm{W/m^2}$	3581.021

Table 21 – Flow Rate Influence: Simulation Proposals

Simulation	Fluid	$\dot{\boldsymbol{m}}$ $[\mathrm{Kg}/\boldsymbol{s}]$	$\boldsymbol{Re}$	$\boldsymbol{u_{in}}$ $[\boldsymbol{m/s}]$
FR1	DIW	0.00302	750	0.1071
FR2		0.02014	5000	0.7146
FR3		0.03022	7500	1.072
FR4		0.04029	10000	1.429
FR5	CNT/DIW	0.00477	750	0.1410
FR6		0.03181	5000	0.9400
FR7		0.04771	7500	1.410
FR8		0.06362	10000	1.880

5.2.1.1. Laminar Flows

At Re=750 (simulations FR1 and FR5), both fluids expectedly display a decrease in their heat transfer performance, maintaining a similar diminishing tendency, with decreasing Re, to the observed during model validation. However, as can be perceived in Figure 21, results indicate the highest value of h is no longer in the tube entry region, but at its lowest. The best enhancement in the heat transfer of the nanofluid over DIW is registered at x/D=135, peaking at 22.84 %. When compared to the enhancements obtained during model validation (displayed in Fig. 17), the average enhancement maintains the increasing tendency with decreasing Re, supporting the experimental observation of Garg et al. (2009) but contradicting the experimental tendencies reported by Silva (2010), as covered in the previous chapter, and Wen and Ding (2004a).

The higher heat transfer enhancement of the nanofluid over DIW at lower Re, indicated by the numerical results, suggests that the most advantageous application of nanofluids is at low Re laminar flows. This notion is also backed by the lower nanofluid pressure drop for such flows, proximate to that of the base fluid alone, when compared to the magnitudes of pressure loss for turbulent flows, these soon to be addressed.

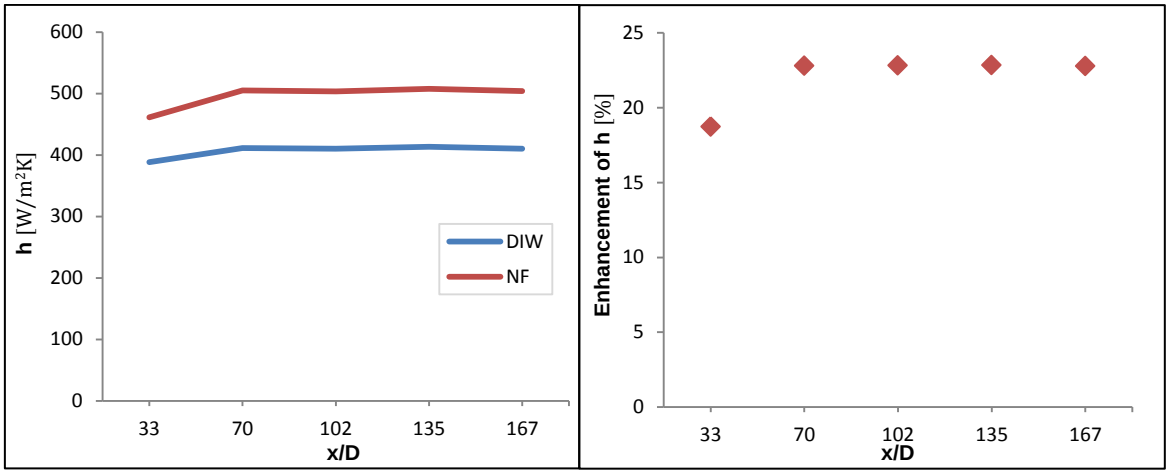

Figure 21 – Positional heat transfer coefficient (left) and respective nanofluid enhancement over DIW (right), at Re=750

Contrary to the observed trend for the validation proposals, Nu displays a diverging trend when matched to the corresponding theoretical predictions calculated using the Shah correlation, which expectedly demonstrate higher heat transfer performances in the tube entry section (Figure 22). A noteworthy variation of the theoretical Nu occurs for DIW from x/D=135 onwards, result of the application of the alternative branch of the Shah equation for these positions, when:

$$\left(Re\ Pr\ {}^{D}/_{x}\right) < 33.3$$

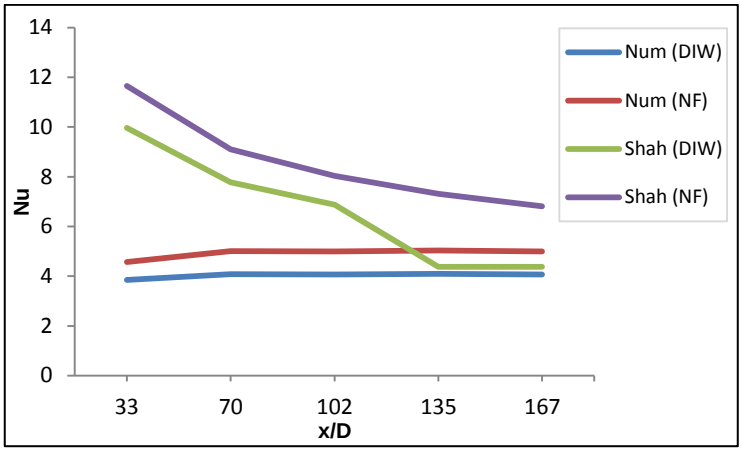

Figure 22 – Comparison of the theoretical (Shah) and numerical (Num) Nusselt numbers as function of position, at Re=750.

5.2.1.2. Turbulent Flows

Fundamentally, the purpose of creating turbulence in the flow is to enhance the fluid heat transfer performance. Turbulence can be applied to a fluid via active techniques, such as fluid mass flow increases or induced vibration, or passive techniques, such as the addition of fins or baffles. As referred in the literature review, active techniques require the addition of power to the heat exchanging systems, be it due to mechanical stimulation devices or increased pumping power. Despite significantly improving the output of heat transfer systems, such practices should be avoided in a long-term sustainability perspective. However, several exigent heat transfer

applications demand significant quantities of heat dissipation which can only be achieved via turbulence maximization. Therefore, the study of nanofluid heat transfer behaviour under turbulent flows will be of interest for potential application in more challenging scenarios.

In order to gain an adequate understanding of fluid performance under turbulent flows, simulations were carried out for three distinct turbulent flows, as presented in Table 21 (simulations FR2 to FR4, for DIW, and FR5 to FR8, for the nanofluid). The resulting average positional h can be observed in Figure 23 (left), where the expected heat transfer improvements, in comparison to the analysed laminar flows (Fig. 15 and 21), can be easily confirmed. Pak and Cho (1998) and Amrohalli et al. (2010) reported similar findings following experimental testing of nanofluids for laminar and turbulent flows.

Figure 23 also exhibits the positional heat transfer enhancements of the nanofluid over DIW for the turbulent flows. In this case, the enhancement in the entry region is half that of the following tube positions, contradicting the experimental results of Nguyen et al. (2007). This can be credited to the high fluid velocities, with increasing Re, not allowing a fully developed flow until reaching x/D=70. Additionally, the already remarked tendency of a decreasing enhancement of h with increasing Re continues for turbulent flows, the average value peaking at 17.23%, at x/D=102. The linear, tiny enhancement decrease with increasing Re (15.69 % at Re=5000 and 14.33 % at Re=10000) supports the outcomes of Foutukian and Esfahany (2010), as well as the claims of Liu and Liao (2010), the latter concluding that the enhancements of h are minimally dependent on Re.

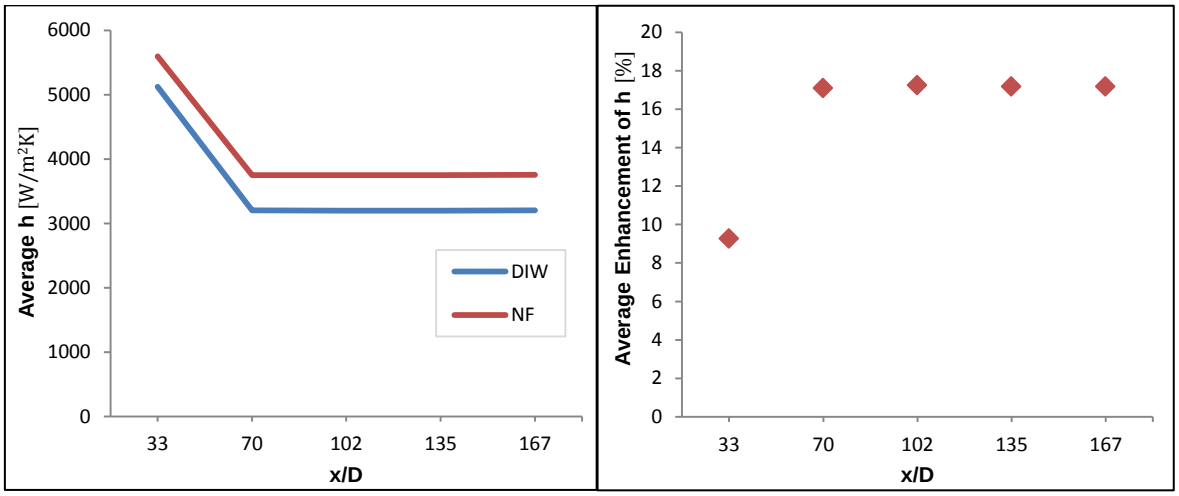

Figure 23 – Average positional heat transfer coefficient (left) and respective nanofluid enhancement over DIW (right), for turbulent flows.

As for Nu, the numerical tendency revealed in the validation results maintains itself, growing linearly with Re, perceptible in Figure 24. For turbulent flows the most common theoretical correlations used in data validation are the Gnielinski (Eq. 13) and Dittus-Boelter (Eq. 14) correlations, both position independent, unlike the Shah correlation for laminar flows. As can be observed in Fig. 24, the numerical data demonstrates good agreement with the Gnielinski equation, displaying a slight over-prediction that decreases with increasing Re. On the other hand the Dittus-Boelter prediction significantly over-predicts the numerical Nu, despite revealing a similar growth trend.

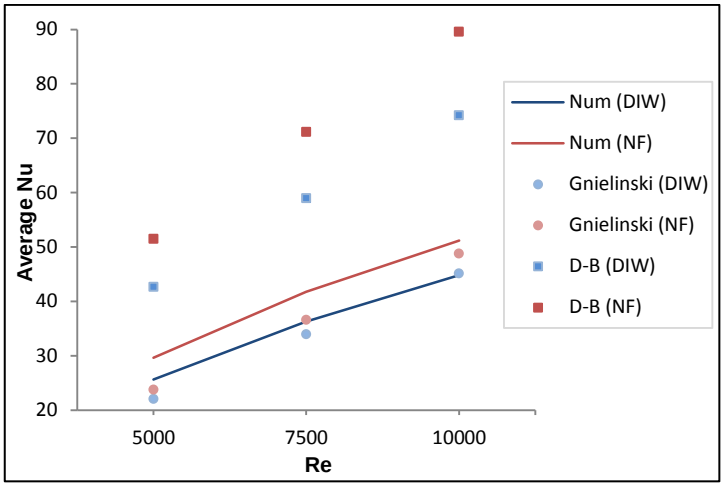

Figure 24 – Comparison of the theoretical (Gnielinski and Dittus-Boelter, D-B) and numerical (Num) average Nusselt numbers as function of Re, for turbulent flows.

An important factor in heat exchanger technology is the undesired fluid pressure drop, quite especially for turbulent flows. Typically, the pressure drop significantly increases with increasing Re, which is the motive for turbulence addition to any given flow requiring increased pumping power. In order to improve exchanger efficiency, this parameter should be minimized. Figure 25 compares the pressure drops, between inlet and outlet of both operating fluids as function of Re. As can be observed, the results indicate that the application of nanofluids will always lead to higher pressure drops, which grow exponentially with increasing turbulence. These could be attributed to the higher viscosity of the nanofluid, the same conclusion reported by He et al. (2007), who also claimed that the difference in the pressure drop of nanofluids and DIW is minimal for laminar flows, which indeed occurs for the present numerical model, at Re=750. In a rational energy management perspective, results indicate that the advantage of nanofluid employment over DIW decreases in turbulent flows, despite the significant heat transfer gains.

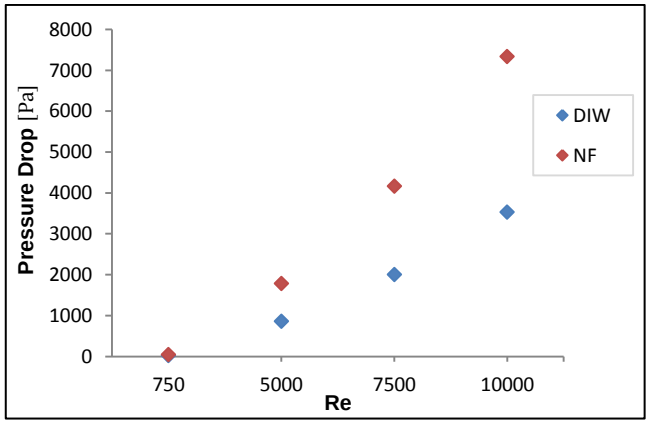

Figure 25 – Comparison of the pressure drops of DIW and the nanofluid, as function of Re.

5.2.2. Thermophysical Properties

The following parametric tests investigate the contribution of nanofluid thermophysical properties to the heat transfer enhancement, under a single-phase approach for five different CNT volume fractions: 0.5, 1, 1.5, 2 and 2.5 vol. %. As referred the single-phase approach cannot

account for volume fraction variations, the fluid is defined as a pure substance. In order to obtain a confident approach that enables such an analysis with a confident degree of precision, individual thermophysical properties required to be varied accordingly to the corresponding volume fraction. Different CNT concentrations obviously lead to different nanofluid thermophysical properties, such as fluid density (ρ), thermal conductivity (k), specific heat capacity (c_P) and dynamic viscosity (μ). To this effect, the employed input fluid parameters for numerical testing should be carefully selected, otherwise the obtained heat transfer results will lack any sort of precision. Therefore, for each of the investigated volume fractions, realistic thermophysical properties need to be defined, these displayed in Table 22.

5.2.2.1. Specific Heat Capacity, Density and Molar Mass

Most investigators studying the heat transfer mechanisms of nanofluids assume a minimal influence of ρ and c_P to the enhancement of h, conceding primary focus on μ and k. Among the available literature, there are no trustworthy experimental or theoretical predictions for the influence of both of these thermophysical properties to the convective heat transfer of nanofluids. Therefore, for each desired volume fraction, ρ and c_P are calculated via the same rationale as the employed for the experimental density and heat capacity (Eq. 19 and 20, respectively). Naturally, this method does lack accuracy, but ultimately enables a reasonable approximation to what should be the true values of those considered the least significant of the thermophysical properties to the heat transfer enhancement. In addition, the numerical material definition requires the definition of the molar mass of the nanofluid. The same rationale, already employed for model validation (Eq. 27), is applied in obtaining this parameter for each of the CNT volume fractions.

5.2.2.2. Thermal Conductivity

A rather debated, non-consensual possible influential convective heat transfer mechanism is the fluid conductivity. Some authors have described the influence of k as being minimal when compared to alternative mechanisms, somewhat reducing the significance of the greater number of studies reported in the literature review. Other authors believe that k is the key parameter responsible for the heat transfer enhancement of nanofluids, dedicating exhaustive investigations to its quantification. In either case, the role performed by k is expected to be more significant to that of ρ or c_P. Therefore, the individual values of k cannot be calculated under the same rationale as the previous properties, requiring a more accurate approach. There are two possible alternatives to the aforementioned rationale, each offering improved precision for k.

Firstly, one may employ any of the several theoretical predictions for nanofluids, covered in Chapter 2. However, most of the correlations exclusively conceived for nanofluids are for spherical nanoparticles, rather than CNTs. In addition, Lamas et al. (2012b) found that those applicable to CNT nanofluids were inadequate in predicting k, a conclusion supported by a clear lack of model convergence yielded under statistical analysis. Typical model shortcomings include a lack of adequate quantification of the influence of percolation network formation or Brownian motion of the CNTs within the base fluids (Lamas et al., 2012b).

The second possibility is the adoption of experimental measurements of k for the required volume fractions. Preceding the experimental investigation of Silva (2010), for a 0.25 vol. % CNT nanofluid, Ponmozhi (2009) and Ponmozhi et al. (2010) conducted experimental measurements (using the THW method) for nanofluids with different CNT concentrations, which include those employed for the current parametric study. Therefore, to enable a decent approximation to the

impact of k on the convective heat transfer, the data obtained by Ponmozhi (2009) at a temperature of 303.15 K, was selected.

5.2.2.3. Dynamic Viscosity

The variation of μ cannot be accurately predicted under the rationale used in Eq. 19, 20 and 27. The considerable dependence of the convective heat transfer on nanofluid viscosity was reported by Mare et al. (2011) following their experimental study of nanofluid application to a PHE. Therefore, an alternative approach is again required. Analogously to the nanofluid conductivity, Ponmozhi (2009) experimentally determined μ for different volume fractions at the Department of Mechanical Engineering of the University of Aveiro. As with the conductivity, the measurement method used is the same as the employed by Silva a year later, μ obtained with a rheometer. The results were posteriorly compared to some of the available theoretical predictions, the author finding that these significantly under-predicted the experimental results. The designated viscosities for the different volume fractions of the parametric study are those experimentally measured by Ponmozhi (2009) at 298.15 K.

5.2.2.4. Summary of Input Parameters

Table 22 displays the used thermophysical properties for the proposed volume fractions of the CNT/DIW mixture and the variables required to be numerically defined for each of the simulations, all undertaken with the same fluid inlet temperature (300 K). As can be deduced from the observation of the last two columns, all proposed simulations are devised to be run at Re=1236. Additionally, the constant wall heat flux boundary condition for all simulations was set to be the same as the heat flux used for model validation, i.e., 3581.021 W/m^2.

Table 22 – Fluid Thermophysical Property Influence: Simulation Input Parameters

CNT Volume Fraction $[vol.\%]$	μ $[N\,s/m^2]$	c_P $[J/kg\,K]$	ρ $[kg/m^3]$	k $[W/m\,K]$	M $[g/mol]$	$\dot{m}$ $[kg/s]$	u_{in} $[m/s]$
0.5	0.00165	4589	1397	0.887	17.985	0.1522	0.243
1	0.00176	4999	1797	0.891	17.954	0.2996	0.202
1.5	0.00181	5409	2197	0.894	17.925	0.5942	0.169
2	0.00185	5819	2597	0.894	17.895	0.8888	0.147
2.5	0.00191	6229	2997	0.921	17.865	1.183	0.131

5.2.2.5. Heat Transfer Results

5.2.2.5.1. Convective Heat Transfer Coefficient

According to the numerical results, increases in CNT volume fraction are accompanied by increases in h of the nanofluid, a trend that can be observed in Figure 26. The same conclusion is reached by most authors of the studies reported in the literature review. Additionally, the numerical data exhibits a linear increase of h for the lower CNT volume fractions, followed by exponential growth behaviour, from 2 vol. % onward. The highest numerical prediction of h occurs at x/D=135 for a CNT volume fraction of 2.5 vol. %, peaking at 1171 $W/m^2\,K$.

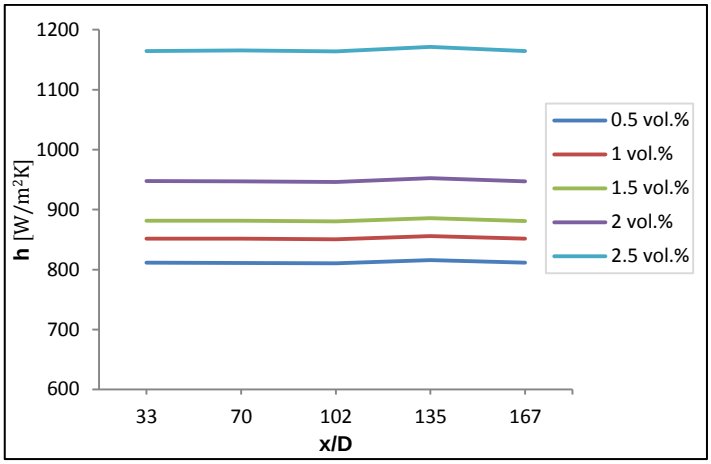

Figure 26 – Positional heat transfer coefficient for different CNT volume fractions, at Re=1236.

Figure 27 (left) displays the average values of h as a function of CNT volume fraction, where the aforementioned tendency is quite noticeable. The enhancement of the different CNT/DIW nanofluids over DIW alone is presented in Fig. 27 (right), which includes the witnessed enhancement for the nanofluid used for numerical model validation (CNT concentration of 0.25 vol. %). As can be observed, the enhancement increases with increasing particle concentrations, the maximum occurring at 2.5 vol. %, at almost 86%.

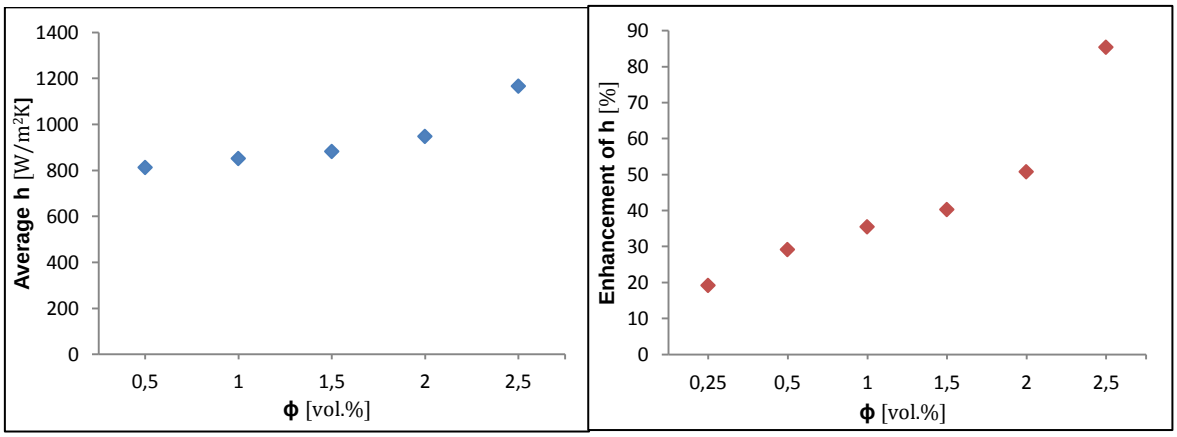

Figure 27 – Average heat transfer coefficient (left) and respective enhancement over DIW (right) as function of CNT volume fraction, at Re=1236.

5.2.2.5.2. Nusselt Number

The positional average Nu for all tested volume fractions is presented in Figure 28 (left), where a comparison between numerical and theoretical results (under the Shah prediction) is also established. When compared to the model validation data, displayed in Fig. 19, the highest numerical rates of advection over diffusion are no longer found in the tube entry region (as the theoretical prediction indicates), but at x/D=135. Additionally, the average numerical values are unexpectedly lower than the matching validation results (Fig. 20), only reaching similar quantities for the highest CNT volume fraction, which can be credited to the differences between the experimental data of Ponmozhi (2009) and Silva (2010). This can be observed in Figure 28 (right), where both sets of data display increases of Nu for increasing nanoparticle concentrations. Once

again, the Shah correlation over-predicts the numerical results, the difference between model data decreasing with increasing CNT volume fractions

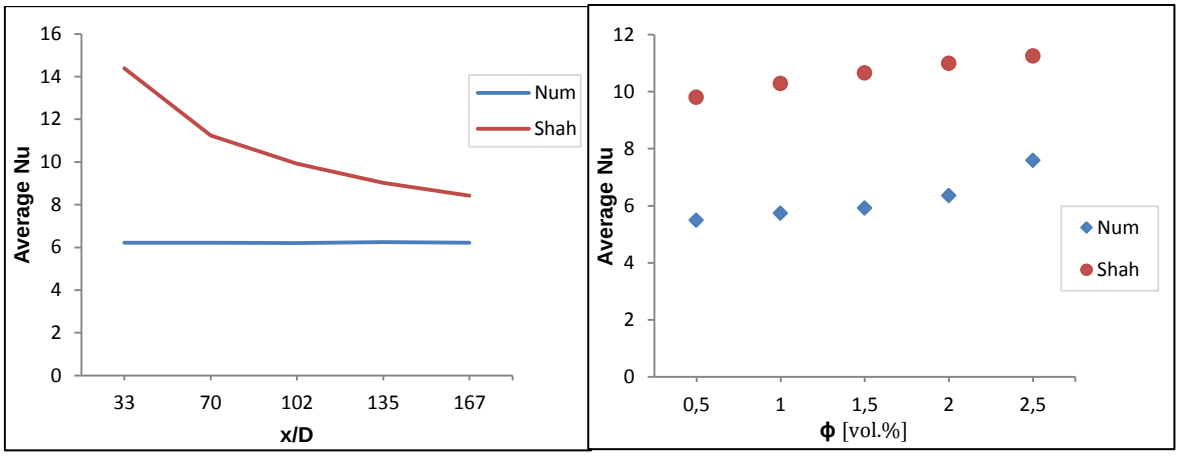

Figure 28 – Average numerical (Num) and theoretical (Shah) Nusselt numbers as function of position (left) and CNT volume fraction (right), at Re=1236.

5.3. Tube Dimensions

With the aim of investigating the legitimacy of the experimental setup, the study of the heat transfer behaviour of the fluids operating in alternatively dimensioned tubes can be significantly insightful. In order to assess the influence of the test tube dimensions, two approaches can be taken:

- An increase in length, to enable the verification of an experimental fully developed thermodynamic flow within the tube;
- A decrease in diameter, to establish a concept of the heat transfer capabilities of the fluids in reduced channel flow.

5.3.1. Length

In theory, if at L=1200 mm, the flow is thermodynamically fully developed, the fluid heat transfer behaviour is bound to repeat itself for L=1500 mm. Therefore, if the numerical model can yield the same results as obtained for the matching model validation simulations, the flow can be considered completely developed. To evaluate this, new model geometry was created and a mesh independence study undertaken (Appendix C). The numerical heat transfer data was gathered for both fluids, the longer tube length implying a recalculation of the heat flux due to the increase in surface area, as can be observed in Table 23. The remaining input parameters are those disposed in Table 20.

Table 23 – Proposed Simulations for L=1500 mm

Simulation	Fluid	q_{cw}'' [W/m^2]
Length1	DIW	2864.78
Length2	CNT/DIW	

The comparison between the positional h for the different tube lengths can be viewed in Figure 29, the data regarding L=1200 mm referring to the model validation simulations proposed in Table 17 (VAL1 and VAL4). As can be observed, these demonstrate good agreement, the data concerning the longer length slightly inferior. This is most likely due to the lower tube surface temperatures that result from an increased surface distribution of the same 108 W supplied by the heating tape. Judging by this close proximity in the heat transfer behaviour for the longer length, one may state that the experimental tube length enables the fluid flow to fully thermally develop before reaching the outlet.

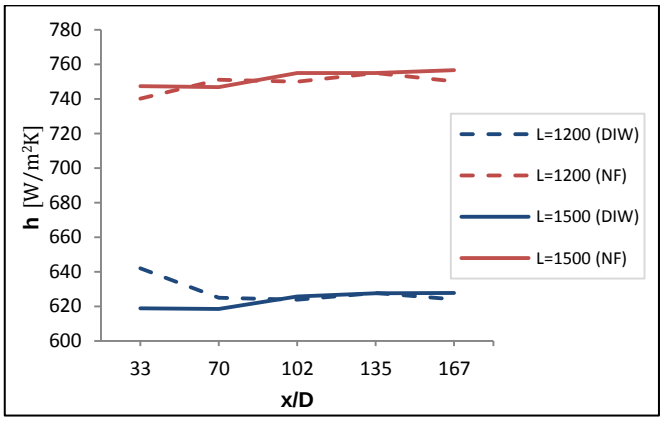

Figure 29 – Comparison of positional heat transfer coefficients for different tube lengths, at Re=1236.

The close data proximity between the tube lengths continues with Nu, as presented in Figure 30. Again, this indicates that the fluid flow is fully developed when reaching the outlet of the experimentally used shorter tube, leading to the conclusion that the current tube length is adequate. However, one must recall that the steady-state flow nature of the numerical model does interfere with data accuracy, as the linearity of the preceding figure indeed suggests.

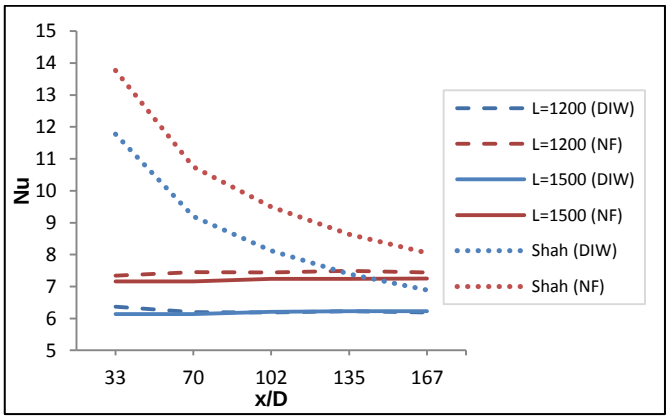

Figure 30 – Comparison of numerical and theoretical (Shah) positional Nusselt numbers for different tube lengths, at Re=1236.

5.3.2. Diameter

As was reported in the literature review, the current trend for heat exchangers is miniaturization allied to the employment of heat transfer enhancement methods, preferably passive

techniques. Of these, great interest has been deposited in the concept of increasing heat transfer surfaces by diameter reduction: where there is one larger channel, improved heat transfer capabilities can be obtained for various smaller channels acting in parallel, thus sparing material costs, space occupancies and required pumping power while maintaining, or even improving, heat transfer performances. In an attempt to understand the nanofluid heat transfer behaviour for a reduced diameter of the tube, two simulations were performed for an inner tube diameter (D) of 2 mm , one for each fluid, as proposed in Table 24. Again, the unspecified input parameters correspond to those displayed in Table 20.

Table 24 – Proposed Simulations for D=2 mm and Relevant Parameters

Simulation	Fluid	$\dot{m}$ $[Kg/s]$	u_{in} $[m/s]$	$q_{cw}{}''$ $[W/m^2]$
Diam1	DIW	0.00166	0.000221	9549.256
Diam2	CNT/DIW	0.00262	0.000290	

As can be observed in Figure 39, the magnitude of h for the smaller tube diameter is far superior to the average h resulting from model validation (Fig. 15). Obviously, the higher heat flux entering the fluid has a significant contribution to these results, consequence of the standard heating tape power (108 W) over a smaller surface. Nonetheless, the gathered results are extremely encouraging in a perspective of nanofluid employment in smaller channels, the nanofluid revealing a maximum enhancement of h, of just under 21 %, over DIW in the tube entry region (surpassing the corresponding enhancement observed during model validation, approximately 19 %).

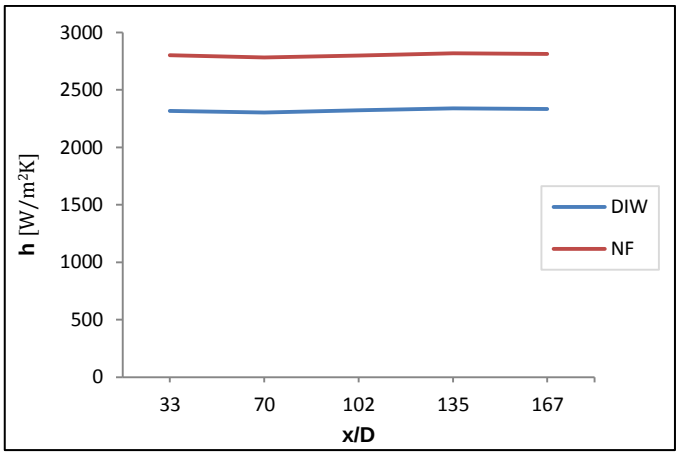

Figure 31 – Comparison of positional heat transfer coefficients for a tube diameter of 2 mm, at Re=1236.

Figure 32 displays the numerical and theoretical predictions of Nu for the smaller tube diameter, both showing reasonable agreement. When compared to the average values of Nu for model validation, displayed in Fig. 19, the current values are slightly smaller. However, this heat transfer data corresponds to half the tube diameter, a combination of smaller diameter tubes will naturally provide superior heat transfer capabilities, with less device volume occupancy requirements.

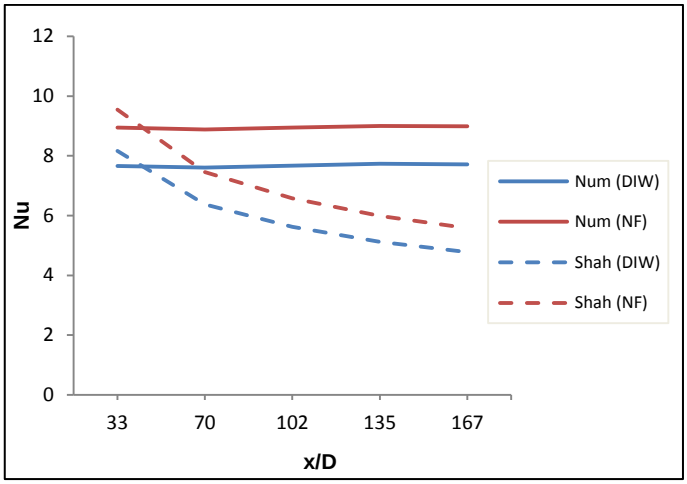

Figure 32 – Comparison of numerical and theoretical (Shah) positional Nusselt numbers for a tube diameter of 2 mm, at Re=1236.

Chapter 6

Conclusions

6.1. Nanofluids for Heat Exchangers

6.1.1. Review

Under the current energy climate, the implementations of measures that simultaneously aid resource preservation and environmental protection have gained significant global priority. The continuous fossil fuel price increases and the recent severity intensification of natural events are testament to mankind's dangerous proximity to the point of no return, as far as long-term sustainability and environmental conservation are concerned. Over the past few decades, scientists and engineers have proposed all kinds of successfully employed improvements in all sorts of industrial areas, but more progress still needs to be made. Any industrial process requiring thermal management typically employs heat exchangers in the corresponding system. As was observed in the literature review, a wide variety of different heat exchanger types and technologies are currently employed in the pursuit of maximum efficiency of heat transfer methods. In a perspective of passively increasing thermal performances, the colloidal dispersion of solid nanoparticles in common base fluids (nanofluids) has recently been proposed. Experimental studies have demonstrated that, compared to the base fluids alone, these display significant heat transfer enhancements, extremely promising in a thermal system sustainability point of view.

6.1.2. Heat Transfer Mechanisms of Nanofluids

In order to predict thermal behaviour for industrial application, a precise understanding of nanofluid thermophysical properties is essential. To that effect, a large amount of studies have been reported in the literature, most emphasized on spherical particle nanofluids. The majority of investigative work in this area has been centred on the quantification of the enhancement of k via two approaches: experimental measurement or theoretical formulation. The most consensual feature of these studies is that the addition of nanoparticles does increase k_{eff} of common fluids and that tubular particle nanofluids exhibit the highest enhancements. However, the mechanisms responsible for such anomalous behaviour remain unknown and theoretical models can only match experimental data for reduced property ranges.

Significantly less attention has been conceded to investigating the convective heat transfer of nanofluids and possible enhancement factors, essential in enabling the practical application of nanofluids in heat exchangers. Of the limited available studies, most report superior enhancements of h to that of k of the same nanofluids, being a strong indicator of the influence of other parameters in the witnessed enhancements. Virtually all experimental results of convective heat transfer, typically studying nanofluid flow through circular tubes, agree that the particle volume fraction is influential to the thermal performance increases. However, higher particle concentrations contribute to higher pressure drop of the fluid flow, which bears the inconvenience of increased pumping requirements. Another noted trend, though not as consensual, is the dependence on the fluid flow state, most authors reporting convective heat transfer increases as function of growing Re. Several authors also found that the thermal enhancement occurred in the tube entry region, proposing the low boundary layer thickness as a possible culprit. Most of the experiment model validations, as well as theoretical studies, apply the single-phase approach in nanofluid behaviour

predictions. The approach treats the solid particle suspension in a liquid as a single-phase fluid, enabling the employment of classic correlations for convective heat transfer. Despite the reduced application due to a higher complexity, authors using the alternative two-phase approach have boasted better agreement with the experimental data. Still, no consensual model has been defined; the mechanisms responsible, as well as their levels of influence are yet to be known. Investigative attempts to test the thermal performance of alternative heat exchanger types can be found in the literature, but these are still quite unique and lack proper validation.

Numerical studies of nanofluid heat transfer performances are the scarcest amongst the available literature, most conducted to evaluate forced convection in circular tubes, as with the majority of experimental investigations. Here, the influence of the definition of boundary conditions and the theoretical assumptions selected is significant. Most studies employ the constant wall heat flux condition and are theoretically based on modifications of classical correlations for laminar and turbulent flow, whenever applicable. With regard to the mentioned anomalous nanofluid behaviour, exhibited in the tube entrances, some authors have employed finer meshes in the region, creating a non-uniformity of overall tube elements. The current thesis proposed a similar study of forced convection, based on data extracted from the experimental research conducted by Silva (2010) and also the experimental measurements obtained by Ponmozhi (2009).

6.2. Numerical Data

6.2.1. Model Performance

Judging by the obtained results, the current numerical model can be deemed reasonably effective for a prototype. The performed validation returned fairly proximate results to that of the experimental data, especially if one is to take into account the employed steady-state flow and single-phase nanofluid assumptions. When heat transfer performance divergences between the two models were found, the numerical data was in better agreement with the majority of the corresponding tendencies reported in the literature review.

When submitted to parametric tests, in Chapter 5, the executed simulations resulted in generally expected trends, again with similar findings to those claimed by other authors, following experimental investigations. As referred, the single-phase fluid approach restricts individual parameter influence analysis, disadvantageous in comparison to a possible dual-phase model.

As for the software processing behaviour, the performed simulations ran smoothly, typically converging between 80 and 100 iterations (defined to terminate at a residual value of 1×10^{-5} between consecutive iterations), at an average processing time of approximately 2 hours each. In general, the employed software demonstrated reasonable adequacy to the study of nanofluid flows, which was expected for a straightforward single-phase nanofluid configuration.

6.2.2. Model Results

In general, the numerical heat transfer results follow the experimental observations, reported by Silva (2010), allowing the conclusion that nanofluid application is more advantageous than the common heat transfer fluids, with witnessed enhancements throughout the conducted investigations. Due to the steady-state analysis, the numerical enhancements of h generally reveal less significance than the experimentally observed, demonstrating a linear tendency with small fluctuations. The numerical value of h was found to increase with increases in Re maintaining its

enhancement over the base fluid, revealing general agreement with the conclusions of most investigators. However, one may assuredly conclude that nanofluids indeed have superior heat transfer capabilities, with great potential to improve typical heat exchanger efficiency.

Usually, the global heat transfer is equivalent to the sum of the contributions of advection and diffusion, these characterized by convective and conductive heat transfers, respectively. Nu is commonly applied to heat transfer fluid problems, a useful parameter in evaluating the contribution of convection over conduction to the transfer process. Accordingly, the typical theoretical correlation used for experimental data validation of heat transfer under laminar flows, the Shah prediction, quantifies this parameter. Both theoretical and numerical predictions indicate higher heat transfer due to convection in the tube entry region, also being where Nu of the nanofluid finds its peak enhancement over DIW. However, the Shah prediction was found to over-predict the convective heat transfer when compared to both numerical and experimental data, which could be credited to the correlation having been conceived for larger diameter conduits.

When submitted to turbulent flows, the numerical model yields superior values of h and of Nu, as most researchers also concluded in the available literature, however the enhancement of h over DIW was found to decrease when compared to the witnessed enhancement for laminar flows. Of the common theoretical predictions of Nu for these flows, the numerical Nu was found to be in good agreement with the Gnielinski correlation, the proximity increasing at higher Re, whereas the Dittus-Boelter displayed significant over-predictions. An increase in Re is accompanied by undesired fluid pressure drops, which was numerically found to be the most disadvantageous feature of the studied nanofluid in relation to DIW. As well as the higher pressure drop of the nanofluid, the developed model also indicates that it evolves exponentially with Re, contrarily to the trend revealed by DIW, under the same conditions, growing in a more linear fashion.

6.2.3. Heat Transfer Mechanisms

Under parametric testing, an estimate of the influence of the CNT volume fraction to the heat transfer was undertaken. To enable a confident approach, the nanofluid thermophysical properties for the varying nanoparticle concentration were required to be as precise as possible. While the expected less influential properties could be calculated under the rationale employed in Eq. 18, 19 and 27, as with the experimental study conducted by Silva (2010), the significant properties demanded more accurate estimates. Therefore, the applied fluid conductivities and viscosities corresponded to the experimental measurements carried out by Ponmozhi (2009). The obtained numerical results indicate an increase in the heat transfer capabilities of the tested nanofluids for increasing CNT volume fractions.

6.3. Future Model Developments

Since the experimental investigations conducted by Ponmozhi (2009) and Silva (2010), several improvements have been applied to the experimental nanofluid preparation and measurement facility. The unanticipated experimental tendencies, reported in Chapter 4, especially regarding the positions of maximum advection or the decrease of Nu with increasing Re, steered to the conclusion that a few setup adjustments were required.

The colloidal stability of the DIW-based nanofluid was found to significantly improve when mixed with ethylene glycol (EG), leading the current working base fluids to typically include EG volume fractions of 30 or 60%. In addition, the CNT settling features are now evaluated using

Fourier transform infrared spectroscopy (FTIR), where infrared radiation is transmitted through the nanofluid sample creating an infrared spectrum that represents the peaks of molecular absorption and transmission. This technique is more accurate than ultraviolet-visible spectrophotometry in determining the quality or consistency of fluid samples, therefore improving the nanofluid quality control prior to experimental testing. (Lamas et al., 2012a)

As for the convective heat transfer experimental test facility, additional thermocouples have been placed for fluid temperature measurement in the same relative positions to that of the ones positioned on the outer tube surface. This is obviously far more accurate than the previous procedure of theoretically calculating the average value of each of the intermediate positioned fluid temperatures using Eq. 23. Additional improvements could include the addition of fluid pressure measurement instruments (for experimental pressure drop measurements) and the substitution of the current pump for one that can also supply steady turbulent flows. The full insulation of the test tube and heating tape should be periodically checked, particularly to ensure that the tube surface thermocouple readings are not influenced by the temperature of the heating tape. The accuracy of the heat transfer results could also improve if the experiments were to be conducted at similar timescales, allowing the system to absorb similar quantities of heat for each study.

The aforementioned progresses lead to more accurate fluid properties which may, in future, also benefit the precision of the numerical model. The current numerical model is still in an early development stage, one may claim still at a macro scale. Future researchers should be aware that several improvements must follow until it can be deemed a powerful nanofluid heat transfer prediction tool, i.e., capable of micro scale analysis. Of these, the two most significant are the fluid material definitions and the nature of the fluid flow analysis.

The single-phase fluid assumption leaves the current model lacking in heat transfer mechanism analysis, quite especially at a molecular level. The next upgrade in material definition should involve a dual-phase approach, which is bound to improve the global precision of the numerical results. Additionally, the model will allow for parametric testing of important parameters such as CNT volume fraction, length, aspect ratio and diameter. However, in order to achieve this, further insight into nanoparticle behaviour, within the base fluid, is required. There is also no indication whether the CFD software can adequately predict the heat transfer performance of base fluids containing nano-scaled particles at low concentrations. The scarcity of CFD studies, reported in the literature review, allied to the relative novelty of nanofluids; do highlight the possibility of software shortcomings when facing colloidal suspensions in base fluids.

The other significant step for future modellers involves the nature of the flow analysis, increased model precision demanding a transient study. The linearity demonstrated by the numerical results is a direct consequence of the current steady-state flow analysis, which is time-independent. Obviously, a transient investigation will lead to a higher accuracy of the numerical heat transfer properties. The downside to this procedure is the added number of required input parameters and the increased processing time, with possible increases in iterative convergence errors.

At present, the nanofluid investigation group is working to achieve accurate distributions of nanofluid viscosity and thermal conductivity with varying temperatures. The recent acquisition of a viscometer will enable a more precise measurement of fluid viscosity distributions. Once established, the resulting data can also be numerically defined, allowing for improved model accuracy.

All of the proposed model innovations share the common requisite of further experimental nanofluid testing. One of the main conclusions derived from the literature review is that the scientific community could well do with further investigation into the convective aspect of the heat transfer. Perhaps too much effort has been expended in determining the thermal conductivity, quite especially if one takes into account its possible minor role in the convective heat transfer enhancements. After all, the thorough understanding of the convective behaviour is unavoidable in enabling realistic nanofluid applications.

Chapter 2 of the present thesis was used as foundation for the chapter *Carbon Nanotubes in a Fluidic Medium: Critical Analysis* of the book *Physical and Chemical Properties of Carbon Nanotubes (Book 2)*, ISBN 980-953-307-485-1

References

Abou-Ziyan, H.S., “Heat Transfer Characteristics of Some Oils Used for Engine Cooling”, *Energy Conversion and Management 45, pp. 2553-2569*, Egypt (2004);

Abreu, B., Lamas, B., Fonseca, A., Martins, N., and Oliveira, M.S.A., “Convective Heat Transfer Characterization of Carbon Based Nanofluids under Laminar Flow Conditions”, *Centre of Mechanical Technology and Automation, University of Aveiro,* Portugal (2012);

Afgan, N.H., Gobaisi, D., Carvalho, M.G., and Cumo, M., “Sustainable Energy Development”, *Renewable and Sustainable Energy Reviews 2, pp. 235-286*, Portugal (1998);

Agostiano, A., Catalano, M., Curri, M.L., Della Monica, M., Manna, L., and Vasanelli, L., “Synthesis and Structural Characterization of CdS Nanoparticles Prepared in a Four-components Water-in-oil Microemulsion”, *Micron 31(3), pp. 253-258*, Italy (2000);

Aiken III, J.D., and Finke, R.G., “A Review of Modern Transition-metal Nanoclusters: Their Synthesis, Characterization, and Applications in Catalysis”, *Journal of Molecular Catalysis A: Chemical 145 (1-2), pp. 1-44*, United States of America (1999);

Ali, F.M., Yunus, W.M.M., Moksin, M.M., and Talib, Z.A., “The Effect of Volume Fraction Concentration on the Thermal Conductivity and Thermal Diffusivity of Nanofluids: Numerical and Experimental”, *Review of Scientific Instruments 81, 074901*, Malaysia (2010);

Amrollahi, A., Rashidi, A.M., Lotfi, R., Meibodi, M.E., and Kashefi, K., “Convection Heat Transfer of Functionalized MWNT in Aqueous Fluids in Laminar and Turbulent Flow at the Entrance Region”, *International Communications in Heat and Mass Transfer 37, pp. 717-723*, Iran (2010);

Anoop, K.B., Sundararajan, T., and Das, S.K., “Effect of Particle Size on the Convective Heat Transfer in Nanofluid in the Developing Region”, *International Journal of Heat and Mass Transfer 52, pp. 2189-2195*, India (2009);

Antisari, M.V., Marazzi, R., and Krsmanovic, R., “Synthesis of Multiwall Carbon Nanotubes by Electric Arc Discharge in Liquid Environments”, *Carbon 41, pp. 2393-2401*, Italy (2003);

Aquaro, D., and Pieve, M., “High Temperature Heat Exchangers for Power Plants: Performance of Advanced Metallic Recuperators”, *Applied Thermal Engineering 27, pp. 389-400*, Italy (2007);

Aris, M.S., Owen, I., and Sutcliffe, C.J., “The Development of Active Vortex Generators from Shape Memory Alloys for the Convective Cooling of Heated surfaces”, *International Journal of Heat and Mass Transfer 54, pp. 3566-3574*, Malaysia (2011);

Atlas Steels, “Grade Data Sheet 316 316L 316H”, A*tlas Specialty Metals,* Australia (2011), available at: http://www.atlassteels.com.au/;

Bazmi, A. and Zahedi, G., “Sustainable Energy Systems: Role of Optimization Modeling Techniques in Power Generation and Supply - A Review”, *Renewable and Sustainable Energy Reviews 15, pp. 3480-3500*, Malaysia (2011);

Behzadmehr, A., Saffar-Avval, M., and Galanis, N., “Prediction of Turbulent Forced Convection of a Nanofluid in a Tube with Uniform Heat Flux Using a Two Phase Approach”, *International Journal of Heat and Fluid Flow 28 (2), pp. 211-219*, Iran (2007);

Bergles, A.E., "Augmentation of Heat Transfer: Heat Exchanger Design Handbook", *Hemisphere Publishing Company*, Washington, United States of America (1983);

Biercuk, M.J., Llaguno, M.C., Radosavljevic, M., Hyun, J.K., and Johnson, A.T., "Carbon Nanotube Composites for Thermal Management", *Applied Physics Letters 80 (15), pp. 2767-2769*; United States of America (2002);

Botha, S.S., "Synthesis and Characterization of Nanofluids for Cooling Applications", *Thesis for the degree of Doctor of Philosophy*, University of the Western Cape, South Africa (2007);

Bruggemann, D.A.G., "The Calculation of Various Physical Constants of Heterogeneous Substances - The Dielectric Constants and Conductivities of Mixtures Composed of Isotropic Substances" *Annual Physics 416, pp. 636-664*, Germany (1935);

Cahill, D.G., "Thermal Conductivity Measurement from 30 to 750 K: the 3ω Method", *Review of Scientific Instruments 61 (2), pp. 802-808*, United States of America (1990);

Chandrasekar, M., Suresh, S., and Bose, A.C., "Experimental Studies on Heat Transfer and Friction Factor Characteristics of Al_2O_3/Water Nanofluid in a Circular Pipe under Laminar low with Wire Coil Inserts", *Experimental Thermal and Fluid Science 34, pp. 122-130*, India (2010);

Cheap Tubes Inc., "Multi Walled Nanotubes > 50 nm Specifications": http://www.cheaptubes.com/MWNTs.htm, Date of last consultation: 31/05/2012;

Chen, H., Yang, W., He, Y., Ding, Y., Zhang, L., Tan, C., Lapkin, A.A., and Bavykin, D.V., "Heat Transfer and Flow Behaviour of Aqueous Suspensions of Titanate Nanotubes (Nanofluids)", *Powder Technology 183 (1), pp. 63-72*, United Kingdom (2008);

Chen, H., Witharana, S., Jin, Y., Kim, C, Ding, Y., "Predicting Thermal Conductivity of Liquid Suspensions of Nanoparticles (Nanofluids) based on Rheology", *Particuology 7 (2), pp. 151-157*, United Kingdom (2009);

Cheng, L., Luan, T., Du, W., and Xu, M., "Heat Transfer Enhancement by Flow-induced Vibration in Heat Exchangers", *International Journal of Heat and Mass Transfer 52, pp. 1053-1057*, China (2009);

Choi, S.U.S., "Nanofluid Technology: Current Status and Future Research." *Energy Technology Division, Argonne National Laboratory,* United States of America (1998);

Choi, S.U.S., and Eastman, J.A., "Enhanced Heat Transfer Using Nanofluids", *Patent US 6221275 B1*, United States of America (2001);

Choi, S.U.S., Zhang, Z.G., Yu, W., Lockwood, F.E., and Grulke, E.A., "Anomalous Thermal Conductivity Enhancement in Nano-tube Suspensions", *Applied Physics Letters 79, pp. 2252-2254*, United States of America (2001);

Choi, S.U.S., Brooks, J.S., Eaton, D.L., Al-Haik, M.S., Hussaini, M.Y., Garmestani, H., Li, D., and Dahmen, K., "Enhancement of Thermal and Electrical Properties of Carbon Nanotube Polymer Composites by Magnetic Field Processing", *Journal of Applied Physics 94 (9), pp. 6034-6039*, United States of America (2003);

Chon, C.H., Kimh, K.D., Lee, S.P., and Choi, S.U.S, "Empirical Correlation Finding the Role of Temperature and Particle Size for Nanofluid (Al2O3) Thermal Conductivity Enhancement", *Applied Physics Letters 87 (15), 153107*, United States of America (2005);

Chun, B., Kang, H.U., and Kim, S.H., "Effect of Alumina Nanoparticles in the Fluid on Heat Transfer in Double-pipe Heat Exchanger System", *Korean Journal of Chemical Engineering 25 (5), pp. 966-971*, South Korea (2008);

Deng, F., Zheng, Q.S., Wang, L.F., and Nan, C.W., "Effects of Anisotropy, Aspect Ratio, and Nonstraightness of Carbon Nanotubes on Thermal Conductivity of Carbon Nanotube Composites", *Applied Physics Letters 90, 021914*, China (2007);

Deng, F., and Zheng, Q., "Interaction Models for Effective Thermal Conductivity and Electric Conductivities of Carbon Nanotube Composites", *Acta Mechanica Solida Sinica 22 (1), pp. 1-17*, China (2009);

Dewan, A., Mahanta, P., Raju, K.S., and Kumar, P.S., "Review of Passive Heat Transfer Augmentation Techniques", *Proc. Institution of Mechanical Engineers Vol. 218 Part A: J. Power and Energy*, India (2004);

Dincer, I., "Energy and Environmental Impacts: Present and Future Perspectives", *Tubitak-Marmara Research Centre*, Turkey (1997);

Ding, Y., Alias, H., Wen, D., and Williams, R.A., "Heat Transfer of Aqueous Suspensions of Carbon Nanotubes (CNT Nanofluids", *International Journal of Heat and Mass Transfer 49, pp. 240-250*, United Kingdom (2006);

Ding, Y., Chen, H., Wang, L., Yang, C., He, Y., Yang, W., Lee, W.P., Zhang, L., and Huo, R., "Heat Transfer Intensification Using Nanofluids", *KONA 25, pp. 23-38*, United Kingdom (2007);

Ding, Y., and Wen, D., "Particle Migration in a Flow of Nanoparticle Suspensions", *Powder Technology 149 (2-3), pp. 84-92*, United Kingdom (2005);

DOE – U.S. Department of Energy, "Fundamentals Handbook: Thermodynamics, Heat Transfer and Fluid Flow, Volume 1", *National Technical Information Service*, Springfield, United States of America (1992);

Duncan, R., Stojolan, V., and Lekakou, C., "Manufacture of Carbon Multi-walled Nanotubes by the Arc Discharge Technique", *Proceedings of the World Congress on Engineering 2007, Vol. II*, United Kingdom (2007);

Eastman, J.A., "Mechanisms of Enhanced Heat Transfer in Nanofluids", *Fluctuations and Noise in Out of Equilibrium Systems Presentation*, United States of America (2005);

Eastman, J.A., Choi, S.U.S., Li, S., Thompson, L.J., and Lee, S., "Enhanced Thermal Conductivity Through the Development of Nanofluids", *Proceedings of the Symposium on Nanophase and Nanocomposite Materials II, vol. 457, Materials Research Society, pp. 3-11*, United States of America (1997);

Eastman, J.A., Choi, S.U.S., Li, S., Yu, W., and Thompson, L.J., "Anomalously Increased Effective Thermal Conductivities of Ethylene Glycol-based Nanofluids Containing Copper Nanoparticles", *Applied Physics Letters 78, pp. 718-720*, United States of America (2001);

Edgar, K., and Spencer, J.L., "The Synthesis of Carbon Nanotubes from Muller Clusters", *Current Applied Physics 6, pp. 419-421*, New Zealand (2006);

Egorova, E.M., and Revina, A.A., "Optical Properties and Sizes of Silver Nanoparticles in Micellar Solutions", *Colloid Journal 64 (3), pp. 334-345*, Russia (2002);

Esumi, K., Ishigami, M., Nakajima, A., Sawada, K., and Honda, H., "Chemical Treatment of Carbon Nanotubes", *Carbon 34, pp. 279-281*, Japan (1996);

European Commission (EC), “Towards Sustainability: The Fifth Environmental Action Programme”, *Official Publications of the European Communities*, Luxembourg (1992);

Evans, W., Fish, J., and Keblinski, P., “Role of Brownian Motion Hydrodynamics on Nanofluid Thermal Conductivity”, *Applied Physics Letters 88, 093116*, United States of America (2006);

Evans, W., Prasher, R., Fish, J., Meakin, P., Phelan, P., and Keblinski, P., “Effect of Aggregation and Interfacial Thermal Resistance on Thermal Conductivity of Nanocomposites and Colloidal Nanofluids”, *International Journal of heat and Mass Transfer 51, pp. 1431-1438*, United States of America (2008);

Feng, Y., Yu, B., and Zou, M., “The Effective Thermal Conductivity of Nanofluids Based on the Nanolayer and the Aggregation of Nanoparticles”, *Journal of Physics D: Applied Physics 40 (10), pp. 3164-3171*, China (2007);

Fiebig, M., “Vortices, Generators and Heat Transfer”, *Trans. IChemE, vol. 76-A, pp. 108-123*, Germany (1998);

Fotukian, S.M., and Esfahany, M.N., “Experimental Investigation of Turbulent Convective Heat Transfer of Dilute γ-Al_2O_3/Water Nanofluid inside a Circular Tube”, *International Journal of Heat and Fluid Flow 31, pp. 606-612*, Iran (2010);

Franck, A., “Measuring Structure of Low Viscosity Fluids in Oscillation using Rheometers with and without a Separate Torque Transducer”, Annual Transaction of the Nordic Rheology Society, Vol. 11, RH090, Germany (2003);

Garg, P., Alvarado, J.L., Marsh, C., Carlson, T.A., and Kessler, D.A., “Na Experimental Study on the Effect of Ultrasonication on Viscosity and Heat Transfer Performance of Multi-wall Carbon Nanotube-based Aqueous Nanofluids”, *International Journal of Heat and Mass Transfer 52, pp. 5090-5101*, United States of America (2009);

Gowda, R., Sun, H., Wang, P., Charmchi, M., Gao, F., Gu, Z., and Budhlall, B., “Effects of Particle Surface Charge, Species, Concentration, and Dispersion Method on the Thermal Conductivity of Nanofluids”, *Advances in Mechanical Engineering 2010, 807610*, United States of America (2010);

Grimm, A., “Powdered Aluminium-containing Heat Transfer Fluids”, *German Patent DE4131516A1*, Germany (1993);

Gubin, S.P., Koksharov, Y.A., Khomutov, G.B., and Yurkov, G.Y., “Magnetic Nanoparticles: Preparation, Structure and Properties”, *Russian Academy of Sciences and Turpion Ltd*, Russia (2005);

Guo, L., Yang, S., Yang, C., Yu, P., Wang, J., Ge, W., and Wong, G.K.L., “Highly Monodisperse Polymer-capped ZnO Nanoparticles: Preparation and Optical Properties”, *Applied Physics Letters 76 (20), pp. 2901-2903*, Hong Kong (2000);

Han, Z., “Nanofluids with Enhanced Thermal Transport Properties.” *Dissertation for the degree of Doctor of Philosophy*, *University of Maryland*, United States of America (2008);

He, Y., Jin, Y., Chen, H., Ding, Y., Cang, D., and Lu, H., “Heat Transfer and Flow Behaviour of Aqueous Suspensions of TiO_2 Nanoparticles (Nanofluids) Flowing Upward through a Verticle Pipe”, *International Journal of Heat and Mass Transfer 50, pp. 2272-2281*, United Kingdom (2007);

Heffington, S.N., “Vibration-induced Droplet Atomization Heat Transfer Cell for Cooling of Microelectronic Components”, *Proceedings of IPACK’01, 15596*, United States of America (2001);

Hemanth, K.D., Patel, H.E., Rajeev, K.V.R., Sundararajan, T., Pradeep, T., and Das, S.K., “Model for Heat Conduction in Nanofluids”, *Physics Review Letters 93, 144301*, India (2004);

Heris, S.Z., Etemad, S.G., and Esfahany, M.N., “Experimental Investigation of Oxide Nanofluids Laminar Flow Convective Heat Transfer”, *International Communications in Heat and Mass Transfer 33, pp. 529-535*, Iran (2006);

Heris, S.Z., Esfahany, M.N., and Etemad, S.G., “Experimental Investigation of Convective Heat Transfer of Al_2O_3/water Nanofluid in Circular Tube”, *International Journal of Heat and Fluid Flow 28, pp. 203-210*, Iran (2007);

Heris, S.Z., Esfahany, M.N., and Etemad, G., “Numerical Investigation of Nanofluid Laminar Convective Heat Transfer through a Circular Tube”, *Numerical Heat Transfer Part A: Applications 52 (11), pp. 1043-1058*, Iran (2007a);

Heris, S.Z., Etemad, S.G., and Esfahany, M.N., “Convective Heat Transfer of a Cu/Water Nanofluid Flowing through a Circular Tube”, *Experimental Heat Transfer 22, pp. 217-227*, Iran (2009);

Heris, S.Z., Kazemi-Beydokhti, A., Noie, S.H., and Rezvan, S., “Numerical Study on Convective Heat Transfer of Al2O3/Water, CuO/Water and Cu/Water Nanofluids through Square Cross-section Duct in Laminar Flow”, *Engineering Applications of Computational Fluid Mechanics 6 (1), pp. 1-14*, Iran (2012);

Hernadi, K., Fonseca, A., Nagy, J.B., Bernaerts, D., Riga, J., Lucas, A., “Catalytic Synthesis and Purification of Carbon Nanotubes”, *Synthetic Metals 77, pp. 31-34*, Belgium (1996);

Hilding, J., Grulke, E.A., Zhang, Z.G., and Lockwood, F., “Dispersion of Carbon Nanotubes in Liquids”, *Journal of Dispersion Science and Technology 24 (1), pp. 1-41*, United States of America (2003);

Hojjat, M., Etemad, S.G., Bagheri, R., and Thibault, J., “Convective Heat Transfer of Non-Newtonian Nanofluids through a Uniformly Heated Circular Tube”, *International Journal of Thermal Sciences 50, pp. 525-531*, Iran (2011);

Hong, H., Wight, B., Wensel, J., Jin, S., Ye, X.R., and Roy, W., “Enhanced Thermal Conductivity by the Magnetic Field in Heat Transfer Nanofluids Containing Carbon Nanotube”, *Synthetic Metals 157, pp. 437-440*, United States of America (2007);

Hong, K.S., Hong, T., and Yang, H.,” Thermal Conductivity of Fe Nanofluids Depending on the Cluster Size of Nanoparticles”, *Applied Physics Letters 88 (3), 031901*, South Korea (2006);

Hong, T., Yang, H., and Choi, C.J., “Study of Enhanced Thermal Conductivity of Fe Nanofluids”, *Journal of Applied Physics 97, 064311*, South Korea (2005);

Hosseini, S.S., Adam, N.M., Azmi, B.Z., Ahmadi, A., and Shahrjerdi, A., “Measuring Thermal Conductivity of Nanofluid by New Method”, *Australian Journal of Basic and Applied Sciences 5 (9), pp. 985-996*, Malaysia (2011);

Hsin, Y.L., Hwang, K.C., Chen, F., and Kai, J., “Production and in-situ Metal Filling of Carbon Nanotubes in Water”, *Advanced Materials 13 (11), pp. 830-833*, China (2001);

Huxtable, S.T., Cahill, D.G., Shenogin, S., Xue, L., Ozisik, R., Barone, P., Usrey, M., Strano, M.S., Siddons, G., Shim, M., and Keblinski, P., "Interfacial Heat Flow in Carbon Nanotube Suspensions", *Nature Materials 2 (11), pp. 731-734*, United States of America (2003);

Hwang, K.S., Jang, S.P., and Choi, S.U.S., "Flow and Convective Heat Transfer Characteristics of Water-based Al_2O_3 Nanofluids in Fully Developed Laminar Flow Regime", *International Journal of Heat and Mass Transfer 52, pp. 193-199*, South Korea (2009);

Hwang, Y., Lee, J.K., Lee, J.K, .Jeong, Y.M., Cheong, S.I., Ahn, Y.C., and Kim, S.H., "Production and Dispersion Stability of Nanoparticles in Nanofluids", *Powder Technology 186 (2), pp. 145-153*, South Korea (2008);

Incropera, F.P., and DeWitt, D.P., "Fundamentals of Heat Transfer 5th Ed.", *John Wiley & Sons Inc*., New Jersey, United States of America (2001);

Jang, S.P., and Choi, S.U.S., "Role of Brownian Motion in the Enhanced Thermal Conductivity of Nanofluids", *Applied Physics Letters 84 (21), pp. 4316-4318*, United States of America (2004);

Jiang, J.S., Gao, L., Yang, X.L., Guo, J.K., and Shen, H.L., "Nanocrystalline NiZn Ferrite Synthesized by High Energy Ball Milling", *Journal of Materials Letters 18, pp. 1781-1783*, China (1999);

Jiang, W., Ding, G., and Peng, H., "Measurement and Model on Thermal Conductivities of Carbon Nanotube Nanorefrigerants", *International Journal of Thermal Sciences 48, pp. 1108-1115*, China (2009);

José-Yacamán, M., Miki-Yoshida, M., Rendón, L., and Santiesteban, J.G., "Catalytic Growth of Carbon Microtubes with Fullerene Structure", *Applied Physics Letters 62, 657*, Mexico (1993);

Ju, Y.S., Kim, J., and Hung, M.T, "Experimental Study of Heat Conduction in Aqueous Suspensions of Aluminium Oxide Nanoparticles", *Journal of Heat Transfer 130 (9), 092403-6*, United States of America (2008);

Juillerat, F., Solak, H.H., Bowen, P., and Hofmann, H., "Fabrication of Large-area Ordered Arrays of Nanoparticles on Patterned Substrates", *Nanotechnology 16 (8), pp. 1311-1316*, Switzerland (2005);

Kalbasi, M., and Saeedi, A., "Numerical Investigation into the Convective Heat Transfer of CuO Nanofluids Flowing Through a Straight Tube with Uniform Heat Flux", *Indian Journal of Science and Technology 5 (S3), pp. 2455-2458*, Iran (2012);

Kalteh, M., Abbassi, A., Saffar-Avval, M., and Harting, J., "Eulerian-Eulerian Two-Phase Numerical Simulation of Nanofluid Laminar Forced Convection in a Microchannel", *International Journal of Heat and Fluid Flow 32, pp. 107-116*, Iran (2011);

Kandlikar, S.G., Joshi, S., and Tian, S., "Effect of Channel Roughness on Heat Transfer and Fluid Flow Characteristics at Low Reynolds Numbers in Small Diameter Tubes", *Proceedings of 35th National Heat Transfer Conference*, United States of America (2001);

Kang, C., Okada, M., Hattori, A., and Oyama, K., "Natural Convection of Water-Fine Particle Suspension in a Rectangular Vessel Heated and Cooled from Opposing Vertical Walls (Classification of the Natural Convection in the Case of Suspension with a Narrow-size Distribution)", *International Journal of Heat and Mass Transfer 44, pp. 2973-2982*, Japan (2001);

Karanikas, S., and Louis, A.A., “Dynamic Colloidal Stabilization by Nanoparticle Halos”, *Physical Review Letters 93 (24), 248303*, United Kingdom (2004);

Keblinski, P., Eastman, J.A., and Cahill, D.G., “Nanofluids for Thermal Transport”, *Materials Today 6, pp. 36-44*, United States of America (2005);

Keblinski. P., Philpot, S.R., Choi, S.U.S., and Eastman, J.A., “Mechanisms of Heat Flow in Suspensions of Nano-sized Particles (Nanofluids)”, *International Journal of Heat and Mass Transfer 45, pp. 855-863*, United States of America (2002);

Keidar, M., and Waas, A.M., “On the Conditions of Carbon Nanotube Growth in the Arc Discharge”, *Nanotechnology 15, pp. 1571-1575*, United States of America (2004);

Khanafer, K., Vafai, K., and Lightstone, M., “Buoyancy-driven Heat Transfer in a Two-dimensional Enclosure Utilizing Nanofluids”, International Journal of Heat and Mass Transfer 46, pp. 3639-3653, United States of America (2003);

Khanafer, K., and Vafai, K., “A Critical Synthesis of Thermophysical Characteristics of Nanofluids”, *International Journal of Heat and Mass Transfer 54, pp. 4410-4428*, United States of America (2011);

Kim, D., Cho, Y., Choi G., and Hong, S., “Carbon Nanotube Synthesis Using a Magnetic Fluid via Thermal Chemical Vapour Deposition”, *Department of Materials Engineering, Chungnam National University*, South Korea (2002);

Kim, J., Kang, Y.T., and Choi, C.K., “Analysis of Convective Instability and Heat Transfer Characteristics of Nanofluids”, *Physics of Fluids 16 (7), pp. 2395-2401*, South Korea (2004);

Kim, Y.J., Ma, H., and Yu, Q., “Plasma Nanocoated Carbon Nanotubes for Heat Transfer Nanofluids”, *Nanotechnology 21, 295703*, United States of America (2010);

Kingston, C.T., Zygmunt, J.J., Dénommée, S., and Simard, B., “Efficient Laser Synthesis of Single-walled Carbon Nanotubes through Laser Heating of the Condensing Vaporization Plume”, *Carbon 42, pp. 1657-1664*, Canada (2004);

Kleinstreuer, C., and Feng, Y., “Experimental and Theoretical Studies of Nanofluid Thermal Conductivity Enhancement: A Review”, *Nanoscale Research Letters 6, 229*, United States of America (2011);

Kolade, B., Goodson, K.E., and Eaton, J.K., “Convective Performance of Nanofluids in a Laminar Thermally Developing Tube Flow”, *ASME Journal of Heat Transfer 131, 052402*, United States of America (2009);

Koo, J., and Kleinstreuer, C., “A New Thermal conductivity Model for Nanofluids”, *Journal of Nanoparticle Research 6, pp. 577-588*, United States of America (2004);

Koo, J., Kang, Y., and Kleinstreuer, C, “A Nonlinear Effective Thermal Conductivity Model for Carbon Nanotube and Nano-fibre Suspensions”, *Nanotechnology 19, 375705*, South Korea (2008);

Korcek, S., Jensen, R., Johnson, M., and Sorab, J., “Maximizing the Fuel Efficiency of Engine Oils: The Role of Tribology”, *TriboTest Vol. 7-3, pp. 187-201*, United States of America (2001);

Kulkarni, D.P., Namburu, P.K., Bargar, H.E., and Das, D.K., “Convective Heat Transfer and Fluid Dynamic Characteristics of SiO_2-Ethylene Glycol/Water Nanofluid”, *Heat Transfer Engineering 29 (12), pp. 1027-1035*, United States of America (2008);

Kurt, H., and Kayfeci, M., “Prediction of Thermal Conductivity of Ethylene Glycol-Water Solutions by Using Artificial Neural Networks”, *Applied Energy 86, pp. 2244-2248*, Turkey (2009);

Kwak, K., and Kim, C., “Viscosity and Thermal Conductivity of Copper Oxide Nanofluid Dispersed in Ethylene Glycol”, *Korea-Australia Rheology Journal 17 (2), pp. 35-40*, South Korea (2005);

Lamas, B., Abreu, B., Fonseca, A., Martins, N., and Oliveira, M, “Assessing Colloidal Stability of Long term MWCNT based Nanofluids”, *Journal of Colloid and Interface Science 381, pp. 17-23*, Portugal (2012a);

Lamas, B., Abreu, B., Fonseca, A., Martins, N., and Oliveira, M.S.A., “A Critical Analysis on the Thermal Conductivity Prediction Models for CNT based Nanofluids”, *Department of Mechanical Engineering, University of Aveiro* ,Portugal (2012b);

Laohalertdecha, S., Naphon, P., and Wongwises, S., “A Review of Electrohydrodynamic Enhancement of Heat Transfer”, *Renewable and Sustainable Energy reviews 11, pp. 858-876*, Thailand (2007);

Lee, J., Hwang, K.S., Jang, S.P., Lee, B.H., Kim, J.H., Choi, S.U.S., and Choi, C.J., “Effecetive Viscosities and Thermal Conductivities of Aqueous Nanofluids Containing Low Volume Concentrations of Al_2O_3 Nanoparticles”, *International Journal of Heat and Mass Transfer 51, pp. 2651-2656*, South Korea (2008);

Lee, S., Choi, S.U.S., Li, S., and Eastman, J.A., “Measuring Thermal Conductivity of Fluids Containing Oxide Nanoparticles”, *Journal of Heat Transfer 121, pp. 280-289*, United States of America (1999);

Leong, K.C., Yang, C., and Murshed, S.M.S., “A Model for the Thermal Conductivity of Nanofluids – The Effect of Interfacial Layer”, *Journal of Nanoparticle Research 8, pp. 245-254*, Singapore (2006);

Li, C.H., and Peterson, G.P., “Experimental Investigation of Temperature and Volume Fraction Variations on the Effective Thermal Conductivity of Nanoparticle Suspensions”, *Journal of Applied Physics 99 (8), 084314*, United States of America (2006);

Li, Q., and Xuan, Y., “Convective Heat Transfer and Flow Characteristics of Cu-Water Nanofluid”, *Science in China (Series E) 45 (4), pp. 408-416*, China (2002);

Li, Q., Flamant, G., Yuan, X., Neveu, P., and Luo, L., “Compact Heat Exchangers: A Review and Future Applications for a New Generation of High Temperature Solar Receivers”, *Renewable and Sustainable Energy Reviews*, China (2011);

Liebenberg, L., Bergles, A.E., and Meyer, J.P., “Towards a Unified Approach for Modeling of Refrigerant Condensation in Smooth Tubes”, *Festschrift, Grenoble, France* (2002);

Liu, M., Lin, M.C., Huang, I., and Wang, C., “Enhancement of Thermal Conductivity with CuO for Nanofluids”, *Chemical Engineering and Technology 29 (1), pp. 72-77*, Taiwan (2006);

Liu, Z., and Liao, L., “Forced Convective Flow and Heat Transfer Characteristics of Aqueous Drag-reducing Fluid with Carbon Nanotubes Added”, *International Journal of Thermal Sciences 49, pp. 2331-2338*, China (2010);

Lotfi, R., Rashidi, A.M., and Amrohalli, A., “Experimental Study on the Heat Transfer Enhancement of MWNT-water Nanofluid in a Shell and Tube Heat Exchanger”, *International Communications in Heat and Mass Transfer 39, pp. 108-111*, Iran (2012);

Lunsford, K.M., “Increasing Heat Exchanger Performance”, *Bryan Research & Engineering Inc.-Technical Papers*, Texas, United States of America (2006);

Maiga, S.E.B., Nguyen, C.T., Galanis, N., and Roy, G., “Heat Transfer Behaviours of Nanofluids in a Uniformly Heated Tube”, *Superlattices and Microstructures 35 (3-6), pp. 543-557*, Canada (2004);

Manca, O., Mesolella, P., Nardini, S., and Ricci, D., “Numerical Study of a Confined Slot Impinging Jet with Nanofluids”, *Nanoscale Research Letters 6, 188*, Italy (2011);

Mansour, R.B., Galanis, N., and Nguyen, C.T., “Effect of Uncertainties in Physical Properties on Forced Convection Heat Transfer with Nanofluids”, Applied Thermal Engineering 27 (1), pp. 240-249, Canada (2007);

Mapa, L.B., and Mazhar, S., “Heat Transfer in Mini Heat Exchanger using Nanofluids”, *Northern Illinois Sectional Conference, Session B-T4-4*, United States of America (2005);

Mare, T., Halelfadi, S., Sow, O., Estelle, P., Duret, S., and Bazantay, F., “Comparison of the Thermal Performances of Two Nanofluids at Low Temperature in a Plate Heat Exchanger”, *Experimental Thermal and Fluid Science 35, pp. 1535-1543*, France (2011);

Martin, C.A., Sandler, J.K.W., Shaffer, M.S.P., Schwarz, M.K., Bauhofer, W., Schulte, K., and Windle, A.H., “Formation of Percolating Networks in Multi-wall Carbon-nanotube-epoxy Composites”, *Composites Science and Technology 64, pp. 2309-2316*, United Kingdom (2004);

Masuda, H., Ebata, A., Teramae, K., and Hishinuma, N., “Alteration of Thermal Conductivity and Viscosity of Liquid by Dispersing Ultra-fine Particles (Dispersion of g-Al_2O_3, SiO_2 and TiO_2 Ultra-fine Particles)”, *Netsu Bussei 4 (4), pp. 227-233*, Japan (1993);

Merchan-Merchan, W., Saveliev, A.V., Kennedy, L., and Jimenez, W.C., “Combustion Synthesis of Carbon Nanotubes and Related Nanostructures”, *Progress in Energy and Combustion Science 36, pp. 696-727*, United States of America (2010);

Meyer, J.P., and Liebenberg, L., “In-tube Passive Heat Transfer Enhancement in the Process Industry”, *Applied Thermal Engineering 27, pp. 2713-2726*, South Africa (2007);

Mohammed, H.A., Bhaskaran, G., Shuaib, N.H., and Saidur, R., “Heat Transfer and Fluid Flow Characteristics in Micro-channels Heat Exchanger using Nanofluids: A Review”, *Renewable and Sustainable Energy Reviews 15, pp. 1502-1512*, Malaysia (2010);

Mohammed, H.A., Bhaskaran, G., Shuaib, N.H., and Abu-Mulaweh, H.I., “Influence of Nanofluids on Parallel Flow Square Microchannel Heat Exchanger Performance”, *International Communications in Heat and Mass Transfer 38, pp. 1-9*, Malaysia (2011);

Munson-McGee, S.H., “Estimation of the Critical Concentration in an Anisotropic Percolation Network”, *Physical Review B 43 (4), pp. 3331-3336*, United States of America (1991);

Murshed, S.M.S., and Castro, C.A.N., “Contribution of Brownian Motion in Thermal Conductivity of Nanofluids”, *Proceedings of the World Congress on Engineering Vol. III*, Portugal (2011);

Murshed, S.M.S., Leong, K.C., and Yang, C., “Enhanced Thermal Conductivity of TiO_2-water based Nanofluids”, *International Journal of Thermal Sciences 44 (4), pp. 367-373*, Singapore (2005);

Murshed, S.M.S., Leong, K.C., and Yang, C., "A Model for Predicting the Effective Thermal Conductivity of Nanoparticles-fluid Suspensions", *International Journal of Nanoscience 5, pp. 23-33*, Singapore (2006);

Murshed, S.M.S., Leong, K.C., and Yang, C., "Thermophysical and Electrokinetic Properties of Nanofluids – A Critical Review", *Applied Thermal Engineering 28, pp. 2109-2125*, Singapore (2008);

Nan, C.W., Shi, Z., Lin, Y., "A Simple Model for Thermal Conductivity of Carbon Nanotube-based Composites", *Chemical Physics Letters 375, pp. 666-669*, China (2003);

Nan, C.W., Liu, G., Lin, Y., and Li, M., "Interface Effect on Thermal Conductivity of carbon Nanotube Composites", *Applied Physics Letters 85 (16), pp. 3549-3551*, China (2004);

Narvaez, J.A., Gschwender, L.J., Snyder, C.E., and Wilkens, R.J., "Measuring the Thermal Conductivity of Nanofluids using Three Different Techniques", *Thermal Conductivity 30, pp. 857-867*, United States of America (2010);

Nasiri, A., Shariaty-Niasar, M., Rashidi, A., Amrollahi, A., and Khodafarin, R., "Effect of Dispersion Method on Thermal Conductivity and Stability of Nanofluid", *Experimental Thermal and Fluid Science 35, pp. 717-723*, Iran (2011);

Nguyen, C.T., Roy, G., Gauthier, C., and Galanis, N., "Heat Transfer Enhancement using Al_2O_3-Water Nanofluid for an Electronic Liquid Cooling System", *Applied Thermal Engineering 27, pp. 1501-1506*, Canada (2007);

Oh, D., Jain, A., Eaton, J.K., Goodson, K.E., and Lee, J.S., "Thermal Conductivity Measurement and Sedimentation Detection of Aluminium Oxide Nanofluids by Using the 3ω Method", *International Journal of Heat and Fluid Flow 29, pp. 1456-1461*, South Korea (2008);

Ohadi, M.M., and Buckley, S.G., "High Temperature Heat Exchangers and Microscale Combustion Systems: Applications to Thermal System Miniaturization", *Experimental Thermal and Fluid Science 25, pp. 207-217*, United States of America (2001);

Okada, M., and Suzuki, T., "Natural Convection of Water-fine Particle Suspension in a Rectangular Cell", *International Journal of Heat and Mass Transfer 40 (13), pp. 3201-3208*, Japan (1997);

Omer, A.M., "Energy, Environment and Sustainable Development", *Renewable and Sustainable Energy Reviews 12, pp. 2265-2300,* United Kingdom (2007);

Pak, B.C, and Cho, Y.I., "Hydrodynamic and Heat Transfer Study of Dispersed Fluids with Submicron Metallic Oxide Particles", *Experimental Heat Transfer 11 (2), pp. 151-170*, United States of America (1998);

Pantzali, M.N., Kazakis, N.A., Tsolakidis, N., Mouza, A.A., and Tihon, J., "Measuring Transport Properties of Nanofluids", *Department of Chemical Engineering, Aristotle University of Thessaloniki*, Greece (2008);

Pantzali, M.N., Kanaris, A.G., Antoniadis, K.D., Mouza, A.A., and Paras, S.V., "Effect of Nanofluids on the Performance of a Miniature Plate Heat Exchanger with Modulated Surface", *International Journal of Heat and Fluid Flow 30, pp. 691-699*, Greece (2009);

Pantzali, M.N., Mouza, A.A., and Paras, S.V., "Investigating the Efficacy of Nanofluids as Coolants in Plate Heat Exchangers (PHE)", *Chemical Engineering Science 64, pp. 3290-3300*, Greece (2009a);

Patel, H.E., Anoop, K.B., Sundararajan, T., and Das, S.K., “Model for Thermal Conductivity of CNT-nanofluids”, *Bulletin of Material Science 31 (3), pp. 387-390*, India (2008);

Paul, G., Chopkar, M., Manna, I., and Das, P.K., “Techniques for Measuring the Thermal Conductivity of Nanofluids: A Review”, *Renewable and Sustainable Energy Reviews 14, pp. 1913-1924*, India (2010);

Pavlova, A.A., Otani, K., and Amitay, M., “Active Performance Enhancement of Spray Cooling”, *International Journal of Heat and Fluid Flow 29, pp. 985-1000*, United States of America (2008);

Peña, J.R.V., Zárate, J.M.O., and Khayet, M., “Measurement of the Thermal Conductivity of Nanofluids by the Multicurrent Hot-wire Method”, *Journal of Applied Physics 104, 044314*, Spain (2008);

Pethkool, S., Eiamsa-ard, S., Kwankaomeng, S., and Promvonge, P., “Turbulent Heat Transfer Enhancement in a Heat Exchanger using Helically Corrugated Tube”, *International Communications in Heat and Mass Transfer 38, pp. 340-347*, Thailand (2011);

Pfautsch, E., “Forced Convection in Nanofluids Over a Flat Plate”, *Dissertation for the Degree of Master of Science, University of Missouri*, United States of America (2008);

Pinto, J.M., and Gut, J.A.W., “Optimal Configuration Design for Plate Heat Exchangers”, *International Journal of Heat and Mass Transfer 47, pp. 4833-4848*, Brazil (2004);

Ponmozhi, J., “Desenvolvimento e Caracterização de Nanofluidos”, *Thesis for the degree of Master of Science, University of Aveiro,* Portugal (2009);

Ponmozhi, J., Gonçalves, F.A.A.M., Ferreira, A.G.M., Fonseca, I.M.A., Kanagaraj, S., Martins, N., and Oliveira, M.S.A., “Thermodynamic and Transport Properties of CNT-Water Based Nanofluids”, *Journal of Nano Research 11, pp. 101-106*, Portugal (2010);

Popov, V.N., “Carbon Nanotubes: Properties and Application”, *Materials Science and Engineering R 43, pp. 61-102*, Belgium (2004);

Prasher, R., Bhattacharya, P., and Phelan, P.E., “Thermal Conductivity of Nanoscale Colloidal Solutions (Nanofluids)”, *Physical Review Letters 94, 025901*, United States of America (2005);

Putnam, S.A., Cahill, D.G., Braun, P.V., Ge, Z., and Shimmin, R.G., “Thermal Conductivity of Nanoparticle Suspensions”, *Journal of Applied Physics 99, 084308*, United States of America (2006);

Putra, N., Roetzel, W., and Das, S.K., “Natural Convection of Nano-fluids”, *Heat and Mass Transfer 39, pp. 775-784*, India (2003);

Rafati, M., Hamidi, A.A., and Niaser, M.S., “Application of Nanofluids in Computer Cooling Systems (Heat Transfer Performance of Nanofluids)”, *Applied Thermal Engineering, 10.1016/j.applthermaleng.2012.03.028*, Iran (2012);

Rea, U., McKrell, T., Hu, L., and Buongiorno, J., “Laminar Convective Heat Transfer and Viscous Pressure Loss of Alumina-water and Zirconia-water Nanofluids”, *International Journal of Heat and Mass Transfer 52, pp. 2042-2048*, United States of America (2009);

Reay, D.A., “Compact heat exchangers, enhancement and heat pumps”, *International Journal of Refrigeration 25, pp. 460-470*, United Kingdom (2002);

Rensmo, H., Ongaro, A., Ryan, D., and Fitzmaurice, D., "Self-assembly of Alkane Capped Silver and Silica Nanoparticles", *Journal of Materials Chemistry 12, pp. 2762-2768*, Sweden (2002);

Romano, J.M., Parker, J.C., and Ford, Q.B., "Application Opportunities for Nanoparticles Made From the Condensation of Physical Vapors", *Advances in Powder Metallurgy and Particulate Materials Vol.2, pp. 12.3-12.2*, United States of America (1997);

Roy, G., Nguyen, C.T., and Lajoie, P., "Numerical Investigation of Laminar Flow and Heat Transfer in a Radial Flow Cooling System with the use of Nanofluids", *Superlattices and Microstructures 35, pp. 497-511*, Canada (2004);

Sachdeva, G., "Computation of Heat Transfer Augmentation in a Plate-fin Heat Exchanger Using Rectangular/Delta Wing*", Dissertation for the degree of Doctor of Philosophy, National Institute of Technology*, India (2010);

Sahoo, N.G., Rana, S., Cho, J.W., Li, L., and Chan, S.H., "Polymer Nanocomposites based on Functionalized Carbon Nanotubes", *Progress in Polymer Science 35, pp. 837-867*, Singapore (2010);

Sastry, N.N.V., Bhunia, A., Sundararajan, T., and Das, S.K., "Predicting the Effective Thermal Conductivity of Carbon Nanotube based Nanofluids", *Nanotechnology 19, 055704*, India (2008);

Schmidt, A.J., Chiesa, M., Torchinsky, D.H., Johnson, J.A., Nelson, K.A., and Chen, G., "Thermal Conductivity of Nanoparticle Suspensions in Insulating Media Measured with a Transient Optical Grating and a Hotwire", *Journal of Applied Physics 103 (8), 083529*, United States of America (2008);

Schnitzler, M.C., and Zarbin, A.J.G., "The Effect of Process Variables on the Characteristics of Carbon Nanotubes Obtained by Spray Pyrolysis", *Journal of Nanoparticle Research 10, pp. 585-597*, Brazil (2008);

Shah, R.K., and Sekulic, D.P., "Fundamentals of Heat Exchanger Design", *John Wiley & Sons Inc.*, New Jersey, United States of America (2003);

Shenogin, S., Bodapati, A., Xue, L., Ozisik, R., and Keblinski, P., "Effect of Chemical Functionalization on Thermal Transport of Carbon Nanotube Composites", *Applied Physics Letters 85 (12), pp. 2229-2231*, United States of America (2004);

Shi, Z., Lian, Y., Liao, F.H., Zhou, X., Gu, Z., Zhang, Y., Iijima, S., Li, H., Yue, K.T., and Zhang, S., "Large Scale Synthesis of Single-wall Carbon Nanotubes by Arc-discharge Method", *Journal of Physics and Chemistry of Solids 61, pp. 1031-1036*, China (2000);

Silva, B.A.A, "Caracterização de Nanofluidos do Ponto de Vista Termo-físico", *Thesis for the degree of Master of Science, University of Aveiro,* Portugal (2010);

Sitprasert, C., Dechaumphai, P., and Juntasaro, V., "A Thermal Conductivity Model for Nanofluids Including Effect of the Temperature-dependent Interfacial Layer", *Journal of Nanoparticle Research 11, pp. 1465-1476*, Thailand (2009);

Sundar, L.S., and Sharma, K.V., "Heat Transfer Enhancements of Low Volume Concentration Al_2O_3 Nanofluid and with Longitudinal Strip Inserts in a Circular Tube", *International Journal of Heat and Mass Transfer 53, pp. 4280-4286*, Malaysia (2010);

Sunden, B., Srihari, N., Rao, B.P., and Das, S.K., “Transient Response of Plate Heat Exchangers Considering Effect of Flow Maldistribution”, *International Journal of Heat and Mass Transfer 48, pp. 3231-3243*, Sweden (2005);

Talapin, D.V., Rogach, A.L., Mekis, I., Haubold, S., Kornowski, A., Haase, M., and Weller, H., “Synthesis and Surface Modification of Amino-stabilized CdSe, CdTe and InP Nanocrystals”, *Colloids and Surfaces A: Physicochemical and Engineering Aspects 202 (2-3), pp. 145-154*, Germany (2002);

Trisakri, V., and Wongwises, S., “Critical Review of Heat Transfer Characteristics of Nanofluids”, *Renewable and Sustainable Energy Reviews 11, pp. 512-523*, Thailand (2007);

Tsitzios, V., Georgakilas, V., Oikonomou, E., Karakassides, M., and Petridis, D., “Synthesis and Characterization of Carbon Nanotube/Metal Nanoparticle Composites Well Dispersed in Organic Media”, *Carbon 44, pp. 848-853*, Greece (2006);

Vaisman, L., Wagner, H.D., and Marom, G., “The Role of Surfactants in Dispersion of Carbon Nanotubes”, *Advances in Colloid and Interface Science 128-130, pp. 37-46*, Israel (2006);

Van Der Ploeg, H.J., and Masters, B.I., “A New Shell-and-tube Option for Refineries”, *Petroleum Technology Quarterly 2, pp. 91-95*, United States of America (1997);

Venerus, D.C., Kabadi, M.S., Lee, S., and Perez-Luna, V., “Study of Thermal Transport in Nanoparticle Suspensions Using Forced Rayleigh Scattering”, *Journal of Applied Physics 100, 094310*, United States of America (2006);

Wang, B., Zhou, L., and Peng, X., “A Fractal Model for Predicting the Effective Thermal Conductivity of Liquid with Suspension of Nanoparticles”, *International Journal of Heat and Mass Transfer 46, pp. 2665-2672*, China (2003);

Wang, X., and Mujumdar, A.S., “A Review on Nanofluids – Part I: Theoretical and Numerical Investigations”, *Brazilian Journal of Chemical Engineering 25 (4), pp. 613-630*, Singapore (2008);

Wang, X., Xu, X., and Choi, S.U.S., “Thermal conductivity of nanoparticle-fluid mixture”, *Journal of Thermophysics and Heat Transfer 13, pp. 474-480*, United States of America (1999);

Warad, H.C., Ghosh, S.C., Hemtanon, B., Thanachayanont, C., and Dutta, J., “Luminescent Nanoparticles of Mn Doped ZnS Passivated with Sodium Hexametaphosphate”, *Science and Technology of Advanced Materials 6, pp. 296-301*, Thailand (2005);

WCED – World Commission on Environment and Development (Brundtland Commission), “Our Common Future”, *United Nations General Assembly* (1987);

Webb, R.L., “Advances in Modeling Enhanced Heat Transfer Surfaces”, *Proceedings of 10th International Heat Transfer Conference, 1, pp. 445–459*, United States of America (1994);

Wegner, K., Walker, B., Tsantilis, S., and Pratsinis, S.E., “Design of Metal Nanoparticle Synthesis by Vapor Flow Condensation”, Chemical Engineering Science 57 (10), pp. 1753-1762, Switzerland (2002);

Wen, D., and Ding, Y., “Effective Thermal Conductivity of Aqueous Suspensions of Carbon Nanotubes (Carbon Nanotube Nanofluids)”, *Journal of Thermophysics and Heat Transfer 18 (4), pp. 481-485*, United Kingdom (2004);

Wen, D., and Ding, Y., "Experimental Investigation into Convective Heat Transfer of Nanofluids at the Entrance Region Under Laminar Flow Conditions", *International Journal of Heat and Mass Transfer 47, pp. 5181-5188*, United Kingdom (2004a);

Wen, D., Lin, G., Vafaei, S., and Zhang, K., "Review of Nanofluids for Heat Transfer Applications", *Particuology 7, pp. 141-150*, United Kingdom (2009);

Wen, M.Y., and Ho, C.Y., "Heat-transfer Enhancement in Fin-and-tube Heat Exchanger with Improved Fin Design", *Applied Thermal Engineering 29, pp. 1050-1057*, Taiwan (2009);

Williams, W.C., "Experimental and Theoretical Investigation of Transport Phenomena in Nanoparticle Colloids (Nanofluids)." *Dissertation for the degree of Doctor of Philosophy, Massachusetts Institute of Technology*, United States of America (2006);

Xia, C., "Spray/Jet Cooling for Heat Flux High to 1kW/cm^{2}", *Eighteenth IEEE Semiconductor Thermal Management Symposium, pp. 159-163*, United States of America (2002);

Xie, H., Wang, J., Xi, T., Liu, Y., Ai, F., and Wu, Q., "Thermal Conductivity Enhancement of Suspensions Containing Nanosized Alumina Particles", *Journal of Applied Physics 91, pp. 4568-4572*, China (2002);

Xie, H., Lee, H., Youn, W., and Choi, M., "Nanofluids Containing Multiwalled Carbon Nanotubes and their Enhanced Thermal Conductivities", *Journal of Applied Physics 94 (8), pp. 4967-4971*, China (2003);

Xie, H., Fujii, M., and Zhang, X., "Effect of Interfacial Nanolayer on the Effective Thermal Conductivity of Nanoparticle-Fluid Mixture", *International Journal of Heat and Mass Transfer 48, pp. 2926-2932*, China (2005);

Xie, H., and Chen, L., "Adjustable Thermal Conductivity in Carbon Nanotube Nanofluids", *Physics Letters A 373, pp. 1861-1864*, China (2009);

Xie, H., Yu, W., Li, Y., and Chen, L., "Discussion on the thermal conductivity enhancement of nanofluids", *Nanoscale Research Letters 6, 124*, China (2011);

Xu, J., Yu, B., Zou, M., and Xu, P., "A New Model for Heat Conduction of Nanofluids based on Fractal Distributions of Nanoparticles", *Journal of Physics D: Applied Physics 39, pp. 4486-4490*, China (2006);

Xuan, Y., and Li, Q., "Heat Transfer Enhancement of Nanofluids", *International Journal of Heat and Fluid Flow 21, pp. 58-64*, China (1999);

Xuan, Y., and Roetzel, W., "Conceptions for Heat Transfer Correlation of Nanofluids", *International Journal of Heat and Mass Transfer 43, pp. 3701-3707*, China (2000);

Xuan, Y., Li, Q., and Hu, W., "Aggregation Structure and Thermal Conductivity of Nanofluids", *AIChe Journal 49 (4), pp. 1038-1043*, China (2003);

Xuan, Y., Yu, K., and Li, Q., "Investigation on Flow and Heat Transfer of Nanofluids by the Thermal Lattice Boltzmann Model", *Progress in Computational Fluid Dynamics 5 (1-2), pp. 13-19*, China (2005);

Xue, L., Keblinski, P., Phillpot, S.R., Choi, S.U.S., and Eastman, J.A., "Two Regimes of Thermal Resistance at a Liquid-solid Interface", *Journal of Chemical Physics 118 (1), pp. 337-339*, United States of America (2003);

Xue, Q., “Model for Effective Thermal Conductivity of Nanofluids”, *Physics Letters A 307, pp. 313-317*, China (2003);

Xue, Q.Z., “Model for the Effective Thermal conductivity of Carbon Nanotube Composites”, *Nanotechnology 17, pp. 1655-1660*, China (2006a);

Xue, Q.Z., “Model for Thermal Conductivity of Carbon Nanotube-based Composites”, *Physica B 368, pp. 302-307*, China (2006b);

Xue, Q., and Xu, W., “A Model of Thermal Conductivity of Nanofluids with Interfacial Shells”, *Materials Chemistry and Physics 90, pp. 298-301*, China (2005);

Yoo, D., Hong, K.S., and Yang, H., “Study of Thermal Conductivity of Nanofluids for the Application of Heat Transfer Fluids”, *Thermochimica Acta 455 (1-2), pp. 66-69*, South Korea (2007);

Yu, W., and Choi, S.U.S., “The Role of Interfacial Layers in the Enhanced Thermal Conductivity of Nanofluids: A Renovated Maxwell Model”, *Journal of Nanoparticle Research 5 (1-2), pp. 167-171*, United States of America (2003);

Yu, W., France, D.M., Routbort, J.L., and Choi, S.U.S., “Review and Comparison of Nanofluid Thermal Conductivity and Heat Transfer Enhancements”, *Heat Transfer Engineering 29(5), pp. 432-460*, United States of America (2008);

Yu, W., France, D.M., Smith, D.S., Singh, D., Timofeeva, E.V., and Routbort, J.L., “Heat Transfer to a Silicon Carbide/Water Nanofluid”, *International Journal of Heat and Mass Transfer 52, pp. 3606-3612*, United States of America (2009);

Zaccai, E., “Over Two Decades in Pursuit of Sustainable Development: Influence, Transformations, Limits”, *Environmental Development 1, pp. 79-90*, Belgium (2012);

Zhang, X., Gu, H., and Fujii, M., “Effective Thermal Conductivity and Thermal Diffusion of Nanofluids Containing Spherical and Cylindrical Nanoparticles”, *Experimental Thermal and Fluid Science 31, pp. 593-599*, China (2007).

Appendixes

Appendix A - Model Development

A1 - Model Geometry

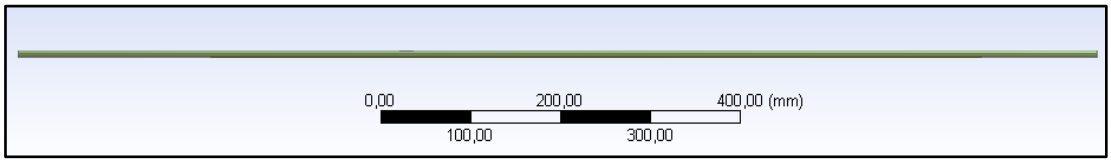

Figure A1 – Front view of the stainless steel test tube

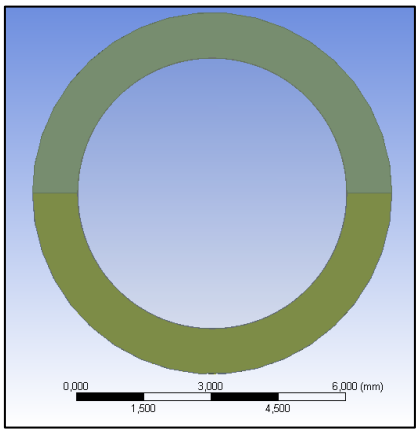

Figure A2 – Side view of the two-part test tube (tube inlet)

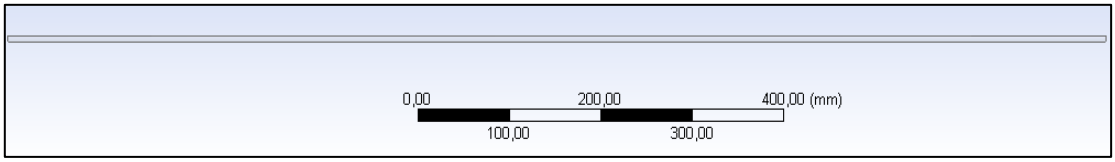

Figure A3 – Front view of the fluid domain

A2 - Mesh Independence

Table A1 – Fixed Parameters of DIW for Mesh Independence Testing

Parameter	Units	Value
Flow rate ($\dot{m}$)	$\mathrm{Kg/s}$	0.006448
Dynamic viscosity (μ)	$\mathrm{N\,s/m^2}$	0.000855
Fluid inlet temperature (T_{in})	K	300
Fluid inlet velocity (u_{in})	$\mathrm{m/s}$	0.2947
Total heat flux (q_{cw}'')	$\mathrm{W/m^2}$	4774.747
Fluid domain timescale	s	≈ Advection time
Solid domain timescale	s	Automatic

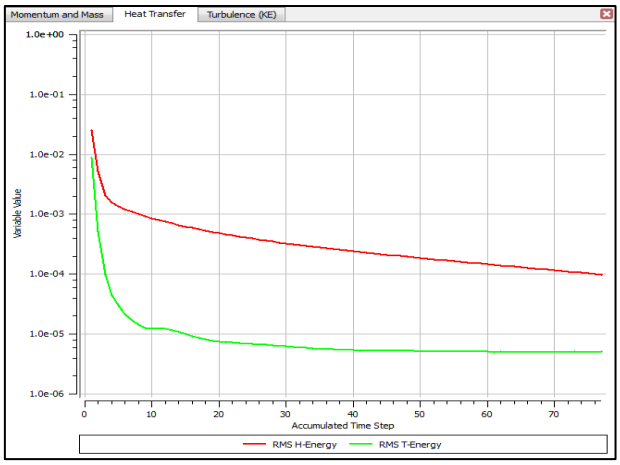

Figure A4 – Mesh independence test: heat transfer iterative convergence.

Appendix B - Model Validation Results

B1 - DIW

Table B1 –Validation Results for DIW

Simulation	x $[m]$	$T_{f,\,num}$ $[K]$	$T_{s,\,num}$ $[K]$	h_{num} $[W/m^2K]$	h_{exp} $[W/m^2K]$	Nu_{num}	Nu_{exp}	Nu_{shah}
VAL1	0	296.85						
	0.2	297.64	304.88	642.15	501.27	6.37	4.91	11.77
	0.42	298.54	305.99	625.06	597.78	6.20	5.85	9.19
	0.61	299.36	306.82	623.97	514.73	6.19	5.04	8.12
	0.81	300.22	307.63	627.93	447.85	6.23	4.38	7.39
	1	301.04	308.49	624.22	534.62	6.19	5.23	6.88
	1.2	301.90						
VAL2	0	299.75						
	0.2	300.33	305.83	841.69	281.38	8.35	2.75	12.96
	0.42	301.01	306.84	793.39	305.75	7.87	2.99	10.12
	0.61	301.62	307.46	792.44	250.67	7.86	2.45	8.94
	0.81	302.26	308.08	796.66	206.55	7.90	2.02	8.13
	1	302.88	308.72	792.58	249.88	7.86	2.04	7.58
	1.2	303.52						
VAL3	0	300.45						
	0.2	300.90	305.36	1036.25	278.31	10.28	2.72	13.96
	0.42	301.44	306.25	960.37	307.08	9.52	3.01	10.90
	0.61	301.93	306.74	959.57	246.40	9.51	2.41	9.49
	0.81	302.45	307.24	963.98	201.19	9.56	1.97	8.63
	1	302.94	307.75	959.97	245.78	9.52	2.40	8.05
	1.2	303.46						

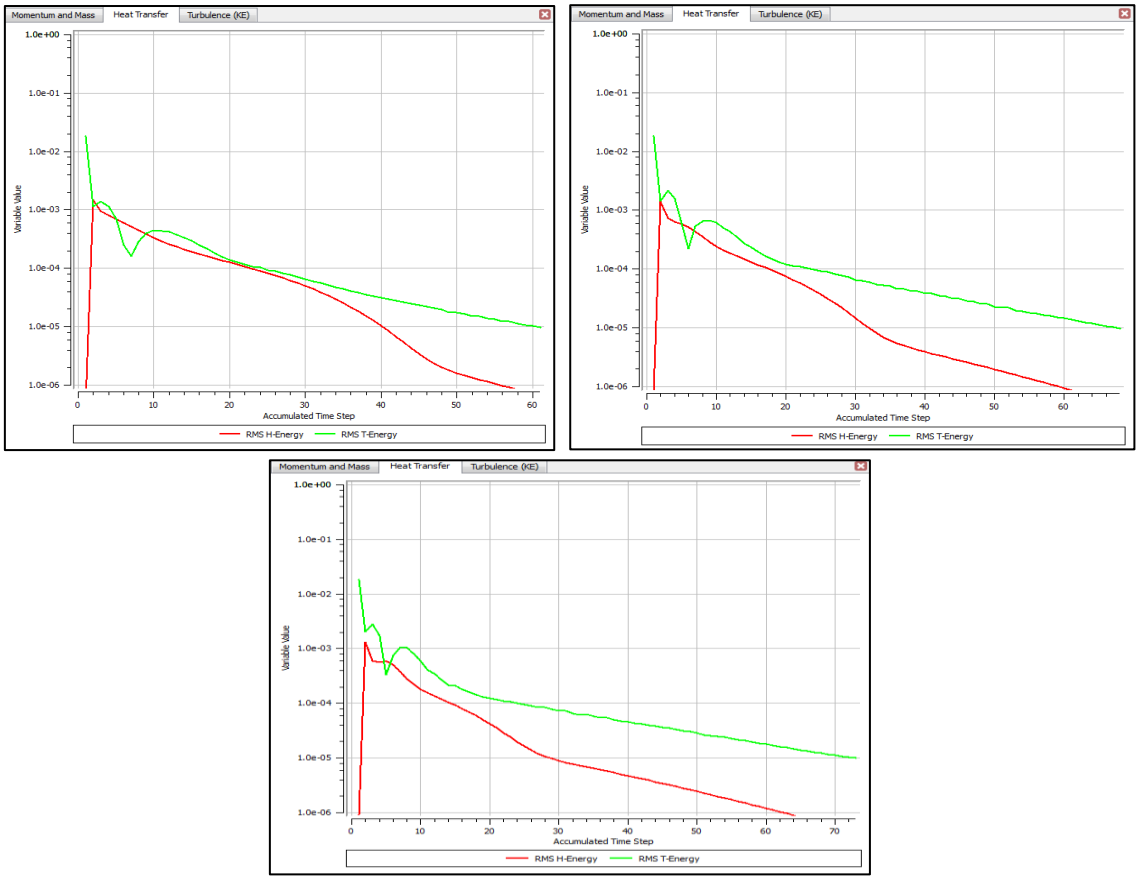

Figure B1 – Model validation: heat transfer iterative convergence for DIW simulations (from top left to bottom: VAL1 to VAL3).

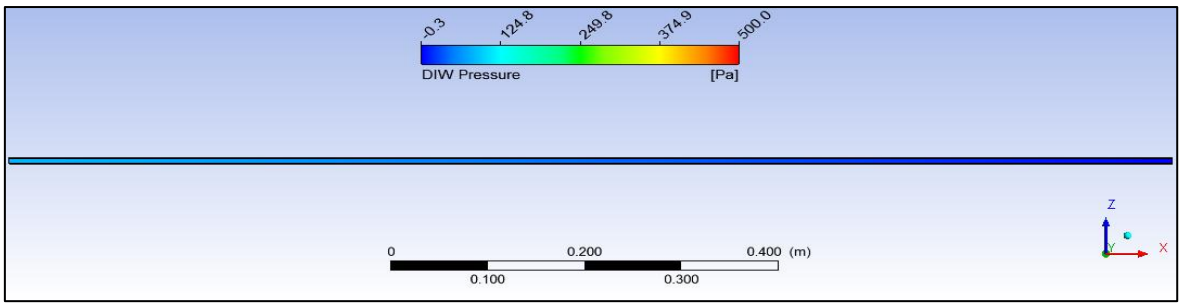

Figure B2 – DIW pressure along tube for simulation VAL1.

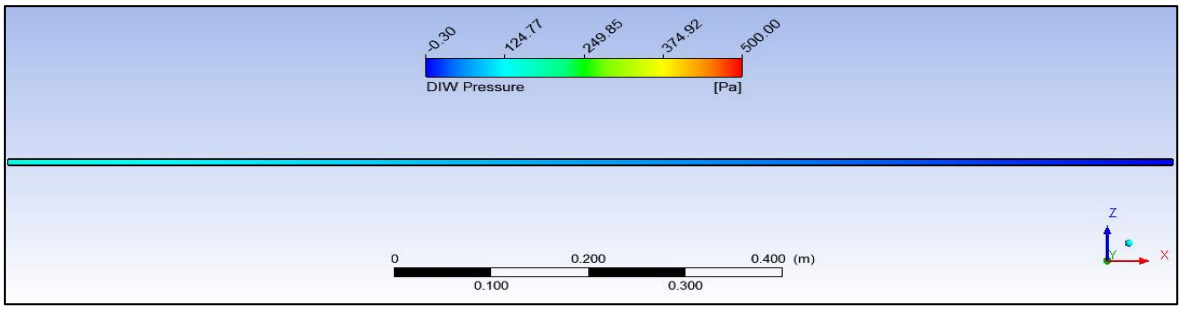

Figure B3 – DIW pressure along the tube for simulation VAL2.

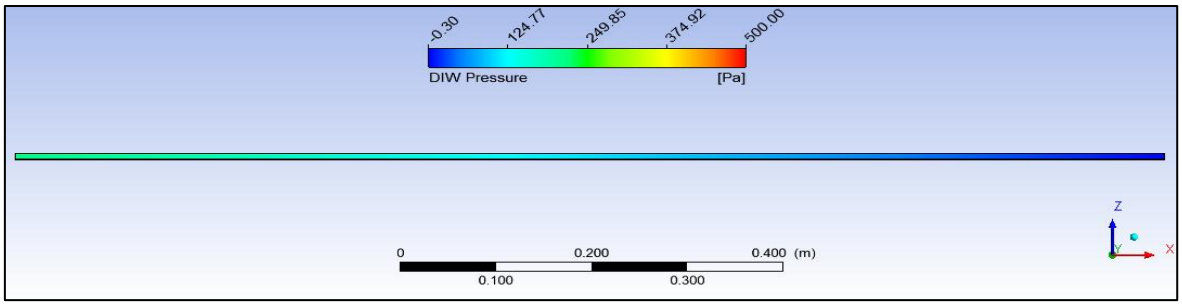

Figure B4 – DIW pressure along the tube for simulation VAL3.

B2 - CNT/DIW Nanofluid

Table B2 –Validation Results for CNT/DIW Nanofluid

Simulation	x $[m]$	$T_{f,\,num}$ $[K]$	$T_{s,\,num}$ $[K]$	h_{num} $[W/m^2K]$	h_{exp} $[W/m^2K]$	Nu_{num}	Nu_{exp}	Nu_{shah}
VAL4	0	297.15						
	0.2	297.63	303.91	740.25	673.44	7.34	6.45	13.77
	0.42	298.17	304.36	751.26	716.50	7.45	6.87	10.75
	0.61	298.67	304.86	750.16	606.25	7.44	5.81	9.49
	0.81	298.19	305.35	755.04	551.79	7.49	5.29	8.63
	1	299.68	305.88	750.28	715.78	7.44	6.86	8.05
	1.2	300.20						
VAL5	0	297.25						
	0.2	297.60	302.37	970.11	385.88	9.62	3.70	15.16
	0.42	298.01	302.88	950.60	412.45	9.43	3.95	11.84
	0.61	298.38	303.25	949.62	327.50	9.42	3.14	10.45
	0.81	298.77	303.62	954.91	290.04	9.47	2.78	9.51
	1	299.14	304.01	949.82	379.87	9.42	3.64	8.87
	1.2	299.53						
VAL6	0	297.05						
	0.2	297.32	301.19	1192.71	447.36	11.83	4.29	16.33
	0.42	297.65	301.67	1147.36	474.30	11.38	4.55	12.75
	0.61	297.94	301.97	1146.79	381.49	11.37	3.66	11.26
	0.81	298.26	302.26	1152.23	332.48	11.43	3.19	10.24
	1	298.56	302.58	1147.08	467.88	11.38	4.48	9.55
	1.2	298.87						

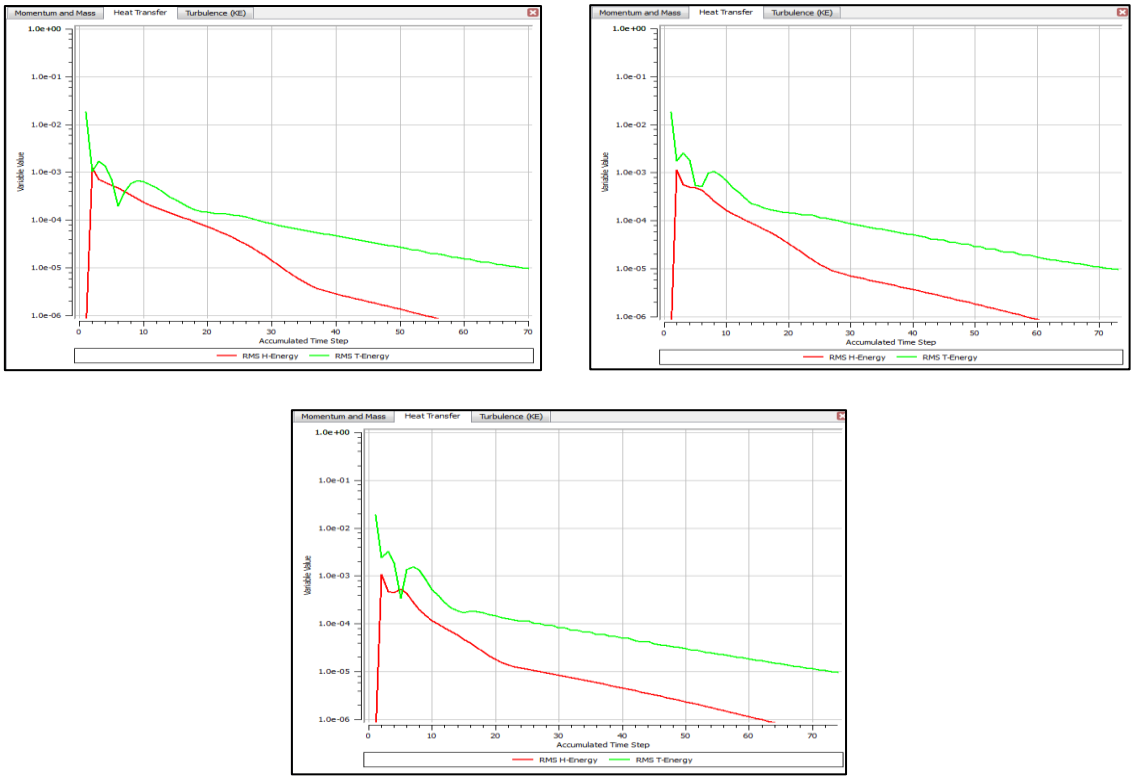

Figure B5 – Model validation: heat transfer iterative convergence for CNT/DIW nanofluid simulations (from top left to bottom: VAL4 to VAL6).

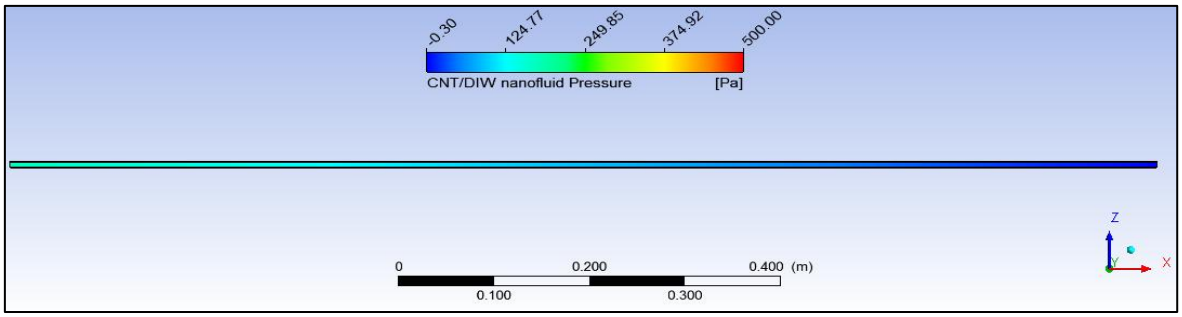

Figure B6 – CNT/DIW nanofluid pressure along the tube for simulation VAL4.

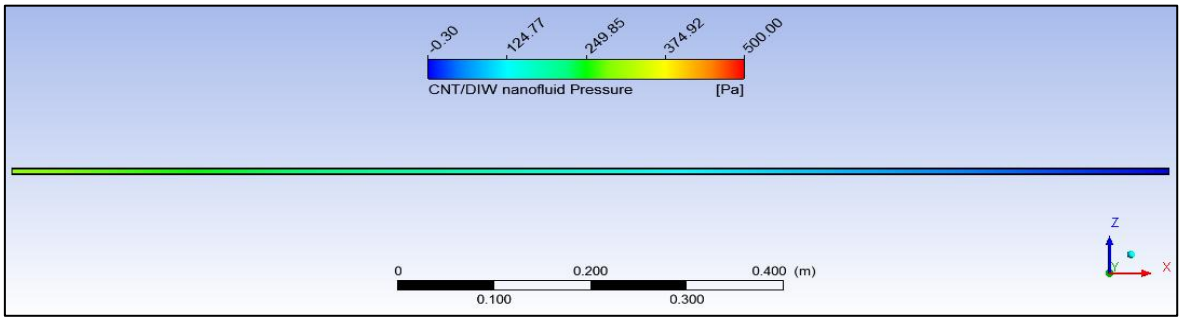

Figure B7 – CNT/DIW nanofluid pressure along the tube for simulation VAL5.

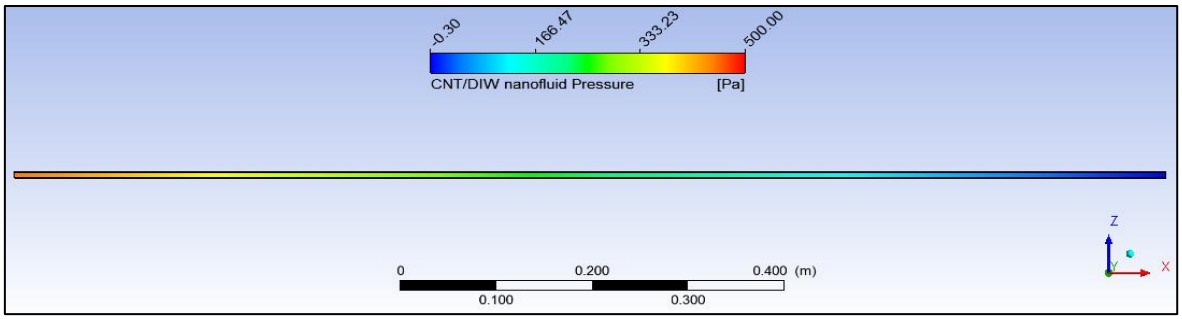

Figure B8 – CNT/DIW nanofluid pressure along the tube for simulation VAL6.

Appendix C - Parametric Study

C1 - Tube Length

Table C1 – Mesh Independence for L=1500 mm: Element Size Proposals

Model Domain	**Model Part**	**Mesh 1** [mm]	**Mesh 2** [mm]	**Mesh 3** [mm]
Fluid	Body	5	1	0.5
	Surface	0.05	0.01	0.005
Tube	Tube1	5	1	0.5
	Tube2	5	1	0.5
Number of Elements		1306472	2118359	4270546

Table C2 – Mesh Independence for L=1500 mm: Mesh Inflation Proposals

Parameter	**Mesh 1**	**Mesh 2**	**Mesh 3**
Number of Layers	8	10	12
Growth Rate	1.2	1.1	1
Maximum Thickness [mm]	1.5	0.15	0.1

Table C3 – Fixed Parameters of DIW for Mesh Independence Testing for L=1500 mm

Parameter	**Units**	**Value**
Flow rate ($\dot{m}$)	$\mathrm{Kg/s}$	0.006448
Dynamic viscosity (μ)	$\mathrm{N\,s/m^2}$	0.000855
Fluid inlet temperature (T_{in})	K	300
Fluid inlet velocity (u_{in})	$\mathrm{m/s}$	0.1767
Total heat flux (q_{cw}'')	$\mathrm{W/m^2}$	2864.789

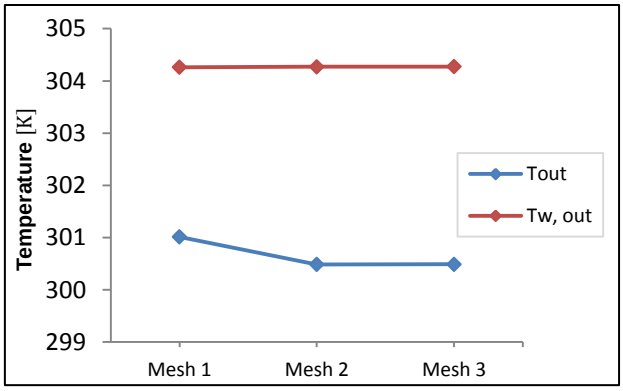

Figure C1 – Mesh independence for L=1500 mm: Temperatures at outlet for tested meshes

C2 - Tube Diameter

Table C4 – Mesh Independence for D=2 mm: Element Size Proposals

Model Domain	**Model Part**	**Mesh 1** [mm]	**Mesh 2** [mm]	**Mesh 3** [mm]
Fluid	Body	5	1	0.5
	Surface	0.05	0.01	0.005
Tube	Tube1	5	1	0.5
	Tube2	5	1	0.5
Number of Elements		423322	704003	883865

Table C5 – Mesh Independence for D=2 mm: Mesh Inflation Proposals

Parameter	**Mesh 1**	**Mesh 2**	**Mesh 3**
Number of Layers	8	10	12
Growth Rate	1.2	1.1	1
Maximum Thickness [mm]	1.5	0.15	0.1

Table C6 – Fixed Parameters of DIW for Mesh Independence Testing for D=2 mm

Parameter	**Units**	**Value**
Flow rate ($\dot{m}$)	$\mathrm{Kg/s}$	0.00166
Dynamic viscosity (μ)	$\mathrm{N\,s/m^2}$	0.000855
Fluid inlet temperature (T_{in})	K	297
Fluid inlet velocity (u_{in})	$\mathrm{m/s}$	0.000221
Total heat flux (q_{cw}'')	$\mathrm{W/m^2}$	9549.296

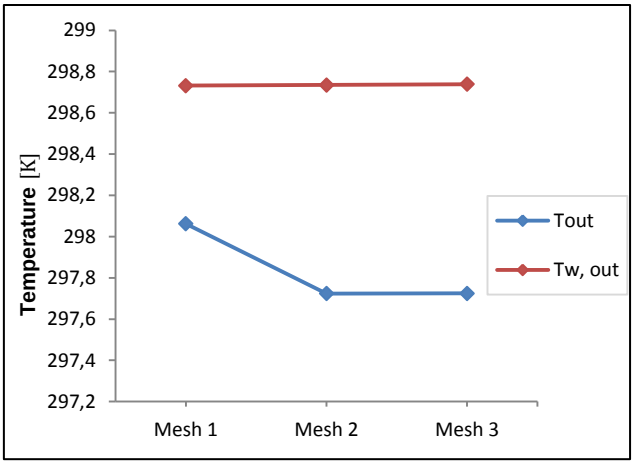

Figure C2 – Mesh independence for D=2 mm: Temperatures at outlet for tested meshes